Title
THEORY OP THE DISSOCIATION OF DIATOMIC MOLECULES AND A STUDY OF THE EMISSION SPECTRA OF IF

Author
Birks, John William.

Publication Date
1974-11-01

THEORY OF THE DISSOCIATION OF DIATOMIC MOLECULES AND A STUDY OF THE EMISSION SPECTRA OF IF

John William Birks
(Ph. D. thesis)

November, 1974

Prepared for the U. S. Atomic Energy Commission
under Contract W-7405-ENG-48

DISCLAIMER

THEORY OF THE DISSOCIATION OF DIATOMIC MOLECULES
AND A STUDY OF THE EMISSION SPECTRA OF IF

Contents

THEORY OF THE DISSOCIATION OF DIATOMIC MOLECULES AND A STUDY OF THE EMISSION SPECTRA OF IF

John William Birks

Inorganic Materials Research Division, Lawrence Berkeley Laboratory
and Department of Chemistry; University of California
Berkeley, California

ABSTRACT

The extent to which diatomic molecules dissociate from all vibrational levels has been investigated by calculating from first principles the collision cross sections for dissociation of H_2 from particular vibration-rotation levels upon collision with Ne atoms. The Ne-H_2 potential energy surface was first calculated by the multiconfiguration self-consistent-field (MCSCF) and configuration interaction (CI) methods. A Monte Carlo classical trajectory study using this surface resulted in cross sections that are smaller than those required to accurately fit the experimental data, when incorporated in a nonequilibrium model of dissociation kinetics. Because of the threshold nature of the dissociation process for all but the highest vibration-rotation levels, the classical cross sections are considered to be a lower bound to the true quantum mechanical cross sections.

The potential energy surface has the interesting property, previously found for the He-H_2 surface, of contracting the H_2 molecule as the Ne atom approaches. The surface demonstrates a cross-over point where the contractive force changes to a stretching force. Such a cross-over point where the contractive force changes to a stretching force. Such a cross-over has been predicted for He-H_2 by Secrest, but points on the He-H_2 surface have not yet been calculated in the region of this cross-over.

An experimental study of the emission spectra of IF in the gas phase reaction of I_2 with F_2 is reported. Emission was observed from both the $B^3\Pi_{o+}$ and the previously unreported $A^3\Pi_1$ excited electronic states. For the $B^3\Pi_{o+}$ state the transition moment and vibrational populations were extracted from the spectra by a least squares method whereby theoretical band shapes were fit to the experimental data. The effect of flow rates of reactants and Ar on the relative emission of the two electronic states suggests that both states are populated by three body atom recombination. It is argued that there is an avoided curve crossing between the two lowest $^3\Pi_{o+}$ states of IF, in which case the ground state dissociation energy of IF is known to be 23229 cm^{-1}.

PART I

THE DISSOCIATION OF DIATOMIC MOLECULES

I. INTRODUCTION

The dissociation of a diatomic molecule X_2 in a "heat bath" of an inert monatomic gas M would appear to be a simple process:

$$X_2 + M \rightarrow X + X + M \qquad (1)$$

Since even at elevated temperatures most of the molecules are in the ground vibrational level one might expect that this process would proceed with an activation energy equal to the dissociation energy D_o and the rate constant be given by the Arrhenius expression

$$k = A \exp(-D_o/kT) \qquad (2)$$

In recent years extensive experimental data for the rates of dissociation of a number of diatomic molecules has been collected.[1,2] An interesting feature of the data is that in every case the observed activation energy is substantially less (by 10-30%) than the bond dissociation energy, D_o. Experimentalists were at first apprehensive about their results, which did not agree with their preconceived notions, and attributed the anomalously low activation energies to experimental error due to boundary layer effects in the shock tube.[2] Subsequent correction for boundary layer effects resulted in even lower values for the activation energy, however, and the effect persisted in experiments using highly dilute mixtures of diatomic molecules in an inert gas.[3] Thus, the problem of the low activation energies in the thermal dissociation of diatomic molecules presents an interesting challenge to the theory of chemical kinetics.

In consideration of this problem one should first begin by realizing that the activation energy and barrier height are not necessarily the same quantity. The activation energy has a purely formal definition

$$E_a = - R \frac{d \ln k}{d (1/T)} \tag{3}$$

and is just the manner in which the logarithm of the rate constant changes with 1/T. Only for the Arrhenius expression, equation 2, does one obtain a value of D_o, the barrier height, for the activation energy. From simple collision theory we know that the pre-exponential or A factor of equation 2 is not temperature independent. In the simple theory of hard-spheres collisions, A is the rate constant for collision, usually denoted Z and is given by

$$A = \pi \sigma^2 (8kT/\pi\mu)^{1/2} \tag{4}$$

where σ is the collision diameter, usually evaluated from viscosity data or used as a fitting parameter, and μ is the reduced mass of the collision pair. The activation energy is then found to be

$$E_a = D_o + \frac{1}{2} RT \tag{5}$$

using the definition of E_a, equation 3. Thus, even for the simple hard-spheres collision theory the activation energy is not simply equal to the barrier height. The observed activation energies deviate from the bond energy by amounts substantially greater than $\frac{1}{2}$ RT, however, and a more complete theory of the dissociation of diatomic molecules is necessary in order to explain the low activation energies.

All of the data for the dissociation of the homonuclear diatomic molecules H_2, N_2, O_2, F_2, Cl_2, Br_2, and I_2 were reviewed up to June 1972 in an article by Johnston and Birks.[4] In this work three models for

the dissociation process were evaluated by comparison with existing data. An important feature of the three models considered was that an equilibrium distribution of molecules among energy levels was not assumed. Instead, a steady-state assumption for the relative vibrational populations was applied, allowing levels to become depleted below their equilibrium values.

The "step ladder" model which allows dissociation only from the top "rung" or vibrational level with dissociation occurring by successive energy transfer steps is a model that has been used frequently in the past.[5] With non-equilibrium effects allowed, this model predicted the wrong temperature dependence of the activation energy, the activation energy being low at low temperatures and increasing with increasing temperature.

The second model considered is the same as the "step ladder" model in that a truncated harmonic oscillator potential is used and vibrational energy transfer is allowed between adjacent rungs only, but differs in that dissociation is allowed to occur from all vibrational levels. This model predicted the correct trend of the activation energy with temperature, and in several cases the activation energies and rate constants agreed quantitatively with the experimental data.

A third model used a more realistic Morse potential and allowed energy transfer to occur between all vibrational levels as well as dissociation from all levels. The results of this more complex model agreed very well with those of the second model, and for this reason the second model was believed to contain all of the features necessary for an understanding of the experimentally observed effect of temperature on the activation energy.

In the context of these models, it is the allowance of a non-equilibrium distribution and the fact that molecules dissociate from a large number of vibrational levels, not just the highest vibrational level, taken together that explains the decrease in activation energy with increasing temperature. This is illustrated by Fig. 1, which is taken from the Johnston and Birks[4] article. This figure compares the product $c_i X_i$, where c_i is the rate constant for dissociation from a particular vibrational level and X_i is the mole fraction for that level, at three temperatures. The rate constant k is the sum over all vibrational levels of these products

$$k = \sum_i c_i X_i \tag{6}$$

The solid lines of Fig. 1 are calculated for non-equilibrium steady-state mole fractions and the dashed lines are the products for an assumed Boltzmann distribution. For F_2 there are seen to be 29 parallel reaction channels with nearly equal contribution to the reaction rate constant from each of these reaction channels in the equilibrium case. However, in the actual case of non-equilibrium many of the upper levels are depleted below their equilibrium values and the number of reaction channels is reduced. The depletion of a given level i is caused both by the rapid loss of molecules in level i to atoms and by level i being skipped as molecules in lower levels go directly to atoms. From Fig. 1 we see that at 500 K there are only about 20 effective reaction channels; at 1000 K the number is about 15; and at 2500 K the number is about 7. This decrease in the number of reaction channels by virtue of the non-equilibrium distribution at high energies causes the rate

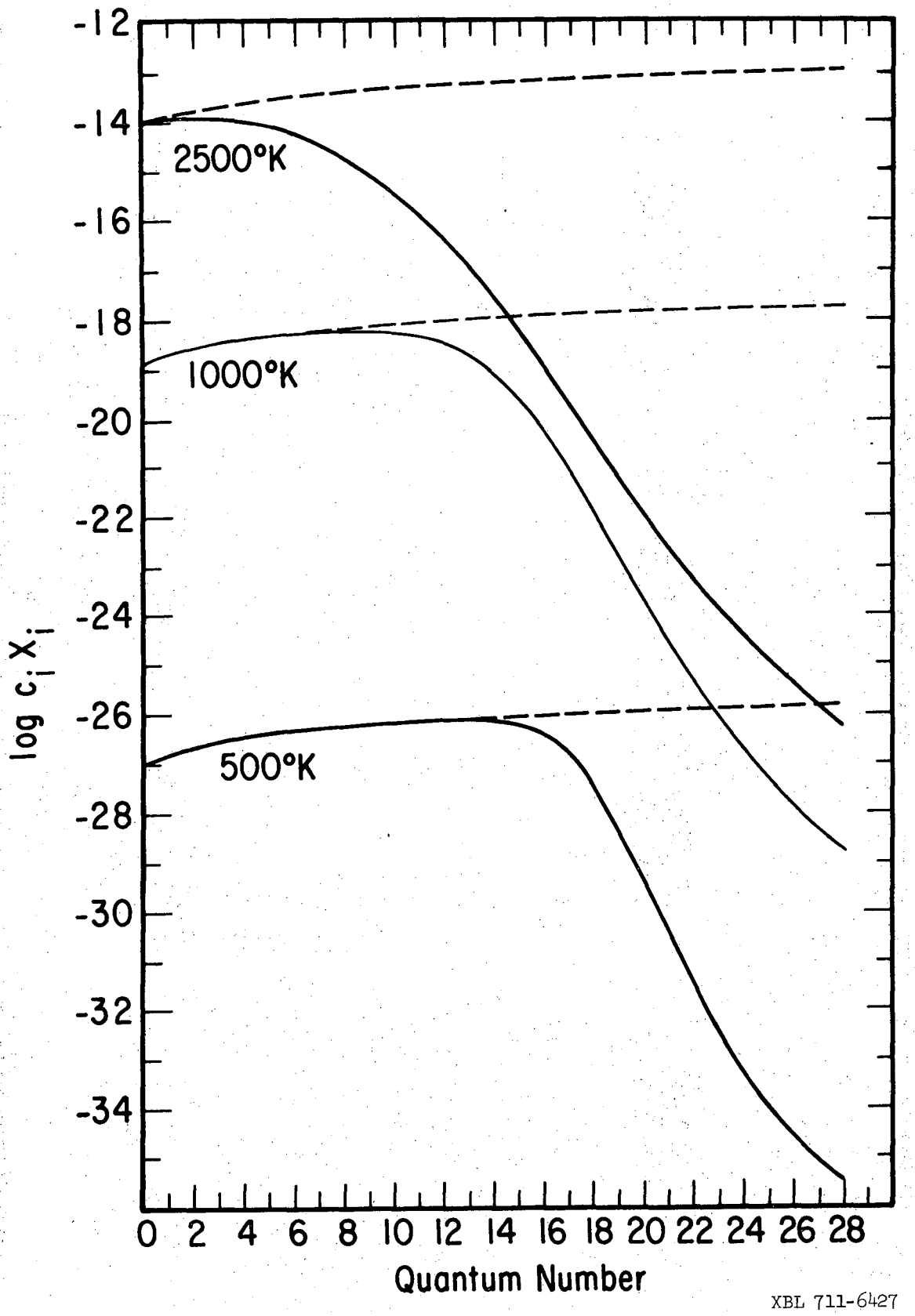

Fig. 1. Distribution function for molecules that react for the vibrational states of F_2. (---) Equilibrium distribution; (—) Non-equilibrium distribution. Note the shrinking number of states that contribute to reaction as one goes to high temperatures.

constant to increase with temperature less rapidly than expected, and thus the activation energy is lower than expected (see equation 3).

Essential to this "explanation" of the effect of temperature on the activation energies is the concept that dissociation occurs from a large number of, perhaps all, vibrational levels. Since the rate constants c_i for dissociation from particular vibrational levels had not been measured, it was necessary that we (Johnston and Birks[4]) arrive at some formula based, in part, on chemical intuition. Because the depletion of upper levels is dependent upon vibrational energy transfer and dissociation coupling, we chose to relate the rate constants c_i to the energy transfer constants. To do this, we assumed that the ratio of dissociation from level i to activation from level i to level i + 1 was governed by the expression

$$\frac{c_i}{a_i} = \beta \frac{\exp[-(D_o-E_i)/kT]}{\exp[-h\nu/kT]} \tag{7}$$

where $\beta > 1$ and is the same for all levels i. In effect, we assumed that dissociation into the continuum of final states has a larger pre-exponential factor than activation to the single next higher state. To evaluate β we assumed that every sufficiently energetic collision resulted in dissociation from the top level. That is,

$$c_t = Z \exp[-(D_o-E_t)/kT] \tag{8}$$

where Z is the rate constant for hard-spheres collisions, given by equation 4. Substituting into equation 7, we obtain the expression for β

$$\beta = \frac{\bar{Z}}{a_t} \exp(-h\nu/kT) \tag{9}$$

A property of harmonic oscillator spectroscopy often used to relate the deactivation rate constant at any level b_i in terms of the deactivation constant between the two lowest levels b_1 is

$$b_i = i\, b_1 \tag{10}$$

From microscopic reversibility, the expression

$$a_i = b_{i+1} \exp(-h\nu/kT) \tag{11}$$

relates the rate constant for activation from level i to i + 1 to the rate constant for deactivation from level i + 1 to i. Combining equations 10 and 11 we have

$$a_i = (i+1)b_1 \exp(-h\nu/kT) \tag{12}$$

and substituting into equation 9 we have for β

$$\beta = \frac{\bar{Z}}{(t+1)b_1} \tag{13}$$

Finally, substitution of equations 12 and 13 into equation 7 yields an expression for the dissociation rate constant from a particular vibrational level

$$c_i = \frac{i+1}{t+1} Z \exp[-(D_o - E_i)/kT] \tag{14}$$

Apart from the factor (i+1)/(t+1) this is just the hard-spheres collision rate constant, the energy barrier being $(D_o - E_i)$.

A Boltzmann distribution of molecules over vibrational levels gives for X_i the result

$$X_i = \frac{1}{f_v} \exp(-E_i/kT) \tag{15}$$

where f_v is the vibrational partition function. The contribution to the dissociation rate constant k from level i is then

$$c_i X_i = \frac{i+1}{t+1} \frac{Z}{f_v} \exp(-D_o/kT) \tag{16}$$

The cancellation of exponents E_i is due to the fact that dissociation from low lying levels, although unfavored by a large energy barrier, is favored by the higher equilibrium population factor. As a result, at equilibrium dissociation occurs equally from all vibrational levels, apart from the factor (i+1)/(t+1). If we include this factor in the collision cross section, we have for the cross sections

$$\pi\sigma^2 = \frac{i+1}{t+1} \pi d^2 \tag{17}$$

where d is the hard-spheres collision diameter, usually evaluated from viscosity data.

Let us consider the example of H_2 dissociating in a heat bath of Ne. The collision diameter is 2.85 Å so that the collision cross-section for dissociation from the top vibrational level is $\sim$ 26 $Å^2$. There are 13 bound vibrational levels for H_2 so that the cross-section for dissociation for the lowest vibrational level is predicted to be ~ 2 $Å^2$.

The good agreement between the simple theory of Johnston and Birks with experiment for a large number of cases and the simple explanation it provides for the change in activation energy with temperature make the theory very appealing, particularly since the theory contains no adjustable parameters. The agreement with the data could be fortuitous, however. For this reason, it is necessary that the

crucial aspect of this theory be put to test. That is, the reaction cross sections for dissociation from particular vibrational levels either be measured or calculated from first principles. The latter approach has been taken in the work described here. The cross sections for dissociation of H_2 by collisions with Ne have been calculated within the framework of the Born-Oppenheimer approximation for the separation of nuclear and electronic motion and the use of classical mechanics to describe the nuclear motion. The procedure used was to first calculate points on the potential energy surface for the Ne-H-H system of atoms from quantum mechanics followed by fitting of these points to an analytic form. Three-dimensional classical trajectories were then calculated on this surface by integrating Hamilton's equations of motion. The trajectories were chosen by a Monte Carlo technique so as to average over initial spacial orientations of the atom and molecule. Collision energies were selected at random from a Maxwellian distribution and the initial vibrational and rotational energies chosen to correspond to quantized states of the H_2 molecule, the vibrational phase being selected at random. From the fraction of trajectories that result in dissociation of the H_2 molecule, it is a simple matter to calculate the reaction rate constant and cross-section for dissociation from particular vibration-rotation levels at the chosen temperature. In the following sections these calculations are described and the results discussed in terms of the theory of dissociation of diatomic molecules previously outlined.

II. CALCULATION OF THE Ne-H-H POTENTIAL ENERGY SURFACE

A. Theory

The calculation of a potential energy surface consists of solving the Schrödinger wave equation for the lowest eigenvalue at a large number of fixed values of the positions of the atomic nuclei. Implicit in such calculations is the Born-Oppenheimer approximation[6] for the separation of nuclear and electronic motion. The Schrödinger wave equation for a stationary state is

$$\mathcal{H}\psi = E\psi \tag{18}$$

where $\mathcal{H}$ is the complete Hamiltonian, consisting of the sum of kinetic energy operators for the nuclei and the electrons plus potential energy terms for the nuclear-nuclear repulsions, the electron-nuclear attractions, and the electron-electron repulsions. The complete Schrödinger wave equation including all of these terms is given by

$$\left\{ \sum_j -\frac{\hbar^2}{2M_j}\nabla_j^2 - \frac{\hbar^2}{2m}\sum_i \nabla_i^2 + \sum_{j<j'} \frac{z_j z_{j'} e^2}{r_{jj'}} - \sum_{i,j} \frac{z_j e^2}{r_{ij}} + \sum_{i<i'} \frac{e^2}{r_{ii'}} \right\} \psi = E\psi \tag{19}$$

where the summations over j and j' are over the nuclei, and the summations over i and i' are over the electrons. In the second term m has no index because all electrons have the same mass. The mass of the nucleus M_j varies according to the atom. The function ψ is the total wavefunction and E is the total energy.

Since the nuclear mass is considerably greater than that of an electron, the mass of the proton being about 1840 times that of the electron, as a first approximation it is reasonable to assume that the nuclei do not move at all. Thus, the Born-Oppenheimer approximation amounts to neglecting the kinetic energy of the nuclei, the first summation in equation 19. Since the nuclei do not move, the third summation, which is the nuclear repulsion energy, is a constant. The total energy is then

$$E = E_N + E_e \tag{20}$$

where E_N is the nuclear repulsion energy and E_e is the electronic energy. Making use of the expression,

$$E_e = E - \sum_{j<j'} \frac{z_j z_{j'} e^2}{r_{jj'}} \tag{21}$$

dropping the first summation in equation 19, and rearranging we obtain

$$\left\{ \sum_i -\frac{\hbar^2}{2m} \nabla_i^2 - \sum_j \frac{z_j e^2}{r_{ij}} + \sum_{i<i'} \frac{e^2}{r_{ii'}} \right\} \psi_e = E_e \psi_e \tag{22}$$

for the electronic Schrödinger wave equation. Within the framework of the Born-Oppenheimer approximation the solution of a problem such as the one considered here consists of solving equation 22 for the electronic energy E_e for a large number of possible positions of the nuclei. Once E_e has been determined as a function of the nuclear coordinates (A, B, $\cdots$, M), it may be used as the potential energy in the wave equation which describes the motion of the nuclei, the nuclear Schrödinger equation, equation, which is given by equation 23.

$$\left\{ \sum_j \frac{\hbar^2}{M_j} \nabla_j^2 + E_e(A,B,\cdots,M) \right\} \psi_N = E_T \psi_N \qquad (23)$$

For example, the lowest eigenvalue E_e may be obtained by solution of equation 5 for various internuclear distances of a diatomic molecule, resulting in the familiar potential energy curve which is usually well described by the empirical Morse potential. This electronic potential energy may be substituted into equation 23 which may then be solved for the stationary state rotation-vibration levels of the molecule.

In the three atom case considered here the solution of equation 22 for various spacial arrangements of the atoms results in a potential energy surface, or more precisely, a manifold of potential energy surfaces. The coordinate system used here for the description of the potential energy as a function of spacial arrangement of the atoms is given by Fig. 2. For θ held constant the potential energy is a function of the two variables R, the H_2 internuclear distance, and X, the distance of the Ne nucleus from the H_2 center of mass, and describes a surface. There is a surface in Cartesian space for every value of θ.

In the present case we are not interested in the stationary state solution of the nuclear Schrödinger equation, except in assigning the initial state and determining the final state of the H_2 molecule. Instead, we are interested in the time evolution of the nuclear motion and must in principle solve the time-dependent nuclear Schrödinger equation. This amounts to the calculation of quantum mechanical trajectories on the potential energy surface. Since such calculations are

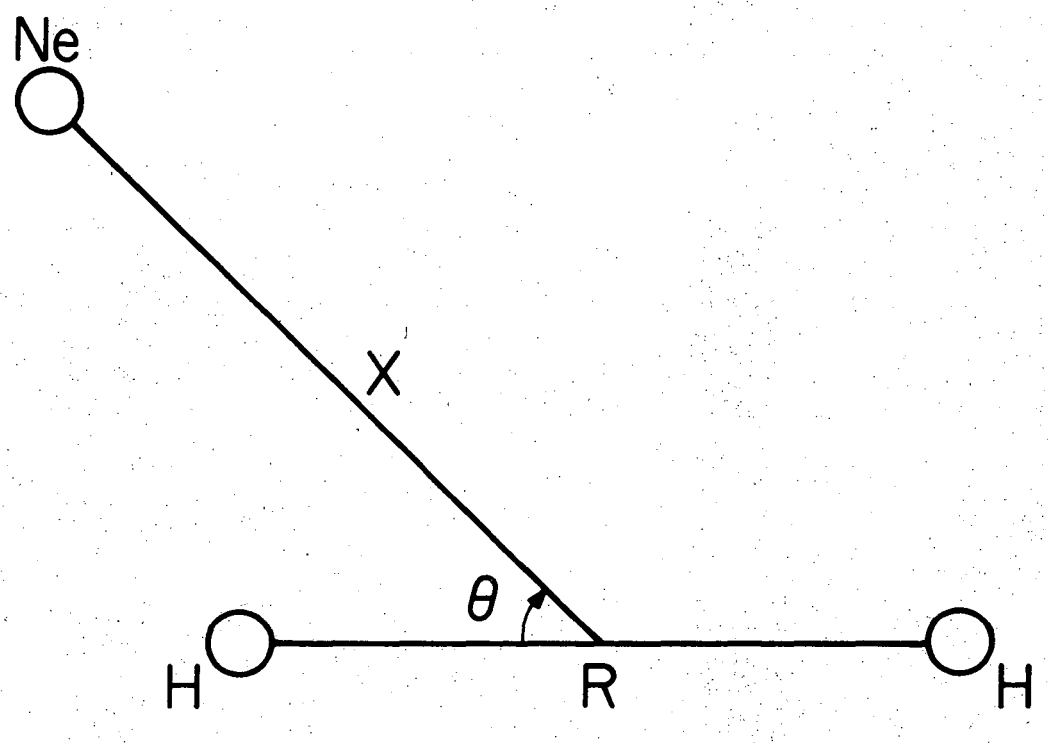

XBL 7410-7505

Fig. 2. Coordinate system for representing the Ne-H-H potential energy surface.

at the present time not practical and since the semiclassical theories of Miller[7] and Marcus[8] are not yet sufficiently developed for application to this problem, it was necessary to calculate trajectories according to the classical equations of motion. Classical trajectory calculations have been successful in calculating the rates of bimolecular exchange reactions.[9]

It should be pointed out that the Schrödinger wave equation, equation 19, neglects relativistic effects. Relativistic contributions to the total energy are substantial, but are ignored in the calculation of potential energy surfaces. This is because relativistic considerations are very complex for even simple systems, but fortunately the surface obtained by ignoring relativistic energy can be expected to be parallel to the true surface. The shape of the potential energy surface is determined primarily by the motion of the valence electrons, whereas electrons that make the greatest contribution to the relativistic energy are electrons in closed inner shells where the classical velocities of such electrons are not insignificant compared to the velocity of light.

The exact solution of equation 5 has been obtained for one-electron atoms and molecules. For two or more electrons the "three body problem" is encountered and only approximate solutions may be obtained. In principle these approximate solutions which are obtained by numerical methods can be found for any required degree of accuracy, the limitations being the size and speed of the computer used. The computation of accurate potential energy surfaces and other aspects of electronic structure is presently a very active and exciting field, and has been

reviewed in a recent book by Schaefer.[10] His book discusses in a general way the approximate methods used for solution of the wave equation and describes the results of a large number of recent calculations. Details of computational methods are discussed in a book by McWeeny and Sutcliffe.[11]

Approximate Methods - Approximate solutions of the Schrödinger equation are in almost all cases based on the "variational principle". For any normalized approximate wavefunction the energy is just the expectation value of the Hamiltonian operator

$$E = \int \psi_e^* \mathcal{H}_e \psi_e \, d\tau \tag{24}$$

The variational principle asserts that the energy E calculated from equation 24 is a rigorous upper bound to the true energy. That is, the energy calculated from any approximate wave function ψ will always lie above the exact energy. For a given functional form of ψ the best wave function is the one for which the parameters have been varied to obtain the lowest energy.

An important application of the variational method is the self-consistent-field (SCF) method due to Hartree and Fock.[12,13] The Hartree-Fock (HF) wave function has the form

$$\psi_e = A(n)\phi_1(1)\phi_2(2)\cdots\phi_n(n) \tag{25}$$

for closed shell atoms and molecules where A(n) is the anti-symmetrizer for n electrons, and there is a spinorbital ϕ for each of the electrons. A spinorbital is a function of the coordinates of one electron only and is the product of a spacial orbital χ and a one electron spin function

α (for $m_s = + 1/2$) or β (for $m_s = - 1/2$).

$$\phi_i = \chi_i\alpha \qquad \text{or} \qquad \phi_i = \chi_i\beta \tag{26}$$

The Hartree-Fock wavefunction may also be written as a Slater determinant

$$\psi_e = \frac{1}{\sqrt{n!}} \begin{vmatrix} \phi_1(1)\phi_1(2)\cdots\phi_1(n) \\ \phi_2(1)\phi_2(2)\cdots\phi_2(n) \\ \vdots \\ \phi_n(1)\phi_n(2)\cdots\phi_n(n) \end{vmatrix} \tag{27}$$

which meets the requirement of being antisymmetric with respect to exchange of any two electrons.

A rather complicated set of integrodifferential equations may be derived by considering the variation of the Slater determinant so as to minimize the energy given by equation 24. These equations may be solved exactly for one electron systems and to a high degree of accuracy for atoms by numerical integration. The resulting energy is called the Hartree-Fock energy. For molecules the orbitals ϕ_i are usually expanded in terms of a set of analytic basis functions. Since the basis set of functions can never be a mathematically complete set, the solution to the Hartree-Fock equations can only be approximate. The best wave function obtained using a finite basis set is called the self-consistent-field (SCF) wave function.

For simplification of the SCF calculation, these calculations are normally carried out within the context of certain symmetry and equivalence restrictions. For Ne-H-H in the linear geometry the SCF

wavefunction may be written

$$\psi_e = A(12)1\sigma\alpha\ 1\sigma\beta\ 2\sigma\alpha\ 2\sigma\beta\ 3\sigma\alpha\ 3\sigma\beta\ 1\pi_{-1}\alpha\ 1\pi_{-1}\beta\ 1\pi_{+1}\alpha\ 1\pi_{+1}\beta\ 4\sigma\alpha\ 4\sigma\beta \tag{28}$$

where the notation $\chi_{1\sigma}\ \alpha(1)$ has been simplified to $1\sigma\alpha$, etc. An example of a symmetry requirement is that each orbital must transform according to one of the irreducible representations of the molecule's point group. Thus variation of σ and π functions is restricted to variation which does not change the symmetry of the functions. A σ function must remain a σ function and cannot have any π character mixed in. An example of an equivalence restriction is that the special function 1σ associated with α spin must be identical to the 1σ function associated with β spin. The solution of the Hartree-Fock equations including symmetry and equivalence restrictions yields the restricted Hartree-Fock (RHF) wave function with energy somewhat above the HF energy.

If the spinorbitals are orthogonal, that is

$$\int \phi_i(1)\phi_j(1)dv(1) = \delta_{ij} \tag{29}$$

where dv(1) indicates integration over the space and spin coordinates of electron 1, then the energy expression can be written

$$E = \sum_i I(i|i) + \sum_i \sum_j [(ij|ij)-(ij|ji)] \tag{30}$$

Here, $I(i|j)$ are the one-electron integrals given by

$$I(i|j) = \int \phi_i^*(1) \left[-\frac{\nabla_1^2}{2} - \sum_A \frac{Z_A}{r_{1A}} \right] \phi_j(1)dv(1) \tag{31}$$

of which $I(i|i)$ is a special case. Two-electron integrals or electron repulsion integrals are given by

$$(ij|k\ell) = \iint \phi_i^*(1)\phi_j^*(2)\frac{1}{r_{12}}\phi_k(1)\phi_\ell(2)\,dv(1)\,dv(2) \tag{32}$$

Integrals of the type $(ij|ij)$ are called "coulomb integrals" and those of the type $(ij|ji)$ are known as "exchange integrals". In evaluation of the integrals use is made of the following properties of spin functions.

$$\begin{aligned} \int \alpha^*(1)\alpha(1)\,ds(1) &= \int \beta^*(1)\beta(1)\,ds(1) = 1 \\ \int \alpha^*(1)\beta(1)\,ds(1) &= \int \beta^*(1)\alpha(1)\,ds(1) = 0 \end{aligned} \tag{33}$$

The Hartree-Fock approximation to the solution of the Schrödinger wave equation is for many purposes very useful. For example, molecular geometries, some one-electron properties, and ionization potentials calculated from RHF wave functions are often in good agreement with experiment.[10] However, the HF and RHF approximations solve for the motion of each electron in the presence of the average potential created by the remaining electrons. These methods neglect the instantaneous (rather than averaged) repulsions between pairs of electrons. The motion of the electrons are actually correlated in that two electrons are unlikely to move very close to each other. The energy due to the instantaneous repulsions is called the "correlation energy" and is usually defined as the difference between the RHF energy and the exact nonrelativistic energy. The correlation energy is usually a small percentage of the total energy of an atom or system of atoms. For the

Ne atom the correlation energy is 0.38 hartrees, which is only 0.3% of the total energy, -129.06 hartree. Although a small percentage of the total energy, 0.38 hartrees is more than twice the energy required to break the H_2 bond. Thus, correlation energy is a very important consideration if we are to understand chemical behavior from electronic structure calculations.

The most useful approach to the problem of correlation energy has been that of configuration interaction (CI). In the Hartree-Fock method each electron of the atom or molecule is assigned to a single spinorbital. There are, of course, an infinite number of other orbitals which could be used to construct other configurations. A CI wavefunction is a linear combination of such configurations with coefficients variationally determined. That is,

$$\psi_e = \sum_i c_i \Phi_i \tag{34}$$

where the Φ's are an orthonormal set of n electron configurations. The coefficients c_i are varied so as to minimize the energy given by equation 24. Use of the variation principle leads to the eigenvalue problem

$$(\underline{H} - \underline{E}\underline{1})\underline{C} = 0 \tag{35}$$

where $\underline{H}$ is a matrix with elements

$$H_{ij} = \int \phi_i^* \mathcal{H}_e \phi_j \, d\tau \tag{36}$$

and $\underline{C}$ isthe matrix containing the coefficients c_i. The eigenvalue problem may be solved by iterative methods yielding M eigenvalues or

energies where M is the number of configurations used. MacDonald's theorem[14] states that the lowest eigenvalue is an upper bound to the true energy of the ground state, and more generally, the k^{th} lowest eigenvalue is a rigorous upper bound to the k^{th} lowest exact energy. For each energy E_i there is a vector C_i which defines the corresponding wave function. In principle the CI method is exact since the exact solution to the Schrödinger equation is approached as the basis set of one-electron functions approaches completeness and all possible configurations are included.

In carrying out a CI calculation it is desirable that both the orbitals ϕ and the CI coefficients c be varied simultaneously. When more than a few configurations are used, however, this is seldom done because of difficulties in solving the complex equations. Calculations in which both the orbitals and CI coefficients are simultaneously varied to obtain the lowest energy are referred to as multiconfiguration self-consistent field (MCSCF) calculations. The first MCSCF calculations were performed by Hartree, Hartree and Swirles[15] on the oxygen atom.

In the present case a 2-configuration MCSCF calculation has been carried out for the Ne-H-H system for both the collinear and perpendicular bisector arrangement of atoms. In addition, a 111-configuration CI calculation has been carried out for the collinear geometry. These calculations are described in more detail in the following section.

B. Details of Calculations

Basis Set. The basis set used for these calculations consists of Guassian functions. The radial part of these functions differ from Slater functions; the former vary as $e^{-\alpha r^2}$, whereas the latter vary as $e^{-\zeta r}$. Slater functions are superior in that fewer functions are required for a given degree of accuracy, only one function being required for the exact solution of one-electron atoms.[16] For nonlinear molecules, however, the necessary integrals are difficult to calculate, requiring considerable computer time. Here Gaussian functions are advantageous, since the integrals may be calculated from closed analytic expressions. The requirement of having two to three times as many Gaussian functions as Slater functions in the basis set increases the time required to reach a solution to the SCF equations, however, via the Roothaan procedure.[17] The Roothaan procedure requires an amount of computer time proportional to the fourth power of the number of basis functions.[10] In order to take advantage of the simplification afforded by Gaussians in the calculation of multi-centered integrals and at the same time minimize the number of required basis functions, theoreticians have begun to make use of contracted Gaussian functions. A contracted Gaussian is a linear combination of functions with fixed coefficients. These coefficients are usually optimized for the atom on which the contracted function is centered and remain fixed in the molecular calculation. In this way the required number of basis functions can usually be reduced by about a factor of two without too large a sacrifice in accuracy, resulting in a savings of a factor of about 16 in computation time.

In the present case, the (9s5p) Gaussian basis for neon of Van Duijneveldt[18] contracted to (5s3p) was used. The exponents α and the contraction coefficients for this (9s5p/5s3p) basis set are given in Table I. The procedure followed to establish a hydrogen basis set is somewhat more complicated, due to the requirement that the H_2 molecule have the correct dissociation energy. The hydrogen basis set was determined by Dean Liskow who took the 5s1p basis set of Huzinaga,[19] contracted to 3s1p and then optimized the s and p Gaussian exponent scale factors by finding the lowest CI energy. This yielded a dissociation energy of 0.168452 Hartree at an interatomic distance of 1.40 Bohr. To parallel the experimental dissociation energy the scale factors were adjusted to fit De. For an s scale factor of 1.20 and p scale factor of 0.85 the dissociation energy was found to be 0.168399 Hartree or 105.7 kcal/mole. The resulting hydrogen basis set is given in Table II. Since the Gaussian exponents were optimized to give the correct dissociation energy for a full 2-electron CI calculation, the MCSCF calculations cannot be expected to result in the correct dissociation energy. As will be seen later, this is not a serious problem since we are only interested in the Ne-H_2 potential energy of interaction. A total of 26 basis functions were used, 14 functions centered on neon, and 6 functions centered on each of the hydrogen atoms.

Configurations. In the general case, a full 2-electron CI calculation requires the consideration of 231 configurations for the present problem which includes 26 orbitals. The number 231 is the number of ways of distributing two electrons among the 21 orbitals remaining after filling the core, and is calculated from the formula

TABLE I. NEON (9s5p/5s3p) BASIS SET

Basis Function	Gaussian Exponent	Contraction Coefficient	Symmetry
1	16501.214801	.000815	1S
1	2477.76179	.006260	1S
1	566.109589	.031596	1S
1	161.628536	.116378	1S
1	53.29324	.301929	1S
2	19.488234		1S
3	7.60176		1S
4	1.632772		1S
5	.481315		1S
6	55.030482	.016995	$2P_x$
6	12.501192	.106925	$2P_x$
6	3.69786	.320808	$2P_x$
7	1.147741		$2P_x$
8	.331057		$2P_x$
9	55.030482	.016995	$2P_y$
9	12.501192	.106925	$2P_y$
9	3.69786	.320808	$2P_y$
10	1.147741		$2P_y$
11	.331057		$2P_y$
12	55.030482	.016995	$2P_z$

TABLE I. (Continued)

Basis Function	Gaussian Exponent	Contraction Coefficient	Symmetry
12	12.501192	.106925	$2P_z$
12	3.69786	.320808	$2P_z$
13	1.147741		$2P_z$
14	.331057		$2P_z$

TABLE II. HYDROGEN BASIS SET

Basis Function	Gaussian Exponent	Contraction Coefficient	Symmetry
1	48.44160	.025374	1S
1	7.28352	.189684	1S
1	1.65168	.852933	1S
2	.46238		1S
3	.14587		1S
4	.7225		$2P_x$
5	.7225		$2P_y$
6	.7225		$2P_z$

$$\sum_{i=1}^{N} i = N(N + 1)/2 \tag{37}$$

where N = 21. The number of configurations that must be included, and thus the size of the matrix to be diagonalized, may be reduced through symmetry considerations. For a collinear arrangement of atoms, the system of atoms belongs to the $C_{\infty v}$ point group, and for a perpendicular arrangement the point group is C_{2v}.[20]

In the C_{2v} case 13 orbitals transform as A_1 symmetry, 1 as A_2 symmetry, 4 as B_1 symmetry, and 8 orbitals transform as B_2 symmetry; and the core may be written $1A_1^2\ 2A_1^2\ 3A_1^2\ 1B_1^2\ 1B_2^2$. Since we need only consider configurations in which the remaining two electrons occupy orbitals of the same symmetry we have the following

$4A_1 \rightarrow 13A_1$	55 configurations
$1A_2$	1 configuration
$2B_1 \rightarrow 4B_1$	6 configurations
$2B_2 \rightarrow 8B_2$	28 configurations

for a total of 90 configurations. For the 2-configuration MCSCF calculation the two configurations used are

$$1A_1^2\ 2A_1^2\ 3A_1^2\ 1B_1^2\ 1B_2^2\ 4A_1^2 \tag{38}$$

$$1A_1^2\ 2A_1^2\ 3A_1^2\ 1B_1^2\ 1B_2^2\ 2B_2^2$$

For the collinear case there are 16 orbitals of σ symmetry, 5 of π_x symmetry, and 5 of π_y symmetry. The core may be written $1\sigma^2\ 2\sigma^2\ 3\sigma^2\ 1\pi_x^2\ 1\pi_y^2$. Accordingly, the configurations are

$4\sigma \rightarrow 16\sigma$	91 configurations
$2\pi_x \rightarrow 5\pi_x$	10 configurations
$2\pi_y \quad 5\pi_y$	10 configurations

for a total of 111 configurations. For the 2-configuration MCSCF calculation the two configurations considered in the collinear case are

$$1\sigma^2\ 2\sigma^2\ 3\sigma^2\ 1\pi_x^2\ 1\pi_y^2\ 4\sigma^2$$

$$1\sigma^2\ 2\sigma^2\ 3\sigma^2\ 1\pi_x^2\ 1\pi_y^2\ 5\sigma^2$$

Computer Programs. The MCSCF calculations were carried out using the computer program package POLYATOM. The integrals used for these calculations were saved as either disk files or as magnetic tape files for the CI calculations. Orbitals from the MCSCF calculations were used with program CIMOL for the CI calculations. Both computer programs, POLYATOM and CIMOL, were obtained from Henry F. Schaefer. Calculations were carried out using the Lawrence Berkeley Laboratory CDC 7600 computer.

C. Results of Calculations

The results of the Ne-H-H potential energy surface calculations are summarized in Table III. The coordinate system for representing points on the surface was previously presented as Fig. 2. The two values of θ at which points were calculated are 0° and 90° for the collinear and perpendicular bisector geometries, respectively. No CI calculations were made for θ = 90° due to difficulties encountered in interfacing the integrals, calculated using the POLYATOM program, to the program CIMOL. Energies in Table III are given in Hartrees, and distances are in Bohrs. V_{MCSCF} and V_{CI} are the total energies obtained by the two respective methods.

TABLE III. RESULTS OF POTENTIAL ENERGY SURFACE CALCULATIONS, ATOMIC UNITS

Θ	R	X	V_{MCSCF}	V'_{MCSCF}	V_{CI}	V'_{CI}	$V'_{CI}-V'_{MCSCF}$	%
0	0.8	2.5	-129.36975	.14734	-129.39333	.14592	-.00142	0.97
0	0.8	3.0	-129.46265	.05586	-129.48623	.05302	-.00284	5.36
0	0.8	3.5	-129.49721	.01988	-129.52072	.01853	-.00135	7.29
0	0.8	4.0	-129.50971	.00738	-129.53313	.00612	-.00126	20.58
0	0.8	6.0	-129.51722	-.00013	-129.53938	-.00013	.00000	0.00
0	1.1	2.5	-129.47985	.17074	-129.50334	.16713	-.00361	2.16
0	1.1	3.0	-129.58100	.06959	-129.60610	.06437	-.00522	8.11
0	1.1	3.5	-129.62684	.02375	-129.64672	.02375	.00000	0.00
0	1.1	4.0	-129.64228	.00831	-129.66212	.00835	.00004	0.48
0	1.1	6.0	-129.65068	-.00009	-129.67056	-.00009	.00000	0.00
0	1.4	2.5	-129.48243	.19580	-129.50552	.19015	-.00585	3.08
0	1.4	3.0	-129.59194	.08629	-129.61831	.07736	-.00893	11.54
0	1.4	3.5	-129.64782	.03039	-129.66544	.03021	-.00018	0.60
0	1.4	4.0	-129.66695	.01126	-129.68441	.01124	-.00002	0.18
0	1.4	6.0	-129.67825	-.00004	-129.69569	-.00004	.00000	0.00

TABLE III. (Continued)

Θ	R	X	V_{MCSCF}	V'_{MCSCF}	V_{CI}	V'_{CI}	$V'_{CI}-V'_{MCSCF}$	%
0	1.7	2.5	-129.44416	.22483	-129.46612	.21773	-.00710	3.26
0	1.7	3.0	-129.56456	.10443	-129.59164	.09221	-.01222	13.25
0	1.7	3.5	-129.61558	.05341	-129.64554	.03831	-.01510	39.41
0	1.7	4.0	-129.63765	.03134	-129.66876	.01509	-.01625	107.69
0	1.7	6.0	-129.66893	.00006	-129.68379	.00006	.00000	0.00
0	2.0	2.5	-129.38223	.26492	-129.40305	.25629	-.00863	3.36
0	2.0	3.0	-129.52276	.12439	-129.54993	.10941	-.01498	13.69
0	2.0	3.5	-129.57907	.06808	-129.61132	.04802	-.02006	41.77
0	2.0	4.0	-129.60482	.04233	-129.63940	.01994	-.02239	112.28
0	2.0	6.0	-129.64696	.00019	-129.65915	.00019	.00000	0.00
0	3.0	3.0	-129.34044	.23346	-129.36475	.21363	-.01983	9.28
0	3.0	3.5	-129.44020	.13370	-129.47745	.10093	-.03277	32.46
0	3.0	4.0	-129.47829	.09561	-129.52918	.04920	-.04641	94.32
0	3.0	4.5	-129.55172	.02218	-129.55648	.02190	-.00028	1.27
0	3.0	5.0	-129.56471	.00919	-129.56928	.00910	-.00009	0.98
0	3.0	6.0	-129.57262	.00128	-129.57711	.00127	-.00001	0.78

TABLE III. (Continued)

Θ	R	X	V_{MCSCF}	V'_{MCSCF}	V_{CI}	V'_{CI}	$V'_{CI}-V'_{MCSCF}$	%
0	4.0	3.5	-129.28293	.25573	-129.31402	.22553	-.03020	13.39
0	4.0	4.0	-129.36637	.17229	-129.42273	.11682	-.05547	47.48
0	4.0	4.5	-129.48125	.05741	-129.48258	.05697	-.00044	0.77
0	4.0	5.0	-129.51286	.02580	-129.51388	.02567	-.00013	0.50
0	4.0	5.5	-129.52775	.01091	-129.52868	.01087	-.00004	0.36
0	4.0	6.0	-129.53429	.00437	-129.53520	.00435	-.00002	0.45
0	5.0	4.0	-129.23230	.29621	-129.27227	.25638	-.03983	15.53
0	5.0	4.5	-129.39726	.13125	-129.39797	.13068	-.00057	0.43
0	5.0	5.0	-129.46602	.06249	-129.46626	.06239	-.00010	0.16
0	5.0	5.5	-129.50067	.02784	-129.50084	.02781	-.00003	0.10
0	5.0	6.0	-129.51671	.01180	-129.51686	.01179	-.00001	0.08

TABLE III. (Continued)

Θ	R	X	V_{MCSCF}	V'_{MCSCF}
90	0.8	3.0	-129.47120	.04589
90	0.8	3.5	-129.50606	.01103
90	0.8	4.0	-129.51363	.00346
90	1.1	3.0	-129.60615	.04444
90	1.1	3.5	-129.63863	.01196
90	1.1	4.0	-129.64660	.00399
90	1.4	2.5	-129.37819	.30001
90	1.4	3.0	-129.64076	.03744
90	1.4	3.5	-129.66570	.01250
90	1.4	4.0	-129.67366	.00454
90	1.7	2.5	-129.52825	.14074
90	1.7	3.0	-129.63324	.03575
90	1.7	3.5	-129.65558	.01341
90	1.7	4.0	-129.66377	.00522

TABLE III. (Continued)

Θ	R	X	V_{MCSCF}	V'_{MCSCF}
90	2.0	2.5	-129.53945	.10770
90	2.0	3.0	-129.61177	.03538
90	2.0	3.5	-129.63276	.01439
90	2.0	4.0	-129.64127	.00588
90	3.0	2.5	-129.50580	.06810
90	3.0	3.5	-129.55928	.01462
90	3.0	4.0	-129.56744	.00646

For each value of the hydrogen internuclear separation R, a calculation was made with the Ne atom held at an essentially infinite distance, X = 100. This facilitated the separation of the Ne-H-H potential energy into two parts, the H_2 potential energy and the Ne-H_2 potential energy of interaction. The H_2 potential energy is well known, both from theoretical calculations and spectroscopic studies. Of interest here is the Ne-H_2 interaction energy V', defined by

$$V'(X,R,\theta) = V(X,R,\theta) - V(\infty,R,\theta) \tag{40}$$

The values of V'_{MCSCF} and V'_{CI} are provided in Table III. Also provided are the differences, $V'_{CI} - V'_{MCSCF}$, and percent differences.

D. Fit of the Ne-H_2 Potential Energy of Interaction to an Analytic Form

Figure 3 presents plots of $\ell n V'_{CI}(X,R,0°)$ against R for the various values of X. The linearity in these plots indicates that for the collinear geometry the potential energy of interaction V'(X,R,0°) may be represented by a function of the form

$$V'(X,R,0°) = A'(X) \exp[\alpha(X)\ R] \tag{41}$$

where $\alpha(X)$ is the slope of the line and A'(X) is the intercept. The slopes and intercepts were determined from least squares fits to the calculated points for X = 2.5, 3.0, 3.5 and 4.0. A fit of $\alpha(x)$ to a second order polynomial in X of the form

$$\alpha(X) = a + bX + cX^2 \tag{42}$$

yielded the results a = -0.74079, b = 0.60491 and c = -0.04930. The fit of this function to the four values of $\alpha(X)$ is shown in Fig. 4.

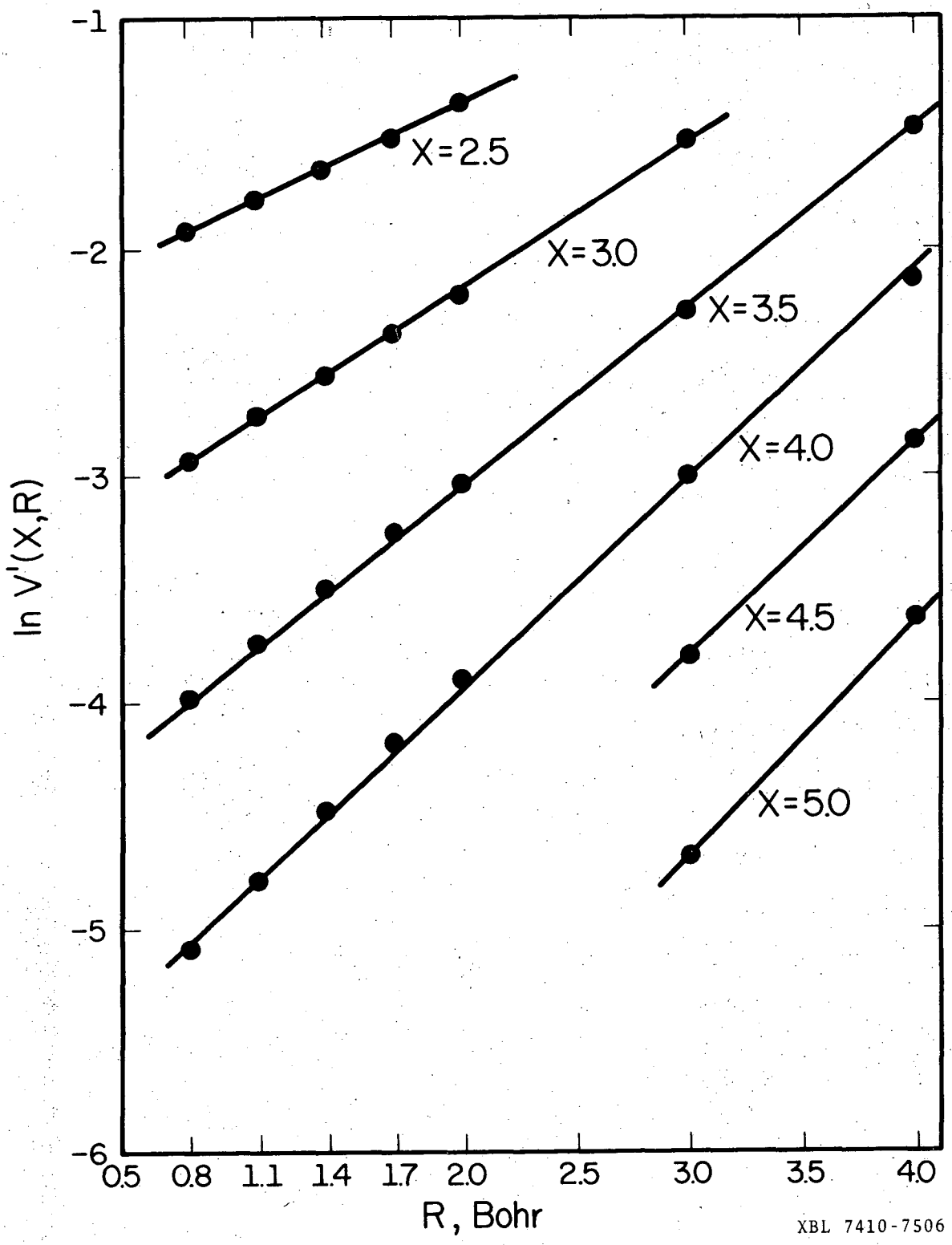

Fig. 3. Plots of V'(X,R) vs. R for fixed values of X and $\theta = 0°$. The linearity of these plots suggests one way of fitting the collinear surface.

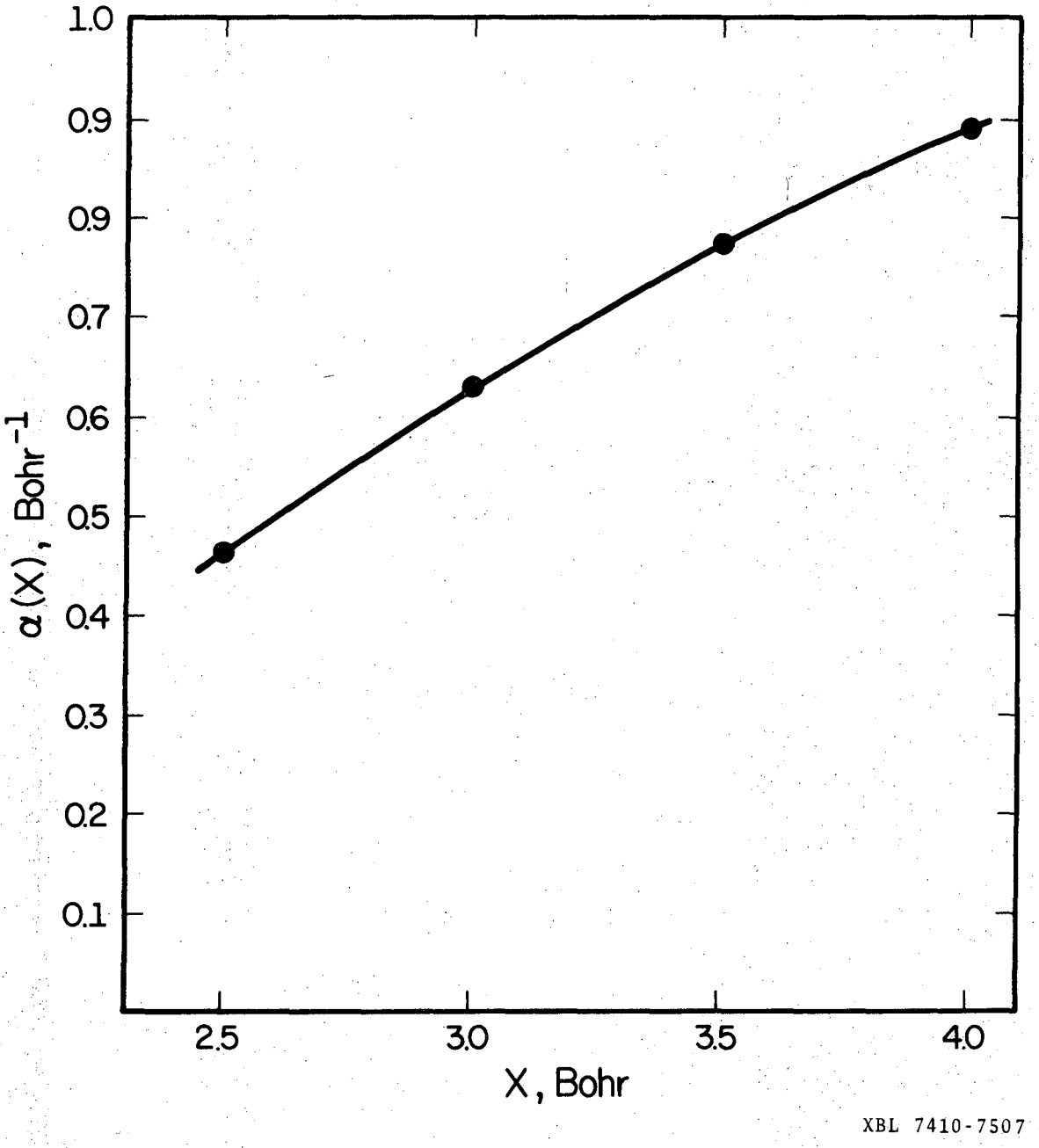

Fig. 4. Comparison of $\alpha(X)$ of equation 42 with the slopes of the lines of Fig. 3 for X = 2.5, 3.0, 3.5, and 4.0.

For the intercepts, a plot of ℓnA(X) against X (Fig. 5) gave a linear plot with slope -2.2909 and intercept 3.4267. The linearity of this plot is to be expected since in the limit as R goes to zero the H_2 molecule becomes a He atom, and the interaction between the He and Ne atoms would be expected to be purely repulsive, varying as $e^{-\beta X}$. Combining these results, we have for the Ne-H_2 potential energy of interaction for the collinear geometry

$$V'(X,R,0°) = \exp[A + BX + CR + DXR + EX^2R] \tag{43}$$

where

$$A = 3.4267,\ B = -2.2909,\ C = -0.74079,\ D = 0.60491,\ E = -0.04930 \tag{44}$$

The variance of the fit can be lowered somewhat by considering the simultaneous variation of all five parameters. A general least squares fitting program, LSQMIN, obtained from the Lawrence Berkeley Laboratory Computing Center was used to find a new set of parameters, resulting in a reduction of the variance by about a factor of three. The "initial guess" for this calculation was the set of parameters 44. The new parameters thus obtained are

$$A = 3.0450,\ B = -2.1583,\ C = -0.46568,\ D = 0.47356,\ E = -0.03633 \tag{45}$$

The possibility of obtaining an even better fit by including the term FXR^2 inside the exponential function of 43 was also investigated. The parameters obtained for this six parameter fit are given by Equation (46).

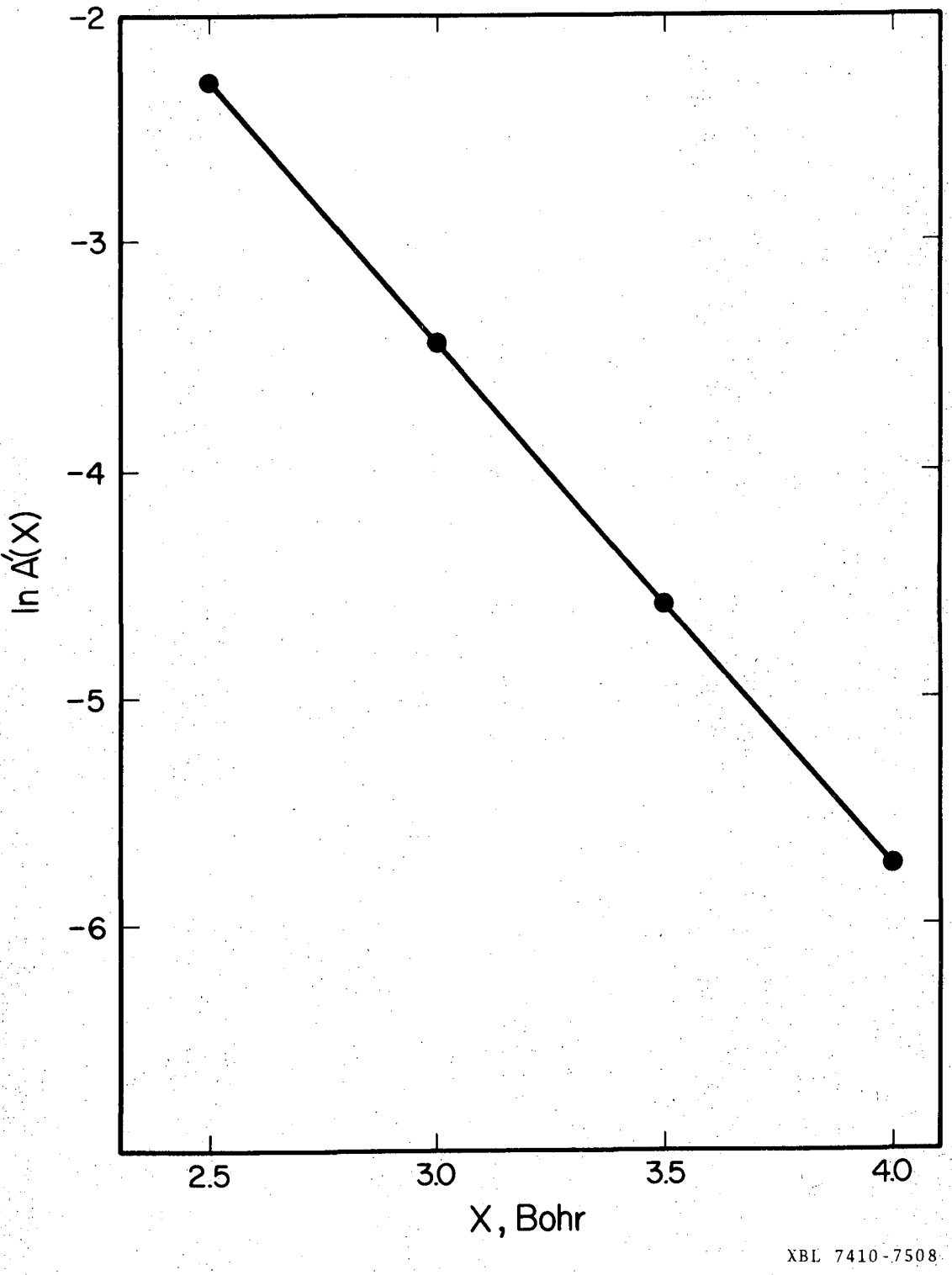

Fig. 5. Plot of the $\log_e$ of the intercept, A', of Fig. 3 is seen to be linear with X.

$$A = 3.4424,\ B = -2.3223,\ C = -0.73964,\ D = 0.62100, \qquad (46)$$

$$E = -0.04568,\ F = -0.005782$$

This resulted in the best fit to the calculated points on the collinear potential energy surface.

An optimized set of parameters was also obtained for the so called "dumbbell potential". This is the empirical form that has so often been used in vibrational energy transfer theory,[21] and has been used in Keck's phase space theory of dissociation and atom recombination.[22] For this model of the interaction potential one assumes that there is a repulsive term of the form $Ae^{-\beta r}$ between the inert gas atom and each of the two atoms of the diatomic molecule. Here r is simply the distance between the inert gas atom Ne and the atom of interest. For a homonuclear diatomic molecule, β is the same for each atom so that the total interaction potential may be written

$$V' = Ae^{-\beta r_A} + Ae^{-\beta r_B} \qquad (47)$$

where the A and B subscripts on r refer to the two different hydrogen atoms. For the collinear case we may replace r_A and r_B by $X - \frac{1}{2} R$ and $X + \frac{1}{2} R$, respectively. We then have for the interaction potential the expression

$$V' = Ae^{-\beta X}[e^{1/2\ \beta R} + e^{-1/2\ \beta R}] \qquad (48)$$

The least squares parameters obtained for a fit to this form of the interaction potential are

$$A = 2.2828,\ \beta = 1.500 \qquad (49)$$

This form of the interaction potential is desirable since only two fitting parameters are required, and because Equation (47) applies to all possible arrangements of the atoms rather than only the collinear arrangement. The variance for the fit was about an order of magnitude larger than that of those fits previously described, however.

The dumbbell potential was also found to be inadequate for the He-H_2 interaction potential by Gordon and Secrest.[23] Dimpfl[24] has suggested that this form for the interaction potential might be improved upon by including an attractive term centered at the diatomic molecule center of mass. For the collinear case the improved dumbbell interaction potential suggested by Dimpfl has the form

$$V' = Ae^{-\beta X}[e^{-\beta R/2} + e^{\beta R/2}] + Be^{-\gamma X} \tag{50}$$

The least squares parameters obtained for this four parameter fit are

$$A = 1.5972,\ \beta = 1.183,\ B = -0.11137,\ \gamma = 0.3235 \tag{51}$$

Increasing the number of parameters from two to four did not substantially improve the dumbbell form of the interaction potential, however. In Table IV a comparison is made between the actual points on the collinear surface and those calculated from each of the analytic fits described. The variance for each fit is also given in Table IV.

For three-dimensional trajectory calculations it is necessary to have an analytic form of the potential energy for all possible arrangements of the atoms. Thus in the present case it is necessary to be able to represent the potential energy for the collinear geometry, the perpendicular bisector geometry, and all angles in between. Since no calculations were made at angles other than 0° and 90° it was necessary

Table IV. Analytic Fits to the Collinear Surface*

X	R	$V_c'I$	Fit 44	Fit 45	Fit 46	Fit 49	Fit 51
2.5	0.8	145.92	145.17	141.85	142.17	127.35	135.19
3.0	0.8	53.02	52.77	53.79	51.52	60.16	60.08
3.5	0.8	18.53	18.81	20.10	18.33	28.42	20.71
4.0	0.8	6.12	6.57	7.40	6.40	13.43	0.79
2.5	1.1	167.13	166.82	164.37	165.17	146.11	152.64
3.0	1.1	64.37	63.75	64.94	63.16	69.02	69.74
3.5	1.1	27.75	23.71	25.15	23.55	32.61	26.05
4.0	1.1	8.35	8.58	9.55	8.57	15.40	3.75
2.5	1.4	190.15	191.70	190.46	191.40	172.28	176.48
3.0	1.4	77.36	77.02	78.40	77.20	81.39	82.93
3.5	1.4	30.23	29.90	31.47	30.16	30.21	33.36
4.0	1.4	11.24	11.21	12.31	11.41	18.16	7.79
2.5	1.7	217.73	220.28	220.69	221.22	207.21	207.46
3.0	1.7	92.21	93.05	94.66	94.06	97.89	100.08
3.5	1.7	38.31	37.69	39.37	38.47	46.25	42.85
4.0	1.7	15.09	14.64	15.87	15.14	21.85	13.04
2.5	2.0	256.29	253.14	255.73	255.01	252.68	246.56
3.0	2.0	109.41	112.42	114.28	114.25	119.37	121.71
3.5	2.0	48.02	47.52	49.25	48.90	56.39	54.82
4.0	2.0	19.94	19.12	20.47	20.00	26.64	19.67
3.0	3.0	213.63	211.13	214.14	213.55	243.36	236.35
3.5	3.0	100.93	102.90	103.91	105.94	114.97	118.26

Table IV. (cont'd.)

X	R	V_cI	Fit 44	Fit 45	Fit 46	Fit 49	Fit 51
4.0	3.0	49.20	46.57	47.75	49.07	54.31	54.78
4.5	3.0	21.90	19.58	20.78	21.23	25.66	21.25
5.0	3.0	9.10	7.64	8.56	8.57	12.12	4.04
3.5	4.0	225.53	222.78	219.25	220.41	241.29	237.25
4.0	4.0	116.82	113.42	111.41	115.00	113.99	120.64
4.5	4.0	56.97	52.32	52.64	54.76	53.85	57.69
5.0	4.0	25.67	21.87	23.13	23.80	25.44	24.21
5.5	4.0	10.87	8.28	9.45	9.44	12.02	6.83
4.0	5.0	256.38	276.19	259.92	257.31	240.82	240.96
4.5	5.0	130.68	139.81	133.35	134.12	113.77	124.28
5.0	5.0	62.39	62.57	62.48	62.36	53.75	61.06
5.5	5.0	27.81	24.75	26.73	25.87	25.39	27.23
6.0	5.0	11.79	8.66	10.44	9.57	12.00	9.48
Variance			6.14×10^{-4}	2.10×10^{-4}	1.51×10^{-4}	4.08×10^{-3}	2.64×10^{-3}

*Energies are in millihartrees, distances in Bohr.

to rely on the previous work of Roberts,[25] Krauss and Mies[26] and Gordon and Secrest[23] for the He-H_2 potential energy to arrive at a reasonable way of representing the angular part of the potential energy surface. Accordingly, the interaction potential was assumed to be separable into two parts,

$$V'(X,R,\theta) = V_1'(X,R)\ V_2'(R,\theta) \tag{52}$$

one part depending only on the variables X and R and one part depending only on the variables R and θ. The latter part, $V_2'(R,\theta)$, was represented by the following function.

$$V_2'(R,\theta) = 1 + \gamma P_2(\cos\theta) + \delta P_2(\cos\theta)\ R \tag{53}$$

Here, P_2 is a Legendre polynomial so that

$$P_2(\cos\theta) = \frac{3}{2}\cos^2\theta - \frac{1}{2} \tag{54}$$

The coefficients γ and δ were determined by considering the ratio of the potential energy of interaction for the perpendicular bisector geometry $V'(X,R,90°)$ to that for the collinear geometry $V'(X,R,0°)$, which is given by

$$\frac{V'(X,R,90°)}{V'(X,R,0°)} = \frac{1 - 1/2\,\gamma - 1/2\ \delta R}{1 + \gamma + \delta R} \tag{55}$$

The following values for γ and δ fit this ratio exactly for X = 4.0 and the two extreme values of R = 0.8 and R = 3.0.

$$\gamma = 0.05623 \text{ and } \delta = 0.4399 \tag{56}$$

It was necessary, unfortunately, to use the MCSCF results for $V'(X,R,90°)$. In the limit of no correlation energy of interaction (X large; R small for $\theta = 0°$, R large for $\theta = 90°$) the MCSCF and CI results for the interaction energy must be identical. It can be seen in Table III that this is certainly the case for the collinear geometry; the values of V'_{CI} and V'_{MCSCF} being nearly the same except when the Ne atom is very near one of the hydrogen atoms (X small, R large). For this reason the coefficients γ and δ were determined at the largest value of X for which there was still a sufficient interaction, so that $V'_{CI}(X,R,0°)$ and $V'_{MCSCF}(X,R,90°)$ contained a minimum amount of correlation energy. The ratio of interaction energies, Equation (55), does not vary with changes in X. Table V compares all such ratios with those calculated from this equation. The ratios listed in Table V are not all constant over changes in X. However, the variation that is present is consistent with the fact that V'_{MCSCF} does not include as much of the correlation energy at small values of X as does V'_{CI}.

For the calculation of 3-D trajectories, described in the next section, the form of the interaction potential used was

$$V'(X,R,\theta) = \frac{1 + \gamma P_2(\cos\theta) + \delta P_2(\cos\theta)}{1 + \gamma + \delta}\,\frac{R}{R}\,V'(X,R,0°) \qquad (57)$$

where $V'(X,R,0°)$ is given by Equation (43). For the potential energy of the hydrogen molecule a Morse potential was used. The total potential energy is then given by

$$V(X,R,\theta) = D_e[1 - \exp(-1.0274r)]^2 + V'(X,R,\theta) \qquad (58)$$

Table V. Values of $\frac{V'(X,R,90°)}{V'(X,R,0°)}$

X \ R	0.8	1.1	1.4	1.7	2.0	3.0
3.0	0.866	0.690	0.484	0.388	0.323	
3.5	0.595	0.504	0.414	0.350	0.300	0.145
4.0	0.565	0.478	0.404	0.346	0.295	0.131
Fit to Eq. 55	0.565	0.474	0.397	0.331	0.275	0.131

where D_e is the dissociation energy, and

$$r = R - R_e$$

where R_e is the equilibrium internuclear distance, 1.40 Bohr. Perspective drawings of this potential energy surface for θ = 0,45 and 90° are provided in Figs. 6a-c.

Fig. 6a. Perspective drawing of the total potential energy surface for $\theta = 0°$. The value of R ranges from 0.5 Bohr on the left to 5.4 Bohr on the right. X varies from 8.4 Bohr nearest the viewer to 2.5 Bohr at the farthest distance from the viewer. A collinear trajectory may be visualized as a frictionless marble rolling on this surface. Beginning in the trough nearest the viewer, the marble rolls up and down the walls of the trough and toward the repulsive wall at the end of the trough. If the velocity along the trough is sufficient for the marble to climb above the dissociation limit and the phase of vibration is favorable, the marble will roll onto the plane on the far right which corresponds to dissociation. Otherwise, the marble rolls back into the trough with greater or lesser vibrational energy, the balance of energy going into the velocity of the marble along the trough.

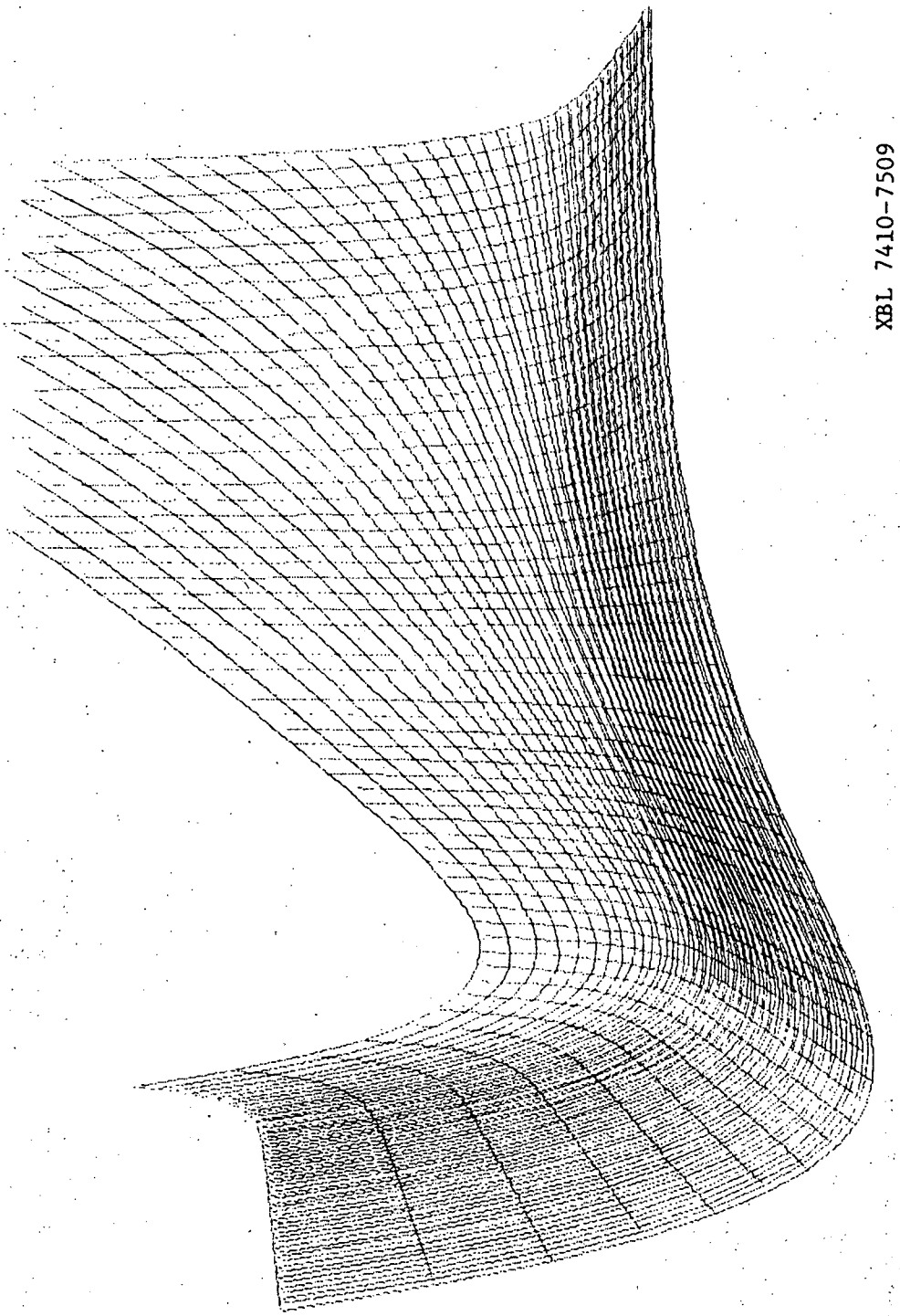

XBL 7410-7509

Fig. 6a

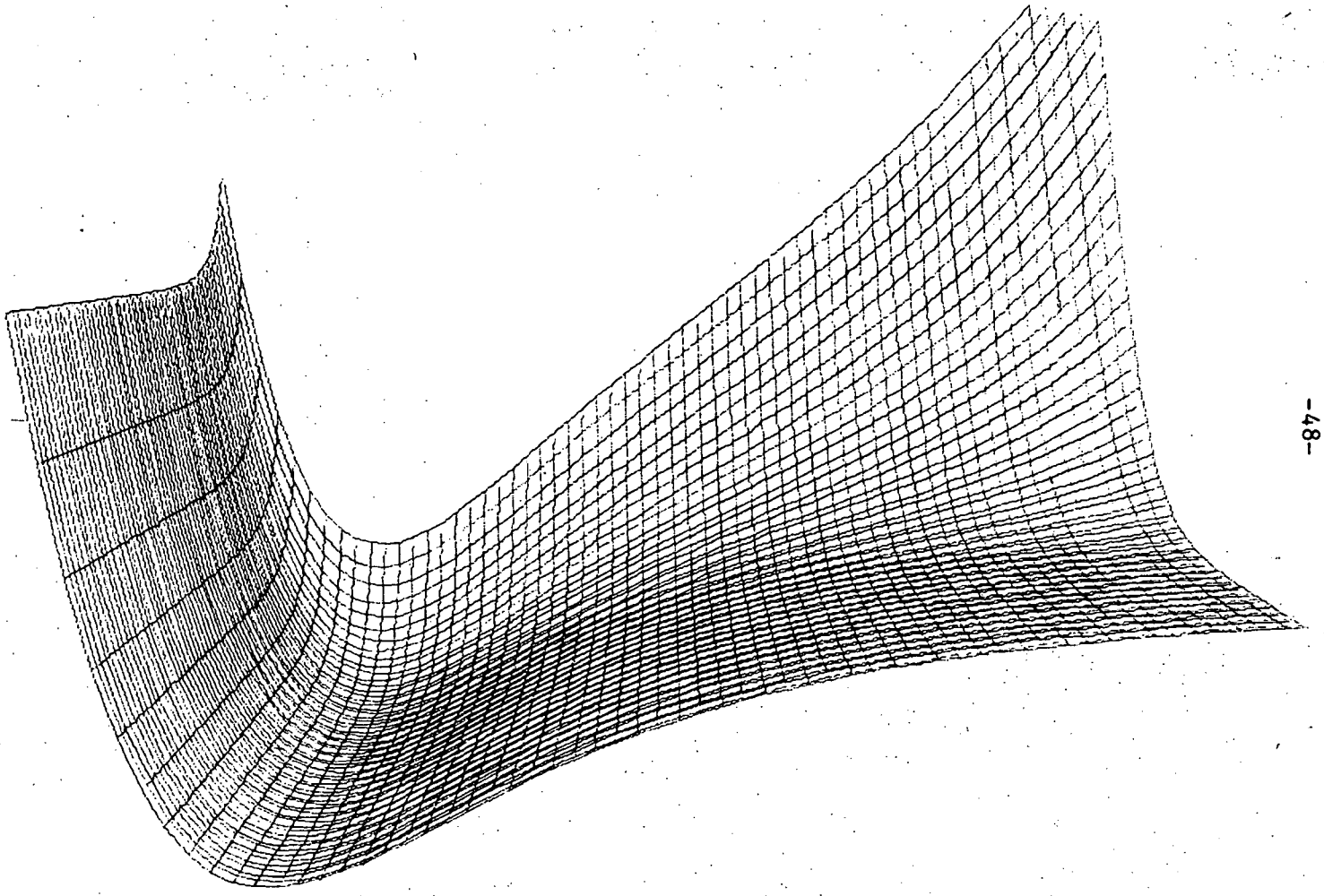

XBL 7410-7510

Fig. 6b. Perspective drawing of the total potential energy surface for $\theta = 45°$. Coordinates are the same as those in Fig. 6a.

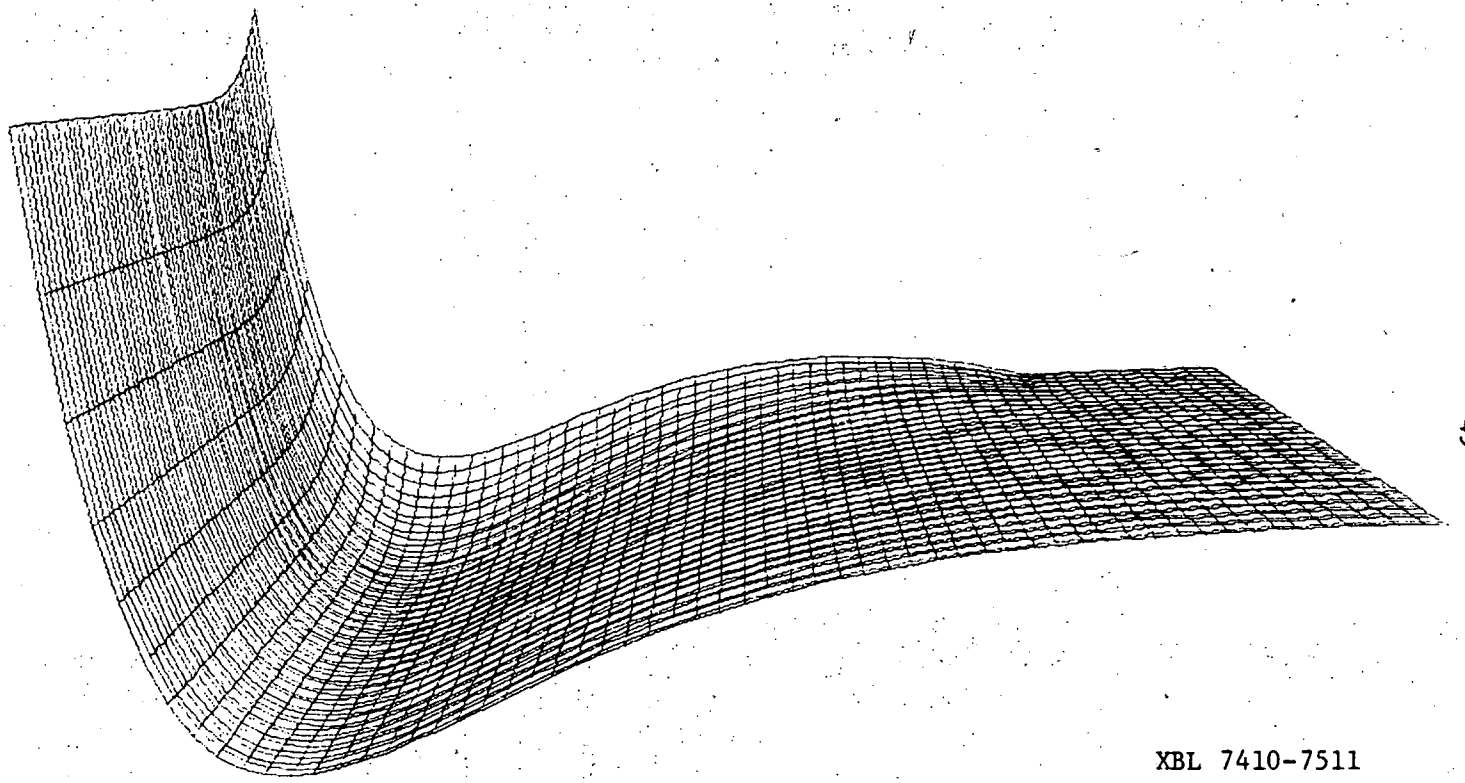

XBL 7410-7511

Fig. 6c. Perspective drawing of the total potential energy surface for $\theta = 90°$. Coordinates are the same as those in Fig. 6a.

III. MONTE CARLO CLASSICAL TRAJECTORY CALCULATIONS

A. Theory

Having obtained a potential energy surface for the system of atoms Ne-H-H, we may now consider the calculation of trajectories on this surface to obtain cross sections and rate constants for the dissociation process. Ideally, one would solve the time dependent nuclear Schrödinger equation, which amounts to the calculation of quantum-mechanical trajectories. For the large number of trajectories required, such a procedure is impractical, however. Furthermore, semi-classical theory is not yet sufficiently advanced for application to this problem. The calculation of classical trajectories is relatively simple, but still time consuming and therefore expensive.

Classical trajectories have been used to describe bimolecular exchange reactions, the best known study being that of Karplus, Porter and Sharma[9] for the reaction

$$H + H_2 \rightarrow H_2 + H \tag{60}$$

Classical trajectories have also been used extensively to study vibrational energy transfer processes.[27] One might expect classical trajectory calculations to better describe the dissociation process than either of these two processes since in the case of dissociation the final states lie in a continuum where classical mechanics certainly applies. In the cases of exchange reactions and vibrational energy transfer processes the final states are quantized. On the other hand, the much larger activation energy for the dissociation process limits the reaction to energies near threshold even at shock tube temperatures,

and it is in this region where classical mechanics and quantum mechanics differ the most. Classical trajectories result in reaction cross sections that are too low near threshold. The justification for the use of classical trajectories in the present case is simply that such calculations are the next logical step in understanding the dissociation process from a theoretical point of view. No doubt, in the future the use of more accurate semi-classical trajectories will be made possible.

We begin by considering a system of three atoms with masses m_A, m_B and m_C with Cartesian coordinates (q_1, q_2, q_3), (q_4, q_5, q_6) and (q_7, q_8, q_9) and conjugate momenta (p_1, p_2, p_3), (p_4, p_5, p_6) and (p_7, p_8, p_9), respectively. The Hamiltonian function H for such a system has the form

$$H = \frac{1}{2m_A}\sum_{i=1}^{3} p_i^2 + \frac{1}{2m_B}\sum_{i=4}^{6} p_i^2 + \frac{1}{2m_C}\sum_{i=7}^{9} p_i^2 + V(q_1, q_2, \cdots q_9) \qquad (61)$$

where $V(q_1, q_2, \cdots q_9)$ is the potential energy. To simplify we introduce the generalized coordinate Q_j defined by

$$\begin{aligned} Q_j &= q_{j+6} - q_{j+3} \\ Q_{j+3} &= q_j - (m_B q_{j+1} + m_C q_{j+6})/(m_B+m_C) \\ Q_{j+6} &= (1/M)(m_A q_j + m_B q_{j+3} + m_C q_{j+6}) \qquad j = 1,2,3 \end{aligned} \qquad (62)$$

where $M = m_A + m_B + m_C$. For this set of coordinates (Q_1, Q_2, Q_3) are the Cartesian coordinates of Particle C with respect to Particle B as the origin, (Q_4, Q_5, Q_6) are the Cartesian coordinates of Particle A with respect to the center of mass of the BC pair as origin, and

(Q_7, Q_8, Q_9) are the Cartesian coordinates of the center of mass of the entire three-particle system. The equations of the inverse transformation are

$$\begin{aligned} q_i &= [(m_B+m_C)/M]Q_{i+3} + Q_{i+6} \\ q_{i+3} &= -[m_C/(m_B+m_C)]\, Q_i - (m_A/M)Q_{i+3} + Q_{i+6} \\ q_{i+6} &= [m_B/(m_B+m_C)]\, Q_i - (m_A/M)Q_{i+3} + Q_{i+6} \qquad i = 1,2,3 \end{aligned} \tag{63}$$

If P_j are the momenta conjugate to Q_j, then

$$p_i = \sum_j P_j\, (\partial Q_j/\partial q_i) \tag{64}$$

and from equations 62 and 64 we find

$$\begin{aligned} p_i &= m_A\, \dot{q}_i = P_{i+3} + (m_A/M)P_{i+6} \\ P_{i+3} &= m_B \dot{q}_{i+3} = -P_i - [m_B/(m_B+m_C)]P_{i+3} + (m_B/M)P_{i+6} \end{aligned} \tag{65}$$

In terms of the new variables Q_i and P_i, the Hamiltonian may be written

$$H = \frac{1}{2\mu_{BC}} \sum_{j=1}^{3} P_j^{\,2} + \frac{1}{2\mu_{A,BC}} \sum_{j=4}^{6} P_j^{\,2} + \frac{1}{2M} \sum_{j=7}^{9} P_j^{\,2} + V(Q_1, \cdots, Q_6) \tag{66}$$

where

$$\mu_{BC} = \frac{m_B m_C}{m_B+m_C} \quad \text{and} \quad \mu_{A,BC} = \frac{m_A(m_B+m_C)}{m_A+m_B+m_C} \tag{67}$$

and the potential energy $V(Q_1, \cdots, Q_6)$ is written with explicit neglect of the center of mass coordinates.

Hamilton's equations for the general dynamical coordinates Q_j and P_j are

$$\dot{Q}_j = \frac{dQ_j}{dt} = \frac{-\partial H}{\partial P_j} \tag{68}$$

$$\dot{P}_j = \frac{dP_j}{dt} = -\frac{\partial H}{\partial Q_j} = -\frac{\partial V}{\partial Q_j} \tag{69}$$

The 18 differential equations describing the motion of the three particles are then

$$\begin{aligned}
\dot{Q}_j &= (1/\mu_{BC})P_j \qquad j = 1,2,3 \\
\dot{Q}_j &= (1/\mu_{A,BC})\, P_j \qquad j = 4,5,6 \\
\dot{Q}_j &= (1/M)P_j \qquad j = 7,8,9 \\
\dot{P}_j &= -\frac{\partial V}{\partial Q_j} \qquad j = 1, \cdots, 6 \\
\dot{P}_j &= 0 \qquad j = 7,8,9
\end{aligned} \tag{70}$$

Since P_7, P_8, and P_9 are constants of the motion, the term containing them may be subtracted out of the Hamiltonian to yield

$$H = \frac{1}{2\mu_{BC}} \sum_{j=1}^{3} P_j^{\,2} + \frac{1}{2\mu_{A,BC}} \sum_{j=4}^{6} P_j^{\,2} + V(Q_1, \cdots Q_6) \tag{71}$$

with 12 simultaneous differential equations to be integrated for the determination of the time variation of the Q_j and P_j.

Assignment of initial values - There are a total of 12 dynamical variables (Q_j, P_j; j = 1, 2, $\cdots$6) to be specified to define the initial state of a collision trajectory. The procedure used in specifying these variables was the same as that used by Karplus, Porter, and Sharma.[9] The method permits the randomization of the initial orientation of the molecule with respect to the Ne atom, the impact parameter b, and the vibrational phase of the molecule according to the appropriate distribution functions. In addition, the collision energy was randomized according to a Maxwellian distribution of relative velocities. Each of the randomly selected trajectories were calculated by integrating numerically the classical equations of motion, and analyzed to determine whether or not the trajectory resulted in dissociation of the diatomic molecule. From the fraction of molecules resulting in dissociation of a large number of trajectories, the reaction cross sections and rate constants for dissociation from particular vibration-rotation states of the H_2 molecule were calculated. This so-called Monte Carlo method of selecting trajectories at random results in great reduction in the number of trajectories that need be calculated.

Figure 7 describes the coordinate system used to assign initial values to the dynamical variables. The z axis is chosen as the direction of the initial relative velocity vector. As a result,

$$P_4^\circ = P_5^\circ = 0 \qquad \text{and } P_6^\circ = \mu_{A,BC}\, V_R \tag{72}$$

where V_R is the initial relative velocity. The coordinate system is oriented so that the atom A and the center of mass of BC lie in the y-z plane, so that

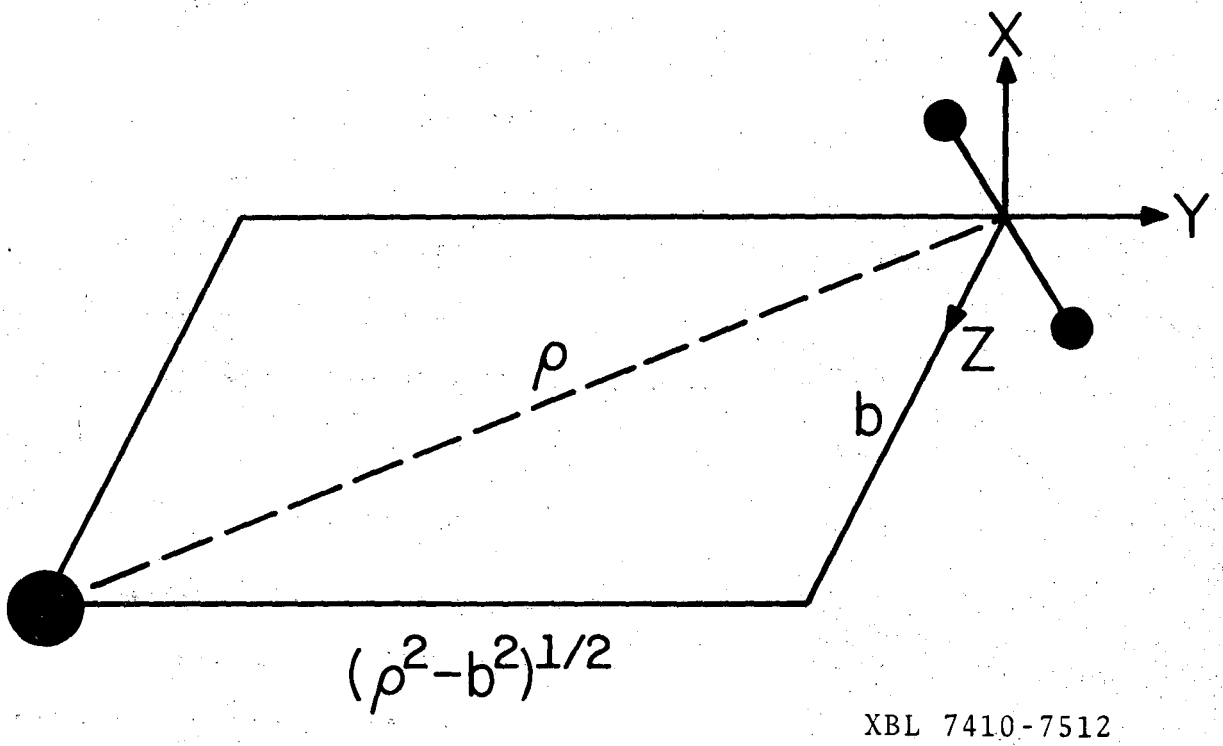

XBL 7410-7512

Fig. 7. Coordinate system for locating the Ne atom with respect to the H_2 molecule. The Ne atom moves in the Y direction in the Y-Z plane with impact parameter b.

$$Q_4^\circ = 0, \quad Q_5^\circ = b, \text{ and } Q_6^\circ = -(\rho^2-b^2)^{1/2} \tag{73}$$

where b is the impact parameter and ρ is the initial distance between A and the center of mass of BC. The value of ρ is required to be great enough that the interaction potential between A and BC is negligible.

The initial state of the H_2 molecule is determined by the six variables Q_j, P_j (j = 1, 2, 3). The orientation of the molecule is specified by the spherical coordinates R, θ, and ϕ. Recalling that Q_1, Q_2 and Q_3 are the Cartesian coordinates of atom C with respect to atom B we have then

$$Q_1^\circ = R\sin\theta\cos\phi, \; Q_2^\circ = R\sin\theta\sin\phi, \text{ and } Q_3^\circ = R\cos\theta \tag{74}$$

where R is the internuclear distance. To simplify the assignment of momenta P_1°, P_2°, and P_3°, we choose to always begin a trajectory at the left or right turning point of the molecule. This also simplifies the randomization of the vibrational phase of the molecule, as discussed below. With R equal to a turning point value, $R_\pm$, there is no momentum along the bond direction ($Q_1P_1 + Q_2P_2 + Q_3P_3 = 0$) and the total internal momentum is simply equal to the angular momentum.

$$P^2 = P_1^{\,2} + P_2^{\,2} + P_3^{\,2} = J(J+1)\hbar^2/R_\pm^2 \tag{75}$$

To specify the components P_1°, P_2°, P_3° we need only fix the angle η of the momentum vector relative to an arbitrarily chosen vector that is perpendicular to the molecular axis. If this vector is taken to be $\vec{R}\times\vec{K}$, where $\vec{R}$ points along the molecular axis and $\vec{K}$ is the unit vector in the Z direction, we have

$$P_1^\circ = -P(\sin\phi\cos\eta + \cos\phi\cos\theta\sin\eta)$$

$$P_2^\circ = P(\cos\phi\cos\eta - \sin\phi\cos\theta\sin\eta) \qquad (76)$$

$$P_3^\circ = P(\sin\theta\sin\eta)$$

Thus, the initialization of each trajectory requires assignments of values to the variables V_r, b, ρ, $R_\pm$, θ, ϕ, η, v and J. Of these variables, v and J are fixed, and the remaining variables are chosen at random from appropriate distribution functions.

Randomization of variables - Variables were in all cases randomized by the use of pseudorandom numbers generated on the computer. For this purpose subroutine RGEN, obtained from the Lawrence Berkeley Laboratory Computing Center, was used. When called, this subroutine returns a pseudorandom number in the range zero to one. The values of v and J were chosen for each set of trajectories so as to obtain rate constants and cross sections for dissociation from particular vibration-rotation levels.

The angles ϕ and η were selected from a uniform distribution between 0 and 2π by use of the two pseudorandom numbers ε_1 and ε_2, thus

$$\phi = 2\pi\varepsilon_1 \qquad \text{and} \qquad \eta = 2\pi\varepsilon_2 \qquad (77)$$

The appropriate value of θ is obtained by selecting $\cos\theta$ from a uniform distribution between -1 and +1. This requires two pseudorandom numbers, ε_3 and ε_4. The variable s is chosen to be -1 if ε_3 is less than 0.5 and +1 if ε_3 is greater than or equal to 0.5. We then have

$$\cos\theta = s\varepsilon_4 \qquad (78)$$

The random number ε_5 is used to assign a value to R, the molecule's internuclear distance, as either the left or right turning point.

$$\begin{aligned} R &= R_+ \qquad \varepsilon_5 < .5 \\ R &= R_- \qquad \varepsilon_5 \geqslant .5 \end{aligned} \tag{79}$$

The values of R_+ and R_- for a particular vibration-rotation level of the molecule may be determined by finding the two values of R that satisfy the equation

$$\frac{J(J+1)\hbar^2}{2\mu_{BC}R^2} + D_e[1-\exp(-1.0274r)]^2 = E_{vJ} \tag{80}$$

where E_{vJ} is the energy of the vibration-rotation level. For E_{vJ} the empirical formula of Stoicheff[41] was used. Equation 80 may be solved for $R_\pm$ by Newton's iterative method as described by Karplus, Porter, and Sharma.[9]

In order to obtain a randomization of the vibrational phase, the molecule was always chosen to be at a turning point as just described, and the coordinate Q_6 was chosen to lie with equal probability between the values $-(\rho_o^2-b^2)^{1/2}$ and $-(\rho_o^2-b^2)^{1/2}-1/2\ \tau_{vJ}$ (see Fig. 7). Using a sixth random number ε_6 we have for Q_6 and ρ

$$Q_6 = -(\rho^2-b^2)^{1/2} = -(\rho_o^2-b^2)^{1/2} - \frac{1}{2}\tau_{vJ}\varepsilon_6 \tag{81}$$

Here τ_{vJ} is the vibrational period of the molecule which must be calculated for each vibration-rotation level of the H_2 molecule. According to Herzberg[28] the formula for the frequency is

$$\nu_{vJ} = c[E(v+\tfrac{1}{2},J)-E(v-\tfrac{1}{2},J)] \tag{82}$$

which is the reciprocal of the period τ_{vJ}. Here c is the velocity of light in a vacuum. The method just described for randomizing the vibrational phase by randomizing the initial distance between the Ne atom and H_2 molecule in a region where there is no interaction is both simple and rigorous.

In the method described here, trajectories are sampled in what might be called "impact parameter space". For each set of trajectories a maximum value of the impact parameter is selected, b_{MAX}. Beyond this value of the impact parameter an insignificant number of trajectories will lead to reaction. The lack of inclusion of trajectories outside this maximum value is easily accounted for in the analysis of trajectory results as will be discussed later. Since the probability that a collision will be characterized by a particular value of the impact parameter is proportional to b^2, we choose b^2 at random from a uniform distribution between 0 and b_{MAX}^2 according to the pseudorandom number ε_7.

$$b^2 = b_{MAX}^2 \, \varepsilon_7 \tag{83}$$

The remaining variable to be assigned is that of V_R, the relative collision velocity. Alternatively, we may assign a value to E_R, the collision energy. The two variables are related, of course, by the equation

$$E_R = \frac{1}{2} \mu_{A,BC} \, V_R \tag{84}$$

One method is to evaluate $S_r(v, J, E_R)$, the reaction cross section, at each of several values of E_R. Integration of $S_r(v, J, E_R)$ over the appropriate energy distribution results in the rate constant for

dissociation from a particular vibration-rotation level at any temperature desired. Eliason and Hirschfelder[29] have shown that the rate constant k_{vJ} is given by

$$k_{vJ} = \left(\frac{2}{kT}\right)^{3/2} (\pi\mu_{A,BC})^{-1/2} \int_o^\infty S_r(E_R,J,v) \exp\left(-\frac{E_R}{kT}\right) E_R dE_R \qquad (85)$$

Note that for the hard-spheres condition, $S_r = \pi\sigma^2$, equation 85 results in the familiar hard-spheres collision rate constant, equation 86.

$$k^{HS} = \left(\frac{8kT}{\pi\mu_{A,BC}}\right)^{1/2} \pi\sigma^2 \qquad (86)$$

For the model with activation energy E_R^* where

$$\begin{aligned} S_r &= 0 \qquad & E_R &< E_R^* \\ S_r &= \pi\sigma^2 \qquad & E_R &\geqslant E_R^* \end{aligned} \qquad (87)$$

one obtains the result

$$k^{act} = \left(\frac{8kT}{\pi\mu_{A,BC}}\right)^{1/2} \pi\sigma^2 \left(\frac{E_R^*}{kT} + 1\right) \exp(-E_R^*/kT) \qquad (88)$$

Generally, S_r is a smoothly increasing function of the collision energy, rising from a value of zero at some threshold energy and leveling off at high energy.

The method described here is to actually evaluate S_r as a function of collision energy by determining the fraction of trajectories that result in dissociation of the diatomic molecule. For a given value of

E_R, the reaction cross-section is given by

$$S_r(E_R,J,v) \cong \pi b_{MAX}^2 \frac{N_r(E_R,J,v)}{N(E_R,J,v)} \tag{89}$$

Here N is the total number of trajectories and N_r is the number of reactive trajectories. This equation is exact in the limit of infinite N. For a finite number of trajectories the standard error s is given by

$$S = \left(\frac{N-N_r}{NN_r}\right)^{1/2} S_r(E_R,J,v) \tag{90}$$

The advantage of obtaining the cross-section as a function of energy is that all of the information necessary for the evaluation of the rate constant at any temperature is obtained. Another method is to include E_R in the collection of variables randomized by the Monte Carlo method. In this method trajectories are calculated for each particular value of the temperature desired. If only a few temperatures are desired, this method is more economical than that of first obtaining the reaction cross section. Furthermore, the activation energy is very large for the dissociation process so that even at a shock tube temperature of 10,000 K the overlap between the S_r curve with the Maxwellian distribution function occurs very near threshold where the uncertainty in the points on the S_r curve is necessarily large (too few trajectories lead to dissociation). The problem of collision energy is avoided by the method whereby collision energies are chosen at random according to the appropriate distribution function characterized by a particular temperature T. In this method we choose E_R to be greater than the

threshold value E_R^*. For energies less than E_R^* the reaction is classically (and quantum mechanically) impossible so those trajectories need not be calculated. The value of E_R was allowed to range from E_R^* to the improbably large value of E_R^* + 10 eV. In accordance with equation 84, the probability of a particular value of E_R was made proportional to $E_R \exp(-E_R/kT)$. For this purpose, a pseudorandom number ϵ_8 was used to select a value of E_R between E_R^* and E_R^* + 10 eV. A special computer routine was written to select E_R. In this method the rate constant k_{vJ} is obtained directly from the fraction of trajectories leading to dissociation, and is given by

$$k_{vJ} \cong \left(\frac{8kT}{\pi\mu_{A,BC}}\right)^{1/2} (\pi b_{MAX}^2)\left(\frac{E_R^*}{kT} + 1\right)\left[\frac{N_r(T,J,v)}{N(T,J,v)}\right] \exp\left(-\frac{E_R^*}{kT}\right) \qquad (91)$$

with standard error given by

$$S = \left[\frac{N-N_r}{NN_r}\right]^{1/2} k_{v,J} \qquad (92)$$

Note the similarity between equations 91 and 88. The factor $(E_R^*/kT + 1) \exp(-E_R^*/kT)$ in equation 91 arises from the fact that we do not sample trajectories for which $E_R < E_R^*$. From equation 91 we see that the hard-spheres collision cross section $\pi\sigma^2$ is given by

$$\pi\sigma^2 \cong (\pi b_{MAX}^2)\left(\frac{E_R^*}{kT} + 1\right)\left[\frac{N_r(T,J,v)}{N(T,J,v)}\right] \qquad (93)$$

The collision cross section is the more interesting quantity since it may be expected to be fairly temperature independent. The variation of this quantity with v and J is of primary interest to this investigation.

B. Results of Trajectory Calculations

Trajectories were calculated by integrating the classical equations of motion, equations 68 and 69. The integration was carried out by means of an Adams-Moulton fifth order integrating routine having a variable step size.[40] Typical reactive and nonreactive trajectories are illustrated in Fig. 8. Each trajectory was integrated until either X, the distance between the Ne atom and H_2 center of mass, became greater than the initial value, or until R, the H_2 internuclear distance, exceeded 10 Bohr. The value assigned to b_{MAX} varied from 0.8 to 8.0 Bohr, depending on the vibration-rotation level under consideration. Calculations were often made for several values of b_{MAX} to be certain that the cross sections not be under estimated due to too small a value of b_{MAX}. Of course, the smaller the value of b_{MAX} used, the greater is the fraction of reactive trajectories so that the statistical error is smaller. For the v = 0, J = 0 level it was necessary to reduce the maximum value of the impact parameter to 1 Bohr in order to obtain a significant fraction of reactive trajectories. On the other hand, for the v = 12, J = 0 level a value of 8 Bohr for b_{MAX} was required so that no reactive trajectories be excluded.

The results of the trajectory calculations are provided in Table VI. All of the calculations were carried out for a temperature of 10,000 K except for a few calculations for which a temperature of 6,000 K was assumed. Although the results are limited with respect to temperature variation, the indication is that over the range of temperature 6,000-10,000 K the collision cross section does not change by much.

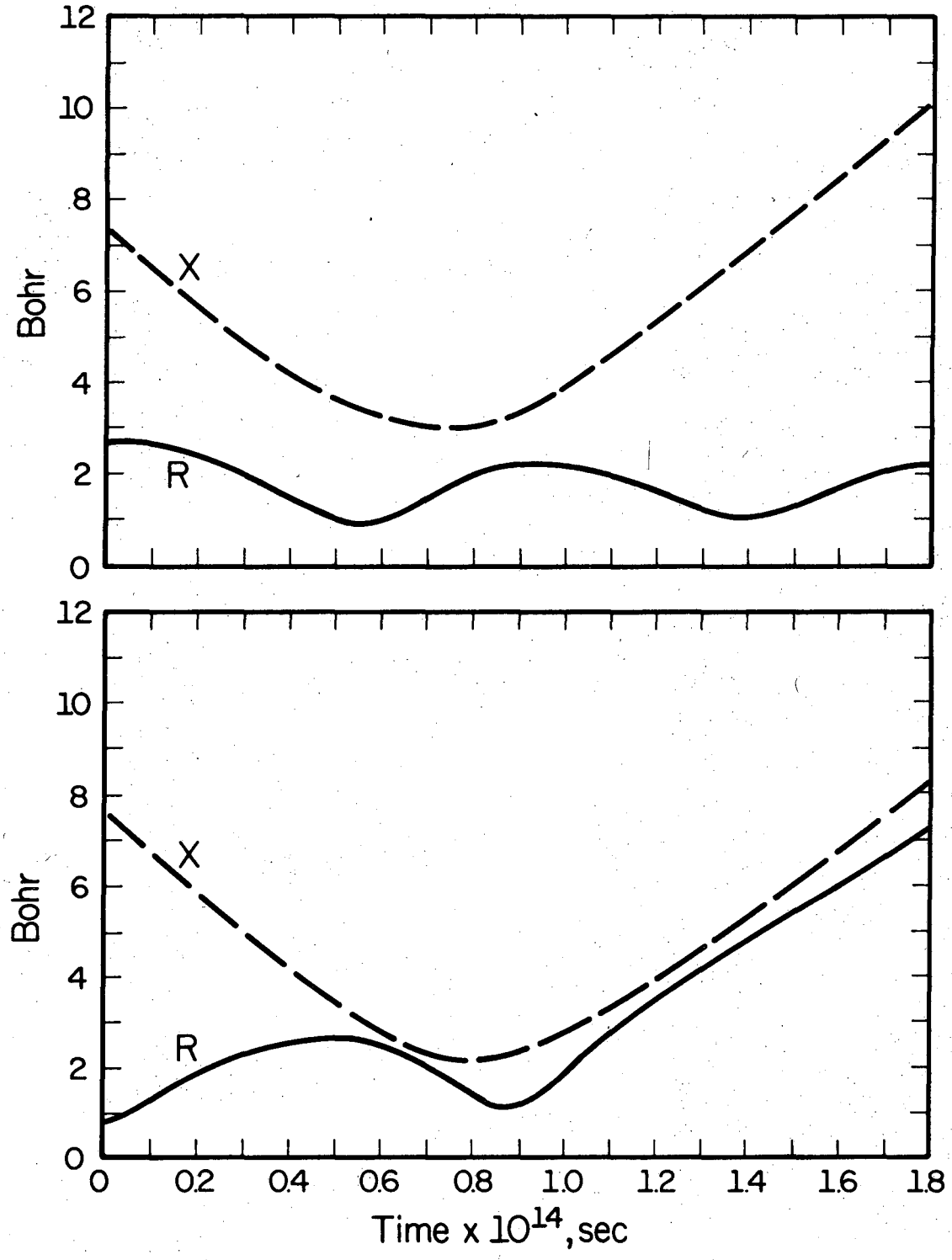

XBL 7410-7513

Fig. 8. Typical nonreactive (upper) and reactive (lower) trajectories for v = 5, J = 0.

Table VI. Results of Trajectory Calculations

v	J	b_{MAX} (Bchr)	N_r/N	$\pi\sigma^2$ (Å)	k_{vJ} (cc/molecule sec)
0	0	0.8	18/1000	0.063 ± .015	3.75×10^{-14}
0	0	1.0	16/1000	0.087 ± .022	5.20×10^{-14}
0	5	1.0	19/1000	0.099 ± .023	7.62×10^{-14}
0	10	1.0	13/1000	0.061 ± .017	8.67×10^{-14}
0	25	8.0	4/200	1.56 ± .77	1.14×10^{-10}
1	0	1.5	17/1000	0.188 ± .045	2.05×10^{-13}
2	0	2.0	9/1000	0.159 ± .053	3.04×10^{-13}
2	5	2.0	25/1000	0.423 ± .084	1.01×10^{-12}
2	10	2.0	16/1000	0.239 ± .059	9.99×10^{-13}
2	24	8.0	20/200	6.41 ± 1.36	6.08×10^{-10}
3	0	2.5	28/1000	0.693 ± .129	2.25×10^{-12}
4	0	3.0	27/1000	0.856 ± .162	4.58×10^{-12}
4	5	3.0	21/1000	0.632 ± .137	4.14×10^{-12}
4	10	3.0	31/1000	0.811 ± .143	8.73×10^{-12}
4	22	8.0	32/200	9.15 ± 1.48	9.72×10^{-10}
5	0	3.0	41/1000	1.15 ± 0.18	9.81×10^{-12}
5	0	4.0	27/1000	1.34 ± 0.26	1.15×10^{-11}
6	0	4.0	34/1000	1.48 ± 0.25	1.96×10^{-11}
6	5	4.0	16/500	1.32 ± 0.32	2.08×10^{-11}
6	10	4.0	16/500	1.12 ± 0.28	2.74×10^{-11}
6	19	8.0	20/200	6.41 ± 1.36	6.02×10^{-10}
7	0	4.0	70/1000	2.65 ± 0.12	5.26×10^{-11}

Table VI (con't.)

	u	J	b_{MAX} (Bchr)	N_r/N	$\pi\sigma^2$ ($\AA^2$)	k_{vJ} (cc/molecule sec)
	8	0	4.0	80/1000	2.61 ± 0.11	7.53×10^{-11}
	8	0	6.0	28/1000	2.06 ± 0.19	5.93×10^{-11}
*	8	0	4.0	67/1000	3.02 ± 0.36	2.79×10^{-11}
	8	5	6.0	11/300	2.51 ± 0.74	8.47×10^{-11}
	8	5	5.0	28/500	2.67 ± 0.49	8.98×10^{-11}
	8	10	5.0	36/500	2.82 ± 0.45	1.39×10^{-10}
	8	10	6.0	23/300	4.33 ± 0.87	2.14×10^{-10}
	8	16	8.0	42/200	12.77 ± 1.75	1.27×10^{-9}
	9	0	5.0	23/300	3.33 ± 0.67	1.36×10^{-10}
	10	0	6.0	24/300	4.20 ± 0.82	2.35×10^{-10}
	10	0	8.0	12/300	3.74 ± 1.06	2.09×10^{-10}
	10	5	8.0	18/300	5.15 ± 1.18	3.29×10^{-10}
	10	10	8.0	54/300	12.10 ± 1.49	1.08×10^{-9}
	10	12	8.0	75/200	21.49 ± 1.96	2.28×10^{-9}
	11	0	8.0	30/300	7.71 ± 1.34	5.75×10^{-10}
	11	5	8.0	54/300	12.61 ± 1.55	1.07×10^{-9}
	11	9	8.0	135/300	25.68 ± 1.64	2.73×10^{-9}
	12	0	6.0	147/300	17.21 ± 1.01	1.67×10^{-9}
	12	0	8.0	79/300	16.44 ± 1.59	1.59×10^{-9}
*	12	0	8.0	76/300	16.85 ± 1.67	1.18×10^{-9}
	12	4	8.0	135/300	26.13 ± 1.67	2.73×10^{-9}
*	12	4	8.0	126/300	24.87 ± 1.69	1.98×10^{-9}

* T = 6000^2K; otherwise T = $10,000^2$K.

The most interesting aspect of the results is the manner in which the collision cross sections change with vibrational quantum number v and rotational quantum number J. For J = 0 the collision cross section increases slowly with increasing vibrational quantum number up to about v = 10, as may be seen in Fig. 9. Beyond v = 10 the cross section rises sharply to a value of about 16.8 $Å^2$ for v = 12. The cross sections are substantially less than those calculated from equation 17 (dashed line).

For a particular vibrational quantum number v, there is little change in the collision cross section with increasing J except as the vibration-rotation level becomes close to the dissociation limit. This may be seen in Table VII where the best values obtained for the collision cross sections are summarized. Note that the values for v = 11, J = 9, and for v = 12, J = 4 are 25.7±1.6 and 26.1±1.7 $Å^2$, respectively. These results agree with the value 25.5 $Å^2$ calculated from the theory of hard spheres, using the collision diameter of 2.85 Å obtained from viscosity data.

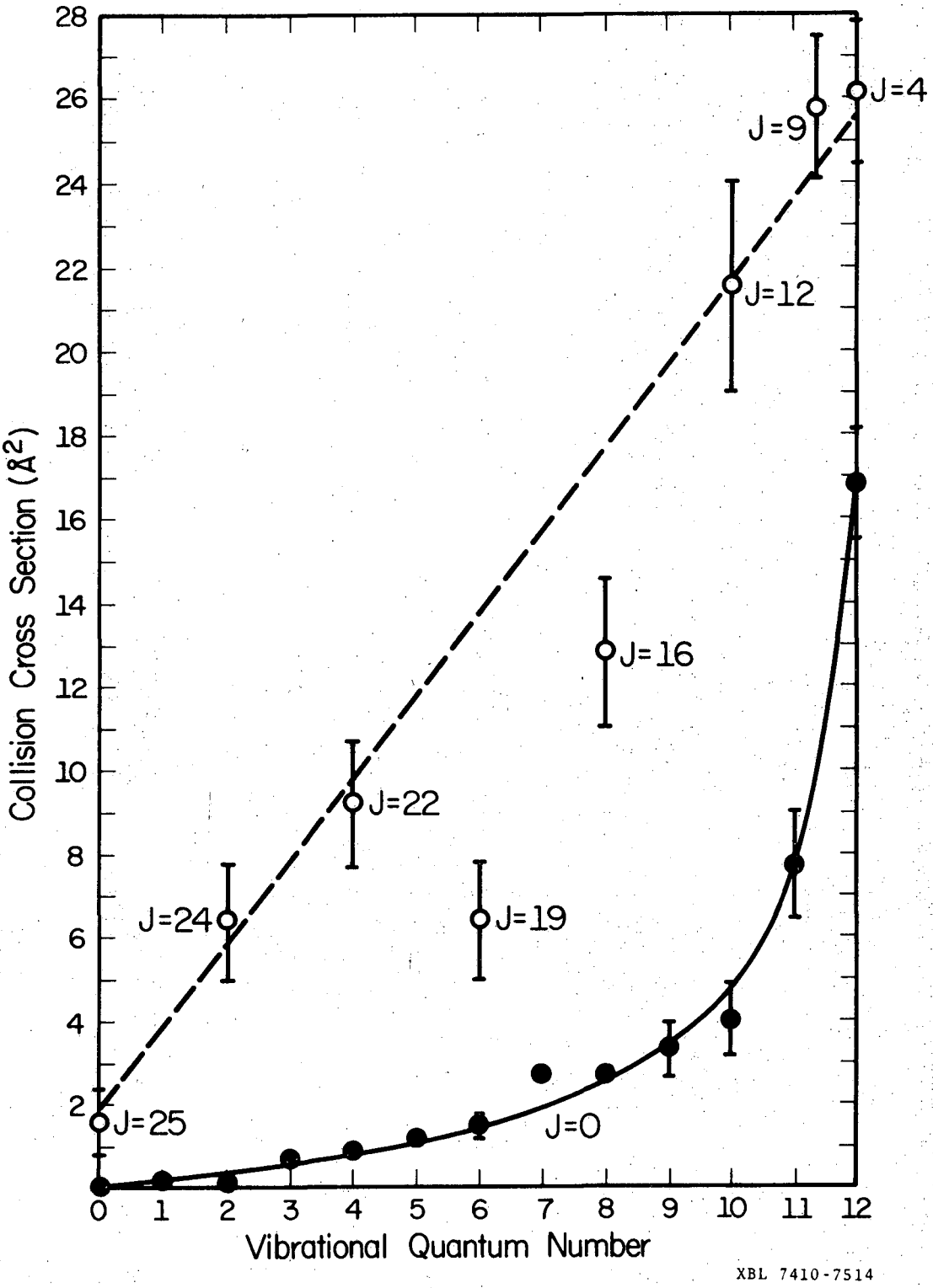

Fig. 9. Collision cross sections, ● for (v, J = 0), and O for the highest bound vibration-rotation levels, calculated from classical trajectories. (——) smooth curve through the (v, J = 0) points and used in Model A. (----) calculated from equation 17 and used in Model B. Error bars are for the standard error. Error bars are not shown when the standard error is less than 0.2 Å^2.

Table VII. Summary of collision cross sections ($\mathring{A}^2$) obtained for T = 10,000 K. Results are tabulated for J = 0,5,10 and for the highest bound rotation-vibration state.

v	J = 0	J = 5	J = 10	J	Highest
0	.075 ± .02	.10 ± .02	.06 ± .02	25	1.6 ± .8
1	.19 ± .05				
2	.16 ± .05	.42 ± .08	.24 ± .06	24	6.4 ± 1.4
3	.69 ± .13				
4	.86 ± .16	.63 ± .14	.81 ± .14	22	9.2 ± 1.5
5	1.2 ± .2				
6	1.5 ± .3	1.3 ± .3	1.1 ± .3	19	6.4 ± 1.4
7	2.7 ± .1				
8	2.6 ± .1	2.5 ± .7	4.3 ± .9	16	12.8 ± 1.8
9	3.3 ± .7				
10	4.0 ± .9	5.2 ± 1.2	12.1 ± 1.5	12	21.5 ± 2.0
11	7.7 ± 1.3	12.6 ± 1.6		9	25.7 ± 1.6
12	16.8 ± 1.3			4	26.1 ± 1.7

IV. CALCULATION OF THE DISSOCIATION RATE CONSTANT AND ACTIVATION ENERGY INCLUDING NONEQUILIBRIUM EFFECTS

A. Introduction

In this section the reaction cross sections presented in the previous section will be used in the simple theory of Johnston and Birks[4] to obtain rate constants and activation energies for the dissociation of H_2 in an inert gas. The model used allows dissociation from all vibrational levels as well as energy transfer processes between all vibrational levels as illustrated by Fig. 10. A Boltzmann distribution of molecules among rotational levels is assumed, but no equilibrium assumption is made with regard to the distribution of molecules among vibrational levels. The rate of dissociation of the molecule A from level i to the continuum of free atoms is

$$R_i = c_i[A_i][M] \tag{94}$$

The rate of chemical reaction is then

$$R = -\frac{d[A]}{dt} = \sum_{i=0}^{t} c_i[A_i][M] \tag{95}$$

and the rate constant k is

$$k = \frac{R}{[A][M]} = \sum_{i=0}^{t} c_i X_i \tag{96}$$

where the definition of the mole fraction X_i has been used. To calculate the rate constant at equilibrium we need only use a Boltzmann distribution for the X_i. To calculate the actual nonequilibrium rate constant we must solve the simultaneous set of differential equations given by

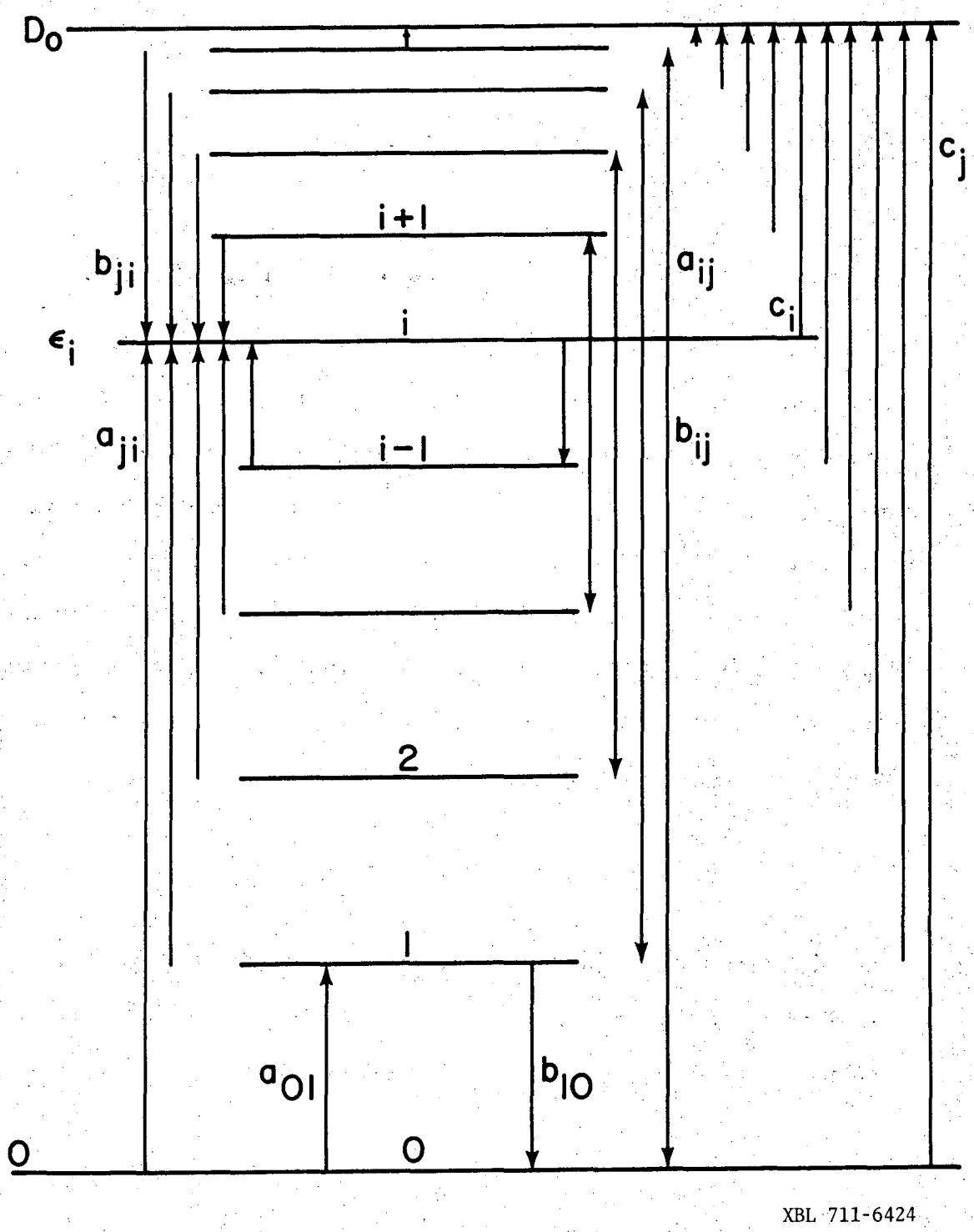

XBL 711-6424

Fig. 10. Model for the dissociation of diatomic molecules involves all activation steps a_{ij}, deactivation steps b_{ij}, and dissociation steps c_i.

$$\frac{d[A_i]}{dt} = [M] \sum_{j=0}^{i-1} a_{ji}[A_j] + [M] \sum_{j=i+1}^{t} b_{ji}[A_j] - [M][A_i]\left\{\sum_{j=0}^{i-1} b_{ij} + \sum_{j=i+1}^{t} a_{ij} + c_i\right\} \quad (97)$$

where a_{ji}, b_{ji} and c_i are the rate constants of Fig. 10. For H_2 there are 13 such differential equations. To obtain the actual distribution of molecules over vibrational levels, we need to solve the set of 13 simultaneous differential equations. It has been shown by detailed computations[30] that, after an extremely short induction period, the relative concentrations $[A_i]/[A]$ assume a steady-state distribution. That is, these ratios do not change with time even though the reactant as a whole is rapidly disappearing, and each state i decreases accordingly. Thus, as an excellent approximation

$$\frac{d([A_i]/[A])}{dt} = \frac{1}{[A]} \frac{d[A_i]}{dt} - \frac{[A_i]}{[A]^2} \frac{d[A]}{dt} \approx 0 \quad (98)$$

Upon substitution of Equations (97) and (95) into Equation (98), we obtained an expression suitable for evaluating the steady-state concentration of A_i by a method of successive approximations, Equation (99).

$$X_i = \frac{\sum_{j=0}^{i-1} a_{ji}X_j \sum_{j=i+1}^{t} b_{ji}X_j}{c_i + \sum_{j=0}^{i-1} b_{ij} + \sum_{j=i+1}^{t} a_{ij} - \sum_{j=0}^{t} c_j X_j} \quad (99)$$

With a set of rate constants a_{ji}, b_{ji} and c_i, we take as the zero approximation the equilibrium mole fractions to find a first approximation to the set of nonequilibrium mole fractions, $X_i (i = 0,1,2,...t)$. This first approximation is then substituted into the right-hand side of Equation (99) to find the second approximation to X_i, and the process can be repeated to any desired degree of convergence.

To calculate the populations of vibrational levels by the above method, one requires knowledge of the deactivation rate constants b_{ji}, the activation rate constants a_{ij}, and the dissociation rate constants c_i. Stevens[31] gives a model for transitions between all bound states of a Morse oscillator which readily permits all values of deactivation constants b_{ji} to be found, Equation (100).

$$b_{i+r,i} = b_{10} x_e^{r-1} [(i + r)\ !/i!r^2] \tag{100}$$

For b_{10} as a function of temperature the experimental results of vibrational relaxation measurements may be used. From the principle of microscopic reversibility, the activation constants a_{ij} are given by

$$a_{i,i+r} = b_{10} x_e^{r-1} [(i + r)\ !/i!r^2] \exp[-(D_o - \varepsilon_i)kT] \tag{101}$$

The method used for assigning values to c_i has been discussed in detail in the Chapter I. Johnston and Birks[4] used the values for c_i given by Equation (14) with collision cross sections given by Equation (17). The differences between the cross sections calculated from Equation (17) and those obtained in the previous section by trajectory calculations are indicated in Fig. 9. The classical trajectory calculations led to substantially lower values for the collision cross sections. In this

section, calculations of the rate constants and activation energies will be compared for the two sets of collision cross sections. In Model A calculations were made using the classical trajectory results for the cross sections. Model B makes use of the cross sections given by Equation (17). Since experimental data is only available for the Ar-H_2 system, the calculations were carried out for Ar-H_2 using the Ne-H_2 collision cross sections. Since the collision diameters evaluated from viscosity data are not very different from the Ne-H_2 and Ar-H_2 systems, the cross sections calculated from Equations (17) are not very different. For these calculations b_{10} was evaluated from the relaxation data for Ar-H_2 of Kiefer and Lutz.[32]

B. Results of Model Calculations

Plots $c_i x_i$ vs vibrational quantum number for Models A (trajectory cross sections) and B (Equation (17)) at three temperatures are provided in Fig. 11. In both models there is an increasing depletion of vibrational levels below the equilibrium values with increasing temperature. In the two models, activation energies decrease with increasing temperature by similar amounts, as seen in Table VIII. Because of the larger collision cross sections for dissociation, levels become depleted at lower temperatures for Model B than for Model A, so that the activation energies decrease somewhat faster with temperature. The principle difference in the two models is the absolute value predicted for the rate constant. Model B predicts a rate constant nearly an order of magnitude larger than that of Model A, and is in much better agreement with the experimental data, Fig. 12. The larger rate constant predicted by Model B is simply due to the larger

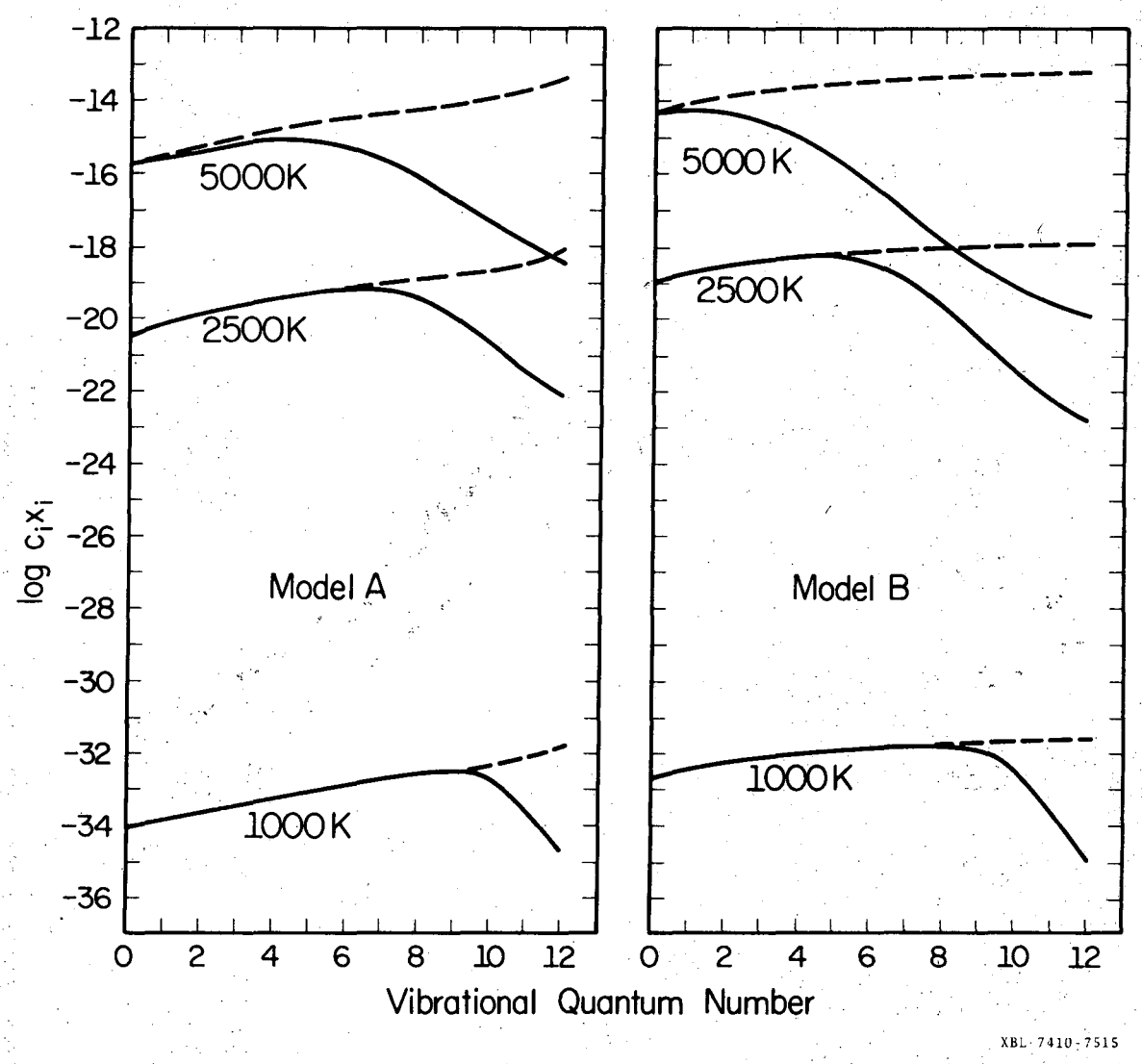

Fig. 11. Comparison of the products $c_i x_i$ in the equilibrium (---) and nonequilibrium (——) cases for Models A (cross sections from classical trajectories) and B (cross sections from equation 17). Both models demonstrate a reduction in the number of states contributing to reaction with increasing temperature.

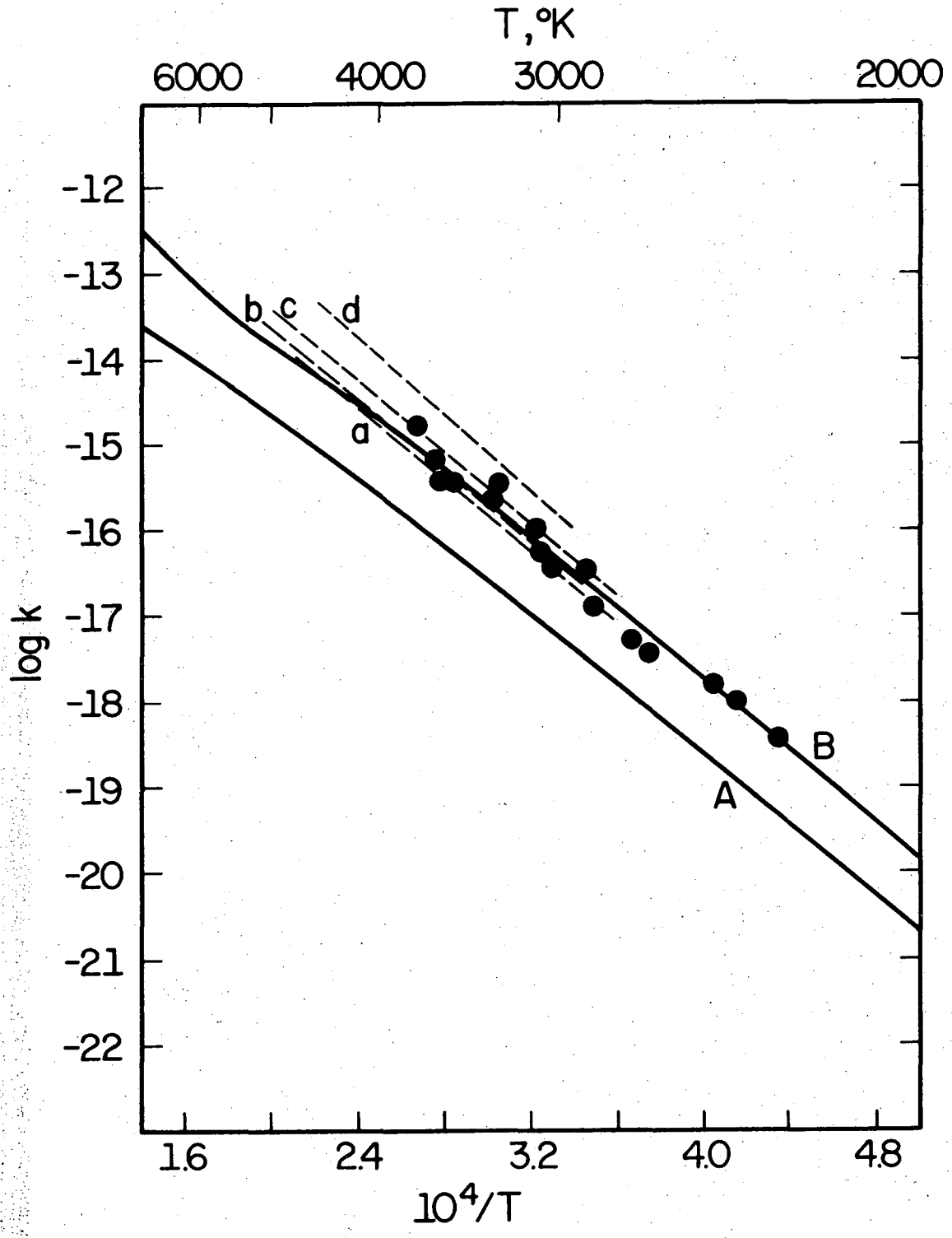

XBL 7410-7516

Fig. 12. Comparison of models A (cross sections from classical trajectories) and B (cross sections from equation 17) with the experimental data for the dissociation of H_2. ● data of Myerson and Watt[37]; (a) data of Sutton[33]; (b) data of Patch[34]; (c) data of Rink[35]; and (d) data of Gardiner and Kistiakowsky[36] where the M is Xe. Rink[35] reported Ar and Xe as having the same efficiency in dissociating H_2.

Table VIII. Activation energies for the dissociation of H_2 by Ar as a function of temperature for nonequilibrium Models A and B and at equilibrium.

T	Model A	Model B	Equilibrium
500	103.0	103.4	104.0
1000	102.4	102.8	104.4
1500	101.1	101.5	104.6
2000	99.3	99.2	104.6
2500	96.8	95.8	104.4
3000	93.9	90.8	104.2
3500	90.6	85.4	103.8
4000	87.5	81.0	103.4
4500	84.8	78.7	102.9
5000	82.7	78.8	102.4
5500	81.4	80.8	101.8
6000			

cross sections for dissociation from individual vibrational levels.

V. DISCUSSION

A. The Ne-H_2 Potential Energy Surface

The interesting aspect of the Gordon-Secrest[23] interaction potential for He-H_2 is that as the He atom approaches the H_2 molecule for the perpendicular bisector geometry, a contractive force is exerted on the H_2 molecule. This is, of course, just the opposite effect from that predicted by the dumbbell potential, in which the force is always in the direction of stretching the H_2 internuclear distance. This effect is also present in the Krauss-Mies[26] He-H_2 potential. Neither Krauss and Mies nor Gordon and Secrest calculated points at sufficiently small values of X (close-in) to show that this effect is actually reversed at small values of X. Realizing that there must be some cross-over point, however, both groups of investigators required that the analytic fit be such that there is a cross-over point where the force exerted on the H_2 bond is zero. For the Gordon-Secrest fit this cross-over occurs at X = 2.01 Bohr, and for the Krauss-Mies fit the value is X = 1.85 Bohr.

In a recent article, Alexander and Berard[38] presented four new ways of fitting the Gordon-Secrest points on the He-H_2 surface. They also calculated probabilities of He-H_2 vibrational energy transfer for each of their four analytic fits and for the Gordon-Secrest fit. They found that the matrix element for the $0 \rightarrow 1$ transition goes to zero for the Gordon-Secrest fit near X = 2. Since none of the four fits of Alexander and Berard exhibited this feature, the transition probability changing smoothly with X, they suggested that the Gordon-Secrest fit was inferior. All four of the Alexander and Berard fits have the property that as the distance X increases the contractive force increases, with no cross-over point.

This, of course is unrealistic. One would, in fact, expect the probability of vibrational energy transfer to be reduced to zero at the cross-over point, since at this point no force is exerted along the H_2 bond

That such a cross-over does exist is demonstrated by the date presented in Table III for the Ne-H_2 interaction potential. Consider first the results for X = 4.0. In table III it can be seen that

$$V'(R = .8) < V'(R = 1.1) < V'(R = 1.7) < V'(R = 2.0) < V'(R = 3.0) \quad (102)$$

so that the force is in the direction of contracting the H_2 internuclear distance, R. For X = 3.5, equation 102 still applies. For X = 3.0, however, we have

$$V'(R = .8) > V'(R = 1.1) > V'(R = 1.7) > V'(R = 2.0) > V'(R = 3.0) \quad (103)$$

and this is seen to be true for X = 2.5 as well. Thus, there is a cross-over point between X = 3.0 and X = 3.5. For X larger than the value of the cross-over point there a contractive force, and for X smaller than the value of the cross-over point, there is a stretching force.

For an analytic fit, the value of X at the cross-over point may be found by taking the derivative of the interaction potential with respect to R, setting the result equal to zero, and solving for X with R = 1.4. The cross-over occurs at slightly different positions for different values of R. The analytic fit (Equation 57) used for the trajectory calculations of the previous section has a cross-over at X = 2.9 Bohr. In consideration of this type of behavior for the interaction potential, it is not surprising that the dumbbell form for the potential results in a poor fit.

B. Collision Cross Sections for Dissociation

Classical trajectory studies tend to underestimate reaction cross sections when the energies sampled are near the threshold for the process.

For this reason the collision cross sections calculated for dissociation from levels other than those near the dissociation limit may be considered a lower bound to the true cross sections. This is illustrated by Fig. 13 which shows that a small positive change in the reaction cross section near threshold can have a substantial effect on the rate constant (Equation 85) due to a better overlap with the energy distribution function, $E\exp(-E/RT)$. At 10,000K the most probable energy is 20 kcal or about 1 ev. Since the threshold for dissociation from v = 0 is 4.5 ev, it is clear the overlap between S_r and the energy distribution function must occur very near the threshold energy. As one goes to higher vibrational levels, the reaction tends to be less of a threshold phenomenon so that the classical approximation is much better, and at the top vibrational level the differences in the classical and quantum mechanical S_r curves would be expected to be of little consequence since the overlap with the energy distribution function would be nearly the same (see Fig. 13).

Perhaps the Johnston-Birks[4] formula (Equation 17) for the collision cross sections over estimates the rates of dissociation from the lower levels as suggested by Bauer,[42] and as indicated in Fig. 9. The much better agreement with the experimental data for H_2 (Fig. 11) when the Johnston-Birks formula is used, however, tends to support the validity of these cross sections rather than those calculated from classical trajectories. The disagreement between the two sets of cross sections varies with vibrational quantum number as one might expect from the previous argument. The agreement is best at v = 12 where the cross sections differ by less than a factor of two and decreases with decreasing vibrational quantum number, the two sets of cross sections differing by about a factor of twenty at v = 0.

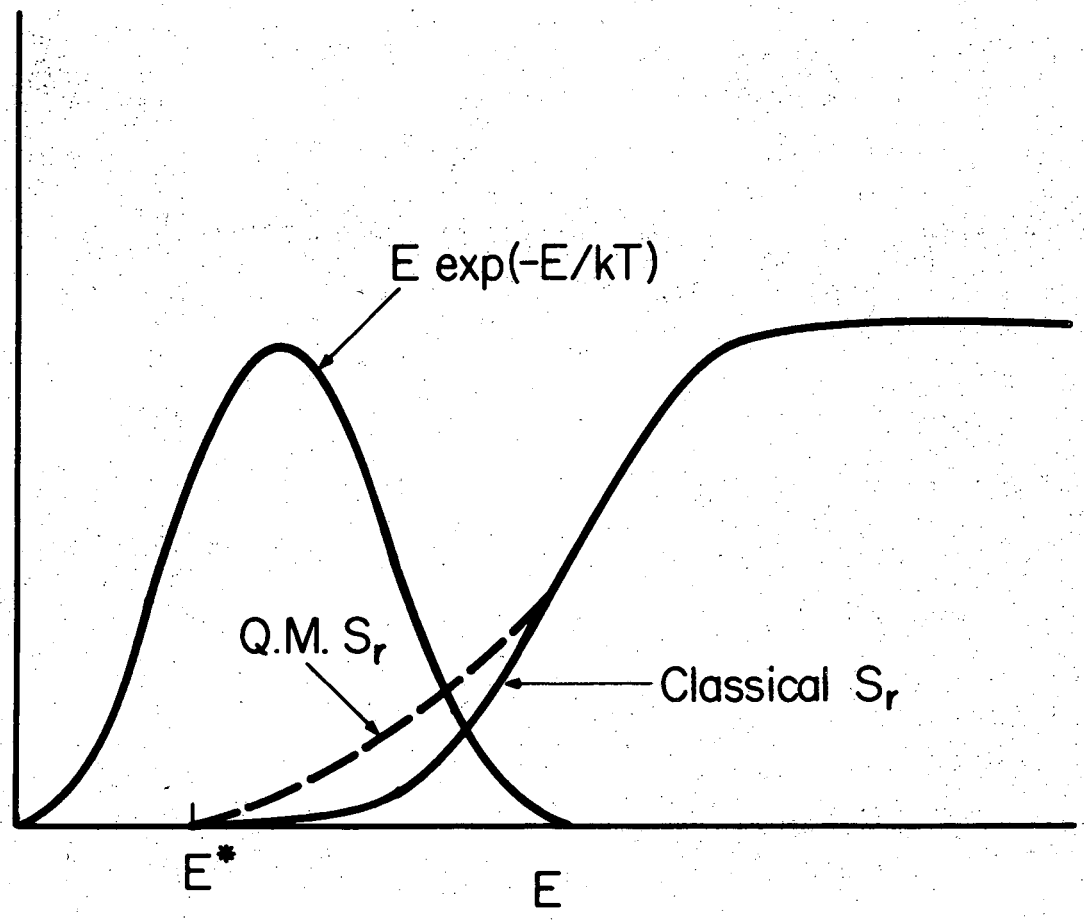

XBL 7410-7517

Fig. 13. The principle difference in the quantum mechanical and classical S_r curves occurs near the threshold E*. Since the rate constant and collision cross section are proportional to the integrated product of the energy distribution function and the S_r curve, the error is greatest when the overlap of these curves is small. This occurs when kT is small compared to the threshold energy E*.

Also plotted in Fig. 9 are the cross sections for dissociation from several of the highest bound vibration-rotation levels. The threshold for dissociation from these levels is much lower than the corresponding (v, J = 0) levels since rotation may contribute to the dissociation process. The agreement between these cross sections and those calculated from the Johnston-Birks formula is remarkable. Since cross sections do not change significantly with rotational quantum number (Table VII) except as the corresponding vibration-rotation levels approach the continuum, this result tends to support the contention that the classical trajectory collision cross sections are underestimated, and that the true quantum mechanical cross sections are more in accord with those of Equation 17. The future application of semi-classical theory will, no doubt, resolve this problem.

C. Activation Energies for the Dissociation of Diatomic Molecules

In shock tube experiments only one variable, the reaction rate constant, is measured as a function of temperature. A good theory should be able to predict this macroscopic quantity, and at the same time provide insight into the presently unmeasurable microscopic processes as well. In particular, it is desirable to know to what extent dissociation occurs by a ladder climbing process (step by step vibrational excitation)[5], by rotational excitation with dissociation occurring from "orbiting resonances",[43,44] and by direct dissociation from a large number of vibration-rotation levels.[4]

Keck[22] has developed a perfectly general phase space theory of diatomic dissociation and atom recombination within the frame-work of classical mechanics. Recognizing that the usual impact parameter sampling technique employed in exchange reaction calculations and as used here is extremely inefficient (too few trajectories lead to reaction) when applied to excitation

reactions, he developed an "inside out" sampling technique. This technique involves selection of initial conditions inside the collision complex, followed by integration of the equations of motion both forward and backward in time to obtain a complete history of the collision. Of course, since classical mechanics is used, the trajectories integrate backward in time to a continuum of vibrational energy levels. In this model, there is a considerable sacrifice of knowledge concerning the details of the dissociation and recombination processes. What is gained is the evaluation of the overall rate constant with improved efficiency. This model provides little insight into the question of why the activation energies decrease with increasing temperature. Much of the application of this model has been a type of curve fitting, the idea being that the experimental data are a measure of the potential energy surface. Keck has evaluated parameters for the dumbbell potential for a large number of atom-diatomic interactions by finding those parameters that make the phase space theory fit the data. Unfortunately, as found in the present calculations for Ne-H_2 and as found by Gordon and Secrest for He-H_2, the dumbbell model does not describe the potential surface sufficiently well.

The opposite approach has been taken here, that of calculating the potential energy surface, calculating trajectories beginning as quantized reactants, and finally evaluating the rate constant using no adjustable parameters. This is the type of approach that is necessary if we are to learn anything of the details of the dissociation and recombination processes. The most interesting aspect of the dissociation reaction is, of course, the manner in which the activation energies change with temperature. Several

theories to explain the low activation energy in terms of the actual microscopic processes involved have been advanced.

Dove and Jones[45] and Johnston and Birks[4] have shown that the "ladder-climbing" model in which molecules undergo collisional transitions between vibrational levels and are eventually excited to the dissociation limit, both underestimates the rate constant by about an order of magnitude and predicts the wrong trend of the activation energy with temperature. Dove and Jones[45] found that the activation energy remained constant near a value of D_o, whereas Johnston and Birks[4] found that the activation energy was lower than D_o and increased with increasing temperature. In subsequent work, Dove and Jones[46] found that if transition probabilities for rotational-translational and vibrational-rotational-translational energy transfer are included, the ladder climbing model correctly predicts both the absolute value of the rate constant and the decrease in activation energy with increasing temperature. No explanation was offered as to why inclusion of rotational energy transfer should have this effect, however.

Kiefer[47] has offered an explanation of the effect of temperature on the activation energy in terms of vibrational-vibrational (VV) energy transfer. Again, in this model dissociation by collision with the M gas is only allowed to occur from the top vibrational level. The collision of two diatomic molecules is envisaged as resulting in dissociation of one molecule at the expense of vibrational energy of the second molecule. The effect is to perturb the Boltzmann distribution over vibrational levels by shoving molecules to lower levels. The reduced steady state population of the highest level results in a reduced rate constant. The effect increases with increasing temperature so that the rate constant increases with temperature less

rapidly than expected, and the activation energy is less than expected. This effect should not persist in sufficiently dilute mixtures of the diatomic molecules in the M gas, however. The extent to which this mechanism retards the rate of reaction depends on the magnitude of the VV energy transfer probabilities, which are still somewhat uncertain.

The most serious omission in the models used to date [5,45-47] has been that of dissociation probabilities for dissociation from levels other than those near the continuum. The Johnston-Birks[4] model includes dissociation from all levels, as discussed previously. In this model it is the depletion of the number of states that react via increased depletion of upper vibrational levels with increasing temperature that explains the effect of temperature on the activation energy. The effect is predicted equally well by the use of the smaller cross sections calculated here. This is because the upper two vibrational levels are substantially depleted, even at temperatures as low as 1000 K (see Fig. 11). The remaining levels constitute nearly parallel reaction channels similar to those given by Equation 14, but with reduced magnitudes, so that the total rate constant is smaller. These results suggest that if the Johnston-Birks model is essentially correct, then the collision cross sections must be larger than those calculated using classical trajectories. As discussed in the previous section, these classical cross sections are only a lower bound, and an order of magnitude error for the ($v = 0$, $J = 0$) cross section would not be surprising in view of the threshold nature of the reaction. The eventual evaluation of microscopic rate constants for the various energy transfer and reaction steps by theoretical and experimental work will, no doubt, shed considerable light on

the dissociation mechanism. The accurate potential energy surface presented here is now available for further theoretical calculations.

REFERENCES

1. J. Troe and H. G. Wagner, Ber. Bunsenges. Phys. Chem. 71, 930 (1967); A. C. Lloyd, Int. J. Chem. Kin. 3, 39 (1971).
2. R. L. Belford and R. A. Strehlow, Ann. Rev. Phys. Chem. 20, 247 (1969).
3. M. Warshay, J. Chem. Phys. 54, 4060 (1971).
4. H. S. Johnston and J. W. Birks, Acct. Chem. Res. 5, 327 (1972). Also available as UCRL-20514.
5. K. E. Shuler, J. Chem. Phys. 31, 1375 (1959); E. E. Nikitin and N. D. Sokolov, J. Chem. Phys. 31, 1371 (1959); H. O. Pritchard, J. Phys. Chem. 65, 504 (1961); O. K. Rice, J. Phys. Chem. 67, 6 (1963); P. V. Marone and C. E. Treanor, J. Phys. Fluids 6, 1215 (1963).
6. M. Born and R. Oppenheimer, Ann. Physik 84, 457 (1927).
7. W. H. Miller, J. Chem. Phys. 53, 1949 (1970); W. H. Miller, J. Chem. Phys. 53, 3578 (1970); W. H. Miller, Chem. Phys. Letters 7, 431 (1970); W. H. Miller, Acct. Chem. Res. 5, 161 (1971); W. H. Miller, J. Chem. Phys. 54, 5386 (1971); C. C. Rankin and W. H. Miller, J. Chem. Phys. 55, 3150 (1971); W. H. Miller, J. Chem. Phys. 58, 1664 (1973).
8. R. A. Marcus, Chem. Phys. Letters 7, 525 (1970); R. A. Marcus, J. Chem. Phys. 54, 3965 (1971); J. N. L. Connor and R. A. Marcus, J. Chem. Phys. 55, 5636 (1971); W. H. Wong and R. A. Marcus, J. Chem. Phys. 55, 5663 (1971); R. A. Marcus, J. Chem. Phys. 57, 4903 (1972); R. A. Marcus, J. Chem. Phys. 56, 311 (1972); J. Stine and R. A. Marcus, Chem. Phys. Letters 15, 536 (1972).
9. M. Karplus, R. N. Porter and R. D. Sharma, J. Chem. Phys. 43, 3259 (1965).
10. H. F. Schaefer III, The Electronic Structure of Atoms and Molecules, (Addison-Wesley, Massachusetts, 1972).

11. R. McWeeny and B. T. Sutcliffe, Methods of Molecular Quantum Mechanics (Academic Press, New York, 1969).

12. D. R. Hartree, Proc. Cambridge Phil. Soc. 24, 89 (1928).

13. V. Fock, Z. Physik 61, 126 (1930).

14. J. K. L. MacDonald, Phys. Rev. 43 830 (1933).

15. D. R. Hartree, W. Hartree, and B. Swirles, Phil. Trans. Roy. Soc. (London) A238, 229 (1939).

16. H. A. Bethe and E. E. Salpeter, Quantum Mechanics of One- and Two-Electron Atoms (Springer-Verlag, Berlin, Gottingen, Heidelberg, 1957).

17. C. C. J. Roothaan, Rev. Mod. Phys. 23, 69 (1951); C. C. J. Roothaan, Rev. Mod. Phys. 32, 179 (1960).

18. F. B. Van Duijneveldt, RJ945, December 1971 (IBM Research Laboratory, San Jose, California 95193).

19. S. Huzinaga, J. Chem. Phys. 42, 1293 (1965).

20. F. A. Cotton, Chemical Applications of Group Theory (Wiley-Interscience, New York, 1971).

21. W. L. Dimpfl and B. H. Mahan, J. Chem. Phys. 60, 3238 (1974).

22. J. C. Keck, J. Chem. Phys. 32, 1035 (1960); J. C. Keck, Adv. Chem. Phys. 13, 85 (1967). V. H. Shui, J. P. Appleton, and J. C. Keck, J. Chem. Phys. 53, 2547 (1970); V. H. Shui and J. P. Appleton, J. Chem. Phys. 55, 3126 (1971); V. H. Shui, J. P. Appleton, and J. C. Keck, J. Chem. Phys. 56, 4266 (1972); V. H. Shui, J. P. Appleton and J. C. Keck, Int. Sym. Combustion 13, 21 (1970).

24. W. L. Dimpfl, Ph.D. Thesis, University of California, Berkeley (August 1973). Available as report LBL-1873.

25. C. S. Roberts, Phys. Rev. 131, 203 (1963).

26. M. Krauss and F. H. Mies, J. Chem. Phys. 42, 2703 (1965).

27. J. D. Kelley and M. Wolfsberg, J. Chem. Phys. 44, 324 (1966).

28. G. Herzberg, Molecular Spectra and Molecular Structure I. Spectra of Diatomic Molecules, 2nd ed. (Van Nostrand, Princeton, 1950).

29. M. A. Eliason and J. O. Hirschfelder, J. Chem. Phys. 30, 1426 (1959).

30. D. G. Rush and H. O. Pritchard, Int. Symp. Combustion 11, 13 (1966).

31. B. Stevens, Collisional Activation in Gases, (Pergamon Press, New York, 1967), p. 39.

32. J. H. Kiefer and R. W. Lutz, J. Chem. Phys. 44, 668 (1966).

33. E. A. Sutton, J. Chem. Phys. 36, 2923 (1962).

34. R. W. Patch, J. Chem. Phys. 36, 1919 (1962).

35. J. P. Rink, J. Chem. Phys. 36, 262 (1962).

36. W. C. Gardiner and G. B. Kistiakowsky, J. Chem. Phys. 35, 1765 (1961).

37. A. L. Myerson and W. S. Watt, J. Chem. Phys. 49, 425 (1968).

38. M. H. Alexander and E. V. Berard, J. Chem. Phys. 60, 3950 (1974).

39. D. Secrest, "On Analytic Fits to the Gordon-Secrest Potential Energy Surface for He-H_2", Preprint, (October, 1974).

40. W. H. Miller and T. F. George, J. Chem. Phys. 56, 5668 (1972). (Appendix C)

41. B. P. Stoicheff, Can. J. Phys. 35, 730 (1957).

42. S. H. Bauer, Private Communication.

43. R. E. Roberts, R. B. Bernstein and C. F. Curtiss, J. Chem. Phys. 50, 5163 (1969).

44. P. A. Whitlock, J. T. Muckerman and R. E. Roberts, J. Chem. Phys. 60, 3658 (1974).

45. J. E. Dove and D. G. Jones, J. Chem. Phys. 55, 1531 (1971).

46. J. E. Dove and D. G. Jones, Chem. Phys. Letters 17, 134 (1972).

47. J. H. Kiefer, J. Chem. Phys. 57, 1938 (1972).

PART II.

AN EXPERIMENTAL STUDY OF THE EMISSION SPECTRA OF IF IN THE GAS PHASE REACTION OF I_2 WITH F_2

I. INTRODUCTION

The emission spectrum of iodine monofluoride (IF) was first reported in 1951 by Durie[1] under low resolution. The rotationally resolved spectrum was later reported by Durie[2], thus confirming the existence of this molecule which is thermodynamically unstable with respect to disproportionation to give the products I_2 and IF_5. Due to absence of a Q branch in the high resolution spectrum, the emission was assigned to the IF ($B^3\Pi_{0^+} \rightarrow X^1\Sigma^+$) transition analogous to other halogen and inter-halogen spectra. In both studies the source of the IF spectrum was an iodine-fluorine flame in which F_2 passed over iodine crystals.

Clyne, Coxon and Townsend[3] studied the emission resulting from the association of ground state I ($^2P_{3/2}$) atoms and F($^2P_{3/2}$, $^2P_{1/2}$) atoms in the presence of singlet oxygen ($^1\Delta_g$, $^1\Sigma_g^+$). They observed many of the same bands as Durie and a number of bands at longer wavelengths that belong to the same band system.

In this study the emission resulting from the gas phase reaction of I_2 with F_2 in a flow system at pressures as low as 4×10^{-3} torr was investigated. In addition to bands belonging to the IF($B^3\Pi_{0^+} \rightarrow X^1\Sigma+$) system, bands in the same wavelength region originating in a lower-lying bound molecular state of IF were observed. The relative amounts of emission from the two excited electronic states varied with the flow rates of I_2

and Ar so that spectra could be obtained in which emission occurred predominantly from either one of the two excited electronic states. This previously unreported emission is here assigned IF($A^3\Pi_1 \rightarrow X^1\Sigma^+$) transition. Emission from the $A^3\Pi_1$ state for diatomic halogens and interhalogens has been reported previously for Br_2[4,5,7] I_2[7], ICl[6] and IBr[4].

The visible and uv spectra of diatomic interhalogens demonstrate interesting curve-crossing effects which have been reviewed by Child and Bernstein.[19] These avoided crossings between a repulsive state and a bound state, both of 0^+ symmetry, result in potential maxima and thus false dissociation limits for the bound state. In this regard IF is a particularly interesting molecule since there arises the possibility of yet another avoided curve crossing between two bound states of 0^+ symmetry, one of which correlates with a spin-orbit excited F* atom and a ground state I atom and the other with a spin-orbit excited I* atom and a ground state F atom. The bond dissociation energy for IF may be determined from a Birge-Sponer extrapolation of the $B^3\Pi_{0_+}$ state in the case that the avoided curve-crossing leading to predissociation is with a bound state rather than a repulsive one.

Since the high resolution emission spectrum of the IF($B^3\Pi_{0_+} \rightarrow X^1\Sigma^+$) transition is known and accurate potential energy curves for the B and X states have been calculated, it is possible to obtain vibrational populations for the B state from low resolution spectra. One may also estimate rotational temperatures from the shapes of the vibrational bands. In this study the effect of pressure on the vibrational populations of the $B^3\Pi_{0_+}$ state was investigated. A mechanism for the rapid reaction between I_2 and F_2 and the population of excited electronic states is proposed and compared with experimental results.

II. EXPERIMENTAL

A. Reaction Cell and Flow System

Figure 1 is a schematic diagram of the apparatus. The reaction cell consisted of a large stainless steel tank with a cylindrical portion 62 cm in diameter and 76 cm long and hemispherical ends. The volume of the cell was 350 liters. Pressures in the cell were measured with a factory calibrated Datametrics Type 1014 Barocel electronic manometer. Effluent gases passed over trays of NaCl heated to 100 °C to exchange F_2 for Cl_2 which was then removed by a liquid nitrogen trap. The cell was continuously pumped on by a mercury diffusion pump and an oil forepump.

Fluorine, obtained from Matheson Co. (98% purity), was passed over activated NaF to remove HF impurity and stored in a 34 liter tank at pressures less than one atomsphere. From this storage tank fluorine was metered into the reaction cell by means of a Vactronics leak valve. Argon of 99.996% purity obtained from Linde Inc. was metered into the cell by a leak valve also and mixed with fluorine prior to entering the cell. Flow rates of fluorine and argon were measured using Hastings-Raydist Model LF-50 calorimetric mass flowmeters.

Analytical reagent grade iodine obtained from Mallincrockdt was held at 313 K in a glass bulb submerged in a constant temperature mineral oil bath. The vacuum line and valves connecting the bulb to the cell were heated to prevent sublimation. Due to the low conductance of the Hastings flow meters and the necessity of heating the flow line it was not possible to measure the iodine flow rates in the same manner as for fluorine and argon. Instead, a needle valve was used to meter the iodine vapor and

the flow rate determined for various settings of the needle valve by closing the cell to the vacuum pump and observing the rise in pressure with time.

B. Optical System and Photon Counting Apparatus

The wave length of the chemiluminescence was measured with a Jarrell-Ash Ebert scanning monochromator having a focal length of 500 mm and an effective aperture ratio of f/8.6. The instrument was equipped with curved entrance and exit slits. Spectra were obtained at a slit width of 0.35 mm and a full slit height of 20 mm. The grating was ruled at 590 lines/mm resulting in a dispersion of 32 Å/mm and was blazed for maximum intensity at 750 nm in first order. The monochromator was calibrated between 430 and 720 nm by scanning twenty-two Ne and four Hg atomic lines. Wavelengths were measured to within 0.2 nm throughout the entire wavelength region. The spectral slit function was found (by scanning a number of atomic lines) to be essentially triangular with a full width at half maximum intensity (FWHM) of 1.12 nm.

The slit of the monochromator was positioned ten cm from the 3.8 cm diameter CaF_2 window of the reaction cell. Light from the exit slit of the monochromator was reflected onto the photocathode of an EMI 9558QA photomultiplier tube having an S-20 type spectral response and a quartz window. The field of view of the optical system is indicated in Fig. 1. The photomultiplier housing was cooled to dry ice temperatures to reduce the thermionic emission from the large photo-sensitive area of the photocathode. The photomultiplier was wired with the photocathode at ground potential and the anode at a high positive potential of 1250 v, chosen

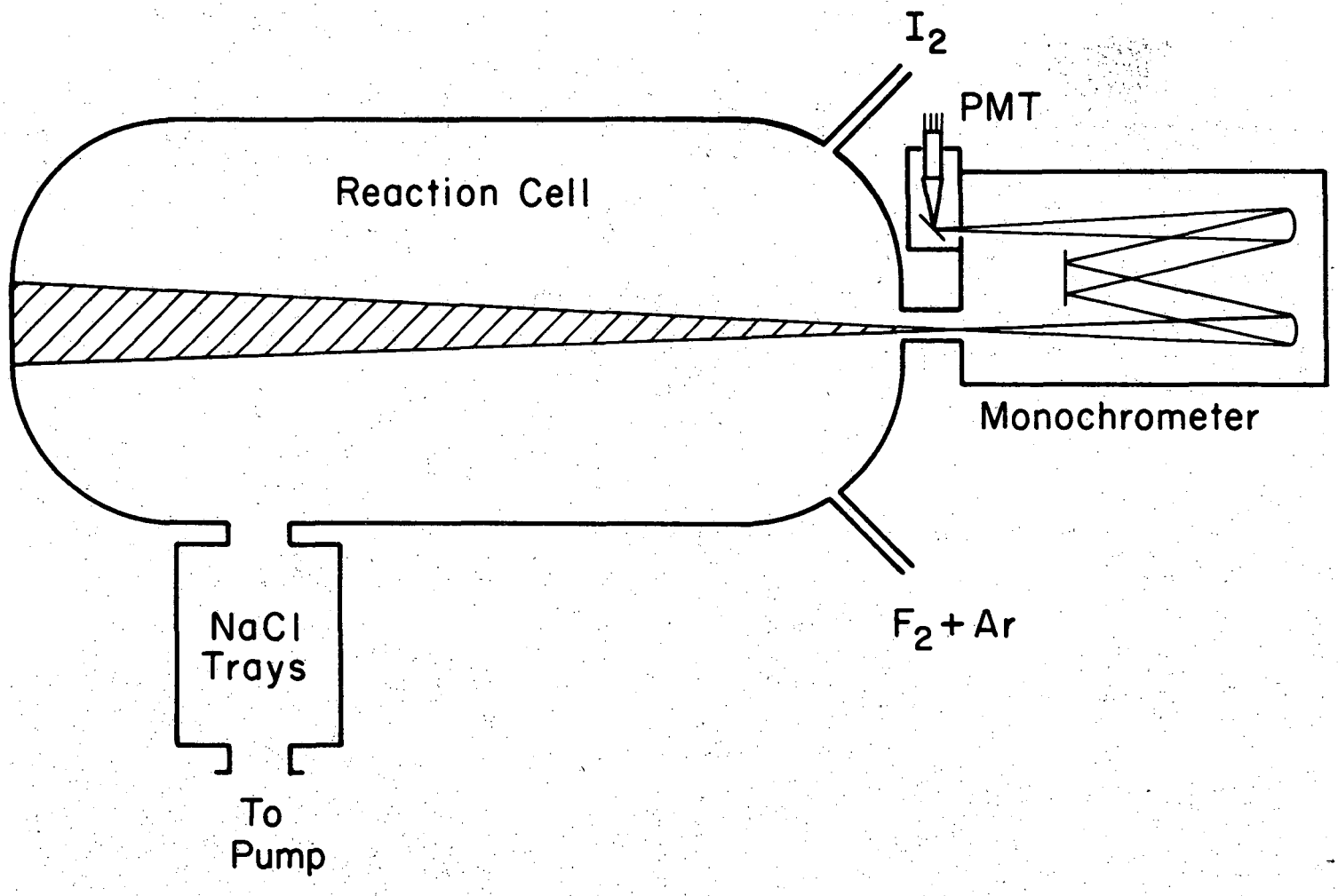

Fig. 1 Schematic Diagram of the Apparatus

for optimum signal to noise ratio. Figure 2 is the wiring diagram for the photo-multiplier tube. The potential difference between the photocathode and first dynode was held at 200 v by a zener diode. Dark current was typically 10 counts/sec. Photon counting was achieved by use of a Solid State Radiations Model 1120 Amplifier-Discriminator and Model 1105 Data Converter Console. The analog voltage proportional to counts/sec was converted to digital form by a digital voltmeter interfaced to a paper tape punch. Spectra were recorded by a Texas Instruments strip chart recorder and simultaneously as a series of data points punched on paper tape.

The wavelength response of the combined optical and electronic detection system was determined by comparing the spectrum obtained upon scanning the light emitted from a General Electric 30A/T24/17 tungsten ribbon lamp with the theoretical spectrum. The power supply for the lamp was stabilized by a photo-feed-back system in which light from the ribbon fell onto a photodiode after passing through a blue Corning No. 5030 filter. The temperature of the tungsten ribbon was measured by a Leeds and Northrup optical pyrometer, calibrated by the D.C. Standards section of the Lawrence Berkeley Laboratory. The theoretical spectrum was calculated using the emissivities of tungsten given by DeVos[9]. The intensity correction factor as a function of wavelength which was applied to all spectra is shown in Fig. 3.

To record a spectrum the monochromator was started scanning from 720 nm at 4 nm/min in the direction of decreasing wavelength. Output from the photon counter with an applied time constant of 11.2 seconds was punched every five seconds or 1/3 nm. Thus 870 data points were recorded in the 72.5 minutes required to scan from 720 nm to 430 nm. The punched tapes

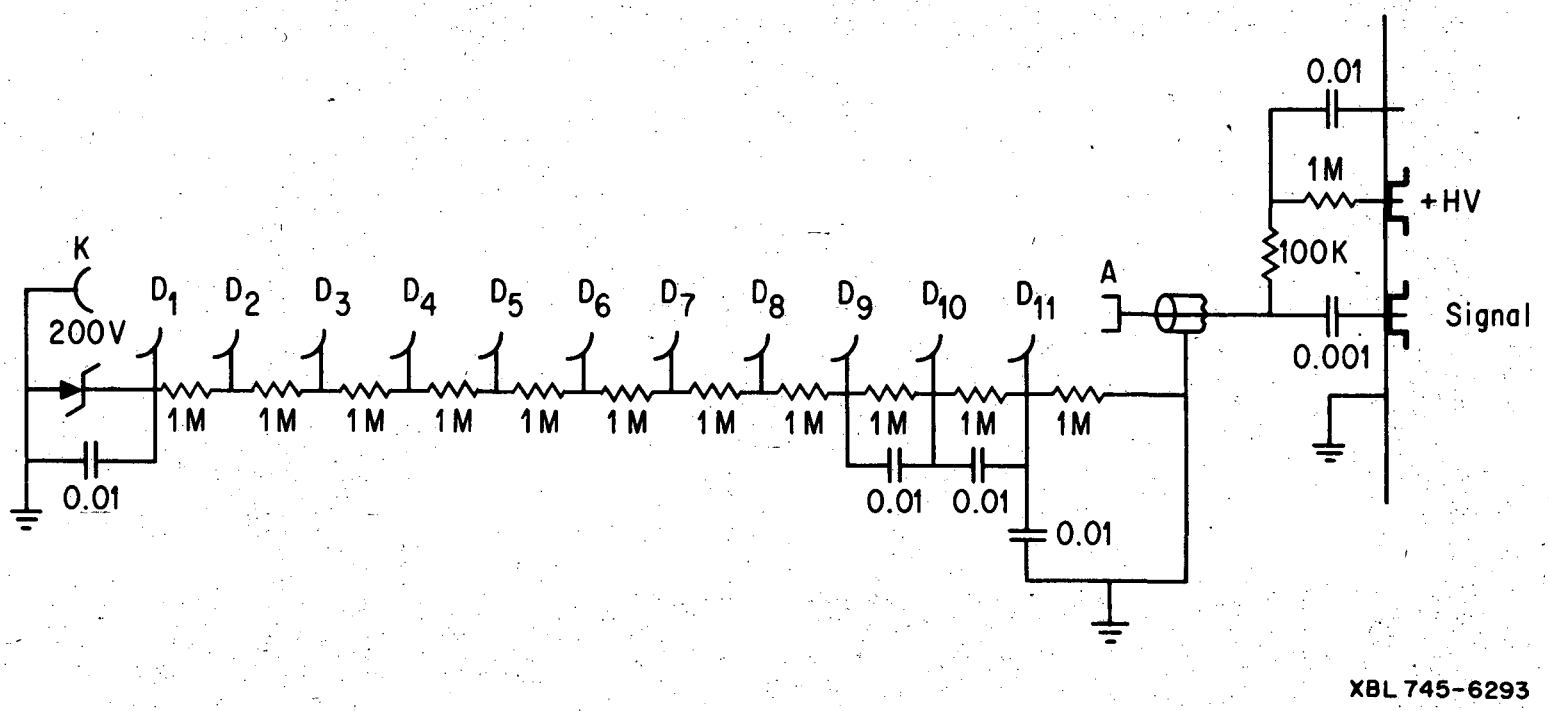

Fig. 2. Wiring diagram for the photomultiplier tube.

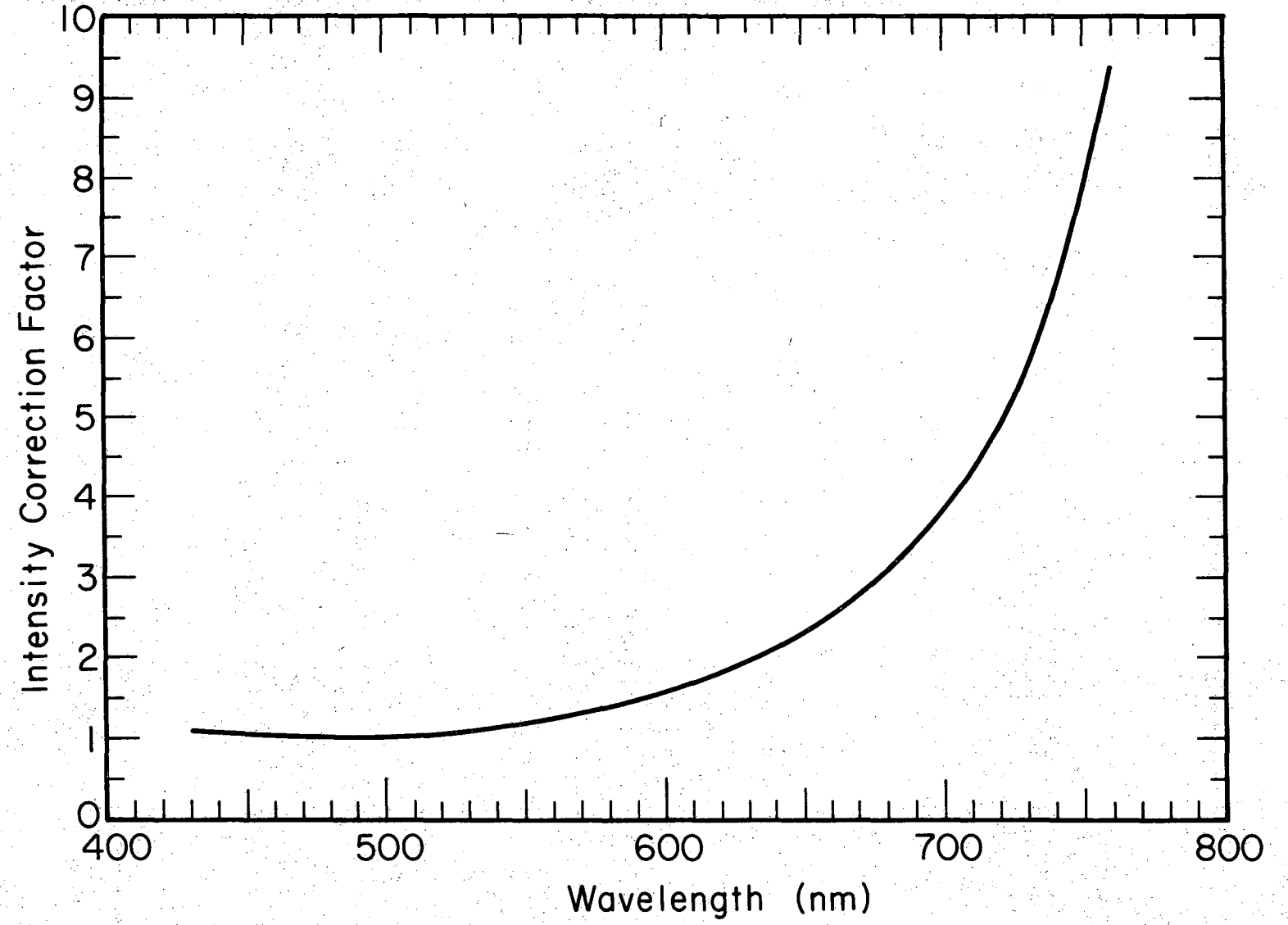

Fig. 3. Intensity correction factor applied to spectra.

were converted to punched cards for easy analysis of the data by a CDC 7600/6600 computer. Wavelength and intensity correction factors were applied to all spectra before computer analysis and plotting. Spectra were found to be highly reproducible in spite of the long scanning times.

III. RESULTS

A. Observation of Emission from Two Excited Electronic States of IF

The reaction of molecular iodine with molecular fluorine resulted in a visible yellow-green emission. The conditions under which seventeen spectra of this emission were recorded are provided in Table I. Spectra were recorded over the wavelength region 430-720 nm for various flow rates of I_2, F_2 and inert gas, Ar. Also included in Table I are the maximum intensities observed for each of the spectra in counts/sec registered by the detector.

Spectra 5 (top) and 9 (bottom) are compared in Fig. 4. All of the bands in Spectrum 5 belong to progressions of the IF($B^3\Pi_{o+} \rightarrow X^1\Sigma^+$) system described by other investigators.[1,2,3,8] Levels up to at least v' = 8 of the $B^3\Pi_{o+}$ state are populated. Table II is the Deslandres table for the B → X band system. In Spectrum 9, which was recorded under different chemical conditions than Spectrum 5, most of the intense bands belong to another band system originating in a bound electronic state of lower energy than the $B^3\Pi_{o+}$ state and terminating in the ground state of IF. Table III is the self-consistent Deslandres table for this new band system. Wavelengths of band originating in vibrational levels up to v' = 10 were measured, and bands originating in levels up to v' = 16 are indicated, these being appreciably overlapped by bands of the B → X system. This banded emission is here assigned to the IF($A^3\Pi_1 \rightarrow X^1\Sigma^+$) transition similar to that observed for Br_2, I_2, IBr and ICl[4-7]. A least squares fit of the term values to an equation of the form

$$G(v) = \omega_e(v+1/2) - \omega_e x_e(v+1/2)^2$$

Table I. Values of Flow Rates, Total Pressure, and Maximum Intensity for the Seventeen Spectra

Spectrum No.	Flow Rates (Std. cc/min)			Total Pressure (mtorr)	Maximum Intensity (counts/sec)
	I_2	F_2	Ar		
1	16.0	24	0	4.75	887
2	"	"	56	12.8	694
3	"	"	68	32.0	1230
4	"	"	89	115	2338
5	"	"	>100	310	2754
6	"	"	0	4.2	681
7	1.0	"	0	3.8	220
8	"	"	0	3.4	205
9	"	"	29	10.0	210
10	"	"	>100	180	81
11	"	"	70	18.1	240
12	23.0	"	0	5.8	939
13	"	42	"	6.7	1277
14	16.0	24	"	4.8	700
15	6.7	"	"	4.2	461
16	2.9	"	"	4.0	311
17	1.0	"	80	70.	110

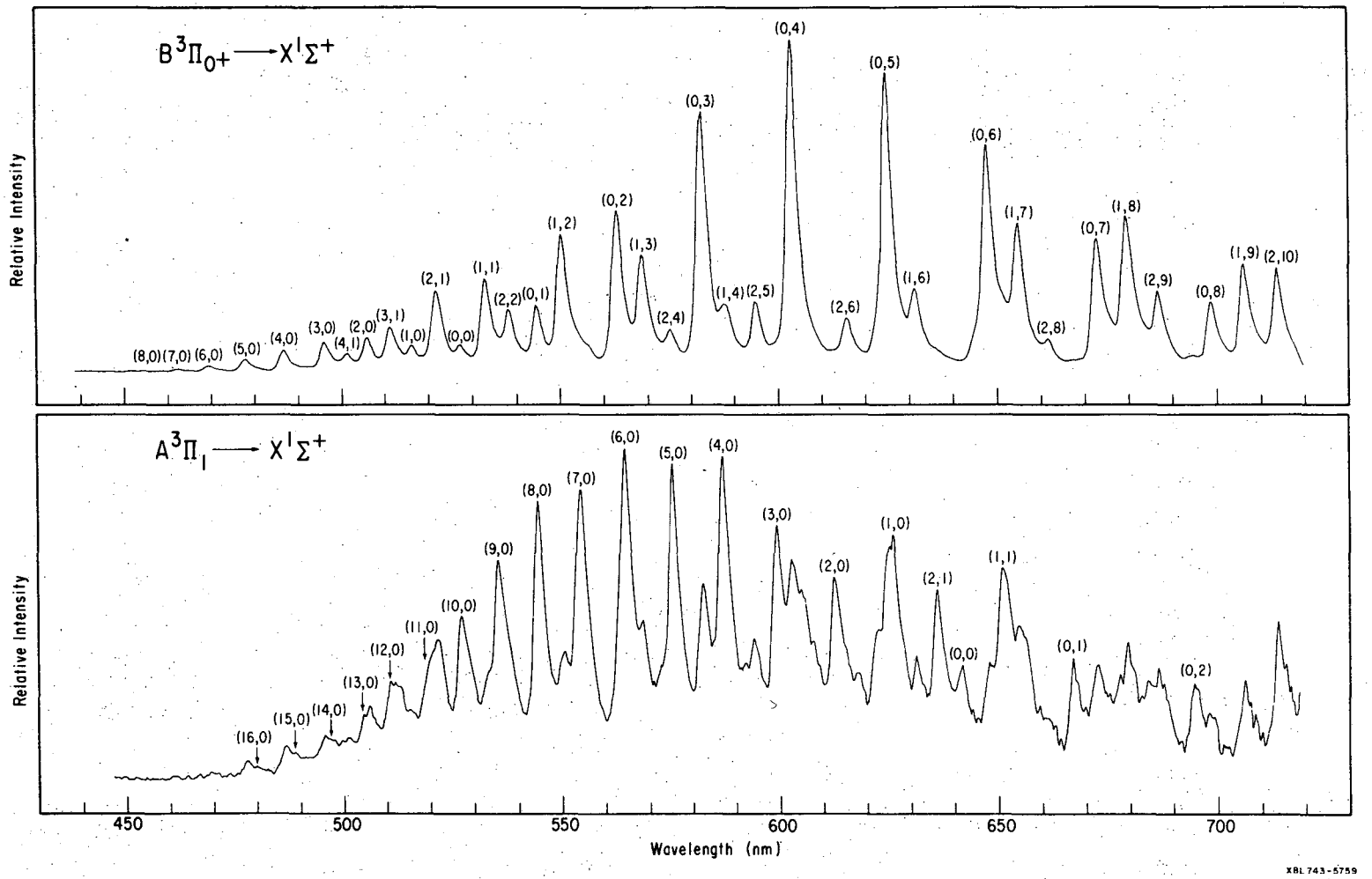

Fig. 4. Comparison of Spectra 5 (upper) and 9 (lower). Positions of the B → X emission bands are indicated in Spectrum 5, and positions of the A → X bands are indicated in Spectrum 9. As can be seen, Spectrum 9 is somewhat contaminated by emission from the B state.

Table II

Deslandres Table For IF($^3\Pi_{0^+} \longrightarrow {}^1\Sigma^+$)

v' \ v''	0		1		2		3		4		5		6		7		8		9		10
0	18955	*606*	18349	*598*	17751	*590*	17161	*585*	16576	*579*	15997	*573*	15424	*566*	14858	*560*	14300				
	404		*406*		*405*		*404*		*404*		*405*		*405*								
1	19359	*604*	18755	*599*	18156	*591*	17565	*585*	16980	*578*	16402	*573*	15829	*566*	15263	*560*	14703	*551*	14152		
	400		*399*		*399*				*400*		*398*		*395*				*401*		*398*		
2	19759	*605*	19154	*599*	18555				17380	*580*	16800	*576*	16224				15104	*554*	14550	*546*	14004
	391		*390*																		
3	20150	*606*	19544																		
	385		*387*																		
4	20535	*604*	19931																		
	377																				
5	20912																				
	369																				
6	21281																				
	360																				
7	21641																				
	349																				
8	21990																				

XBL 741-5506

Table III

Deslandres Table For $IF(^3\Pi_1 \longrightarrow {}^1\Sigma^+)$

v' \ v''	0		1		2
0	15591	(607)	14984	(598)	14386
	(371)		(370)		
1	15962	(608)	15354		
	(365)		(364)		
2	16327	(609)	15718		
	(362)				
3	16689				
	(347)				
4	17036				
	(343)				
5	17379				
	(336)				
6	17715				
	(332)				
7	18047				
	(318)				
8	18365				
	(306)				
9	18671				
	(308)				
10	18979				

XBL 741-5508

gives the results ω_e = 380.5 cm^{-1} and $\omega_e x_e$ = 3.8 cm^{-1} for the $A^3\Pi_1$ state of IF.

B. Effect of Varying the Flow Rates of I_2, F_2 and Ar on the Emission Spectra

For the nearly stoichiometric flow rates of 24 and 23 std cc/min of fluorine and iodine, respectively, a total pressure of 5.8 mtorr resulted with all of the intense bands observed belonging to the IF($B^3\Pi_{o+} \rightarrow X^1\Sigma^+$) transition. Holding the fluorine flow rate at this constant value and lowering the iodine flow rate resulted in a decrease in the emission from the $B^3\Pi_{o+}$ state while emission from the $A^3\Pi_1$ state remained constant. This is demonstrated by the series of spectra 12, 14, 15, 16 and 7 which have been decomposed into components of emission from the A and B states by comparison of the A(5,0) and B(0,3) band intensities (Fig. 5).

The effect of varying the flow rate of fluorine was not thoroughly investigated. Spectrum 13 was the only spectrum recorded in which the fluorine flow rate was varied from 24 std. cc/min. The increased flow rate of fluorine in Spectrum 13 compared to that of Spectrum 12 resulted in an increase in total intensity from 939 to 1277 counts/sec with the intensity of emission from each of the two excited electronic states increasing by the same proportion.

The effect of increased Ar pressure on the emission spectra is demonstrated by two series of spectra. In the first series, Spectra 1-5, the iodine flow rate was held at the high value of 16 std cc/min and the flow rate of Ar was successively increased. In Fig. 6 it is seen that the effect of added Ar was an increase in intensity of the B → X transition, leveling off at the highest pressures studied. The A → X emission, which was a small percentage of the total intensity observed, decreased with

increased Ar pressure. Thus at the highest pressure studied (Spectrum 5) the B → X spectrum was obtained free of any contamination by A → X emission. In a second series of spectra, Spectra 8-11 and 17, the iodine flow rate was held at the low value of 1 std cc/min and the effect of added pressure due to Ar studied. Moderate increases in Ar pressure increased the emission intensity of both the A → X and B → X systems while higher pressures severely decreased the emission from the $A^3\Pi_1$ state as shown in Fig. 7. The effect of Ar on emission from the $B^3\Pi_{o+}$ state at lower iodine flow rates is seen to be quite different from that at high iodine flow rates.

Besides increasing the total pressure in the cell, the flow of Ar reduced the pumping speed of the system and thus increased the residence times of all species. The residence time can be computed from the flow rates and total pressure assuming no change in molarity. It varied from 0.2 to 2.0 sec over the range of conditions studied. In the series of spectra in which Ar flow rates were increased while the iodine flow rate was held at the higher constant value (Spectra 1-5), the intensity of the B → X emission varied linearly with the cell residence time as can be seen in Fig. 8.

C. Determination of Vibrational Populations and Rotational Temperatures of the $B^3\Pi_{o+}$ Electronic State

If one assumes that a single rotational temperature describes the distribution of molecules among rotational levels, the intensity of a vibration-rotation line in spontaneous emission may be shown to be[10]

$$I_{v''J''}^{v'J'} = \frac{64\pi^4 B_{v'} S_{J''}^{J'}}{3hkT_r} \exp\left\{-\frac{B_{v'}J'(J'+1)}{kT_r}\right\} \nu^3 \langle v' \,|\mathrm{Re}|\, v''\rangle^2 N_{v'} \qquad (1)$$

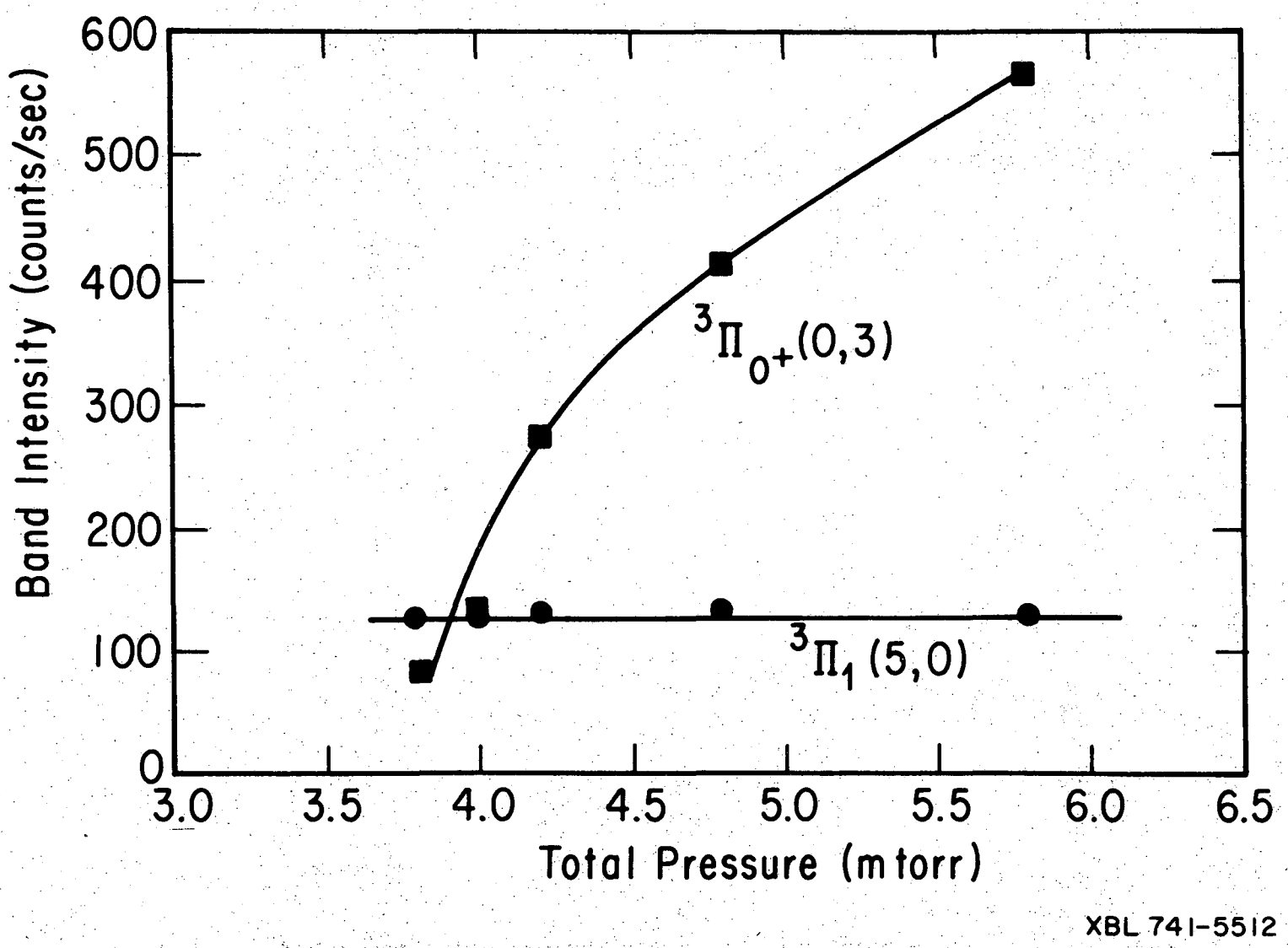

Fig. 5. Effect of pressure due to I_2 on emission from the A and B states as measured by the A(5,0) and B(0,3) band intensities.

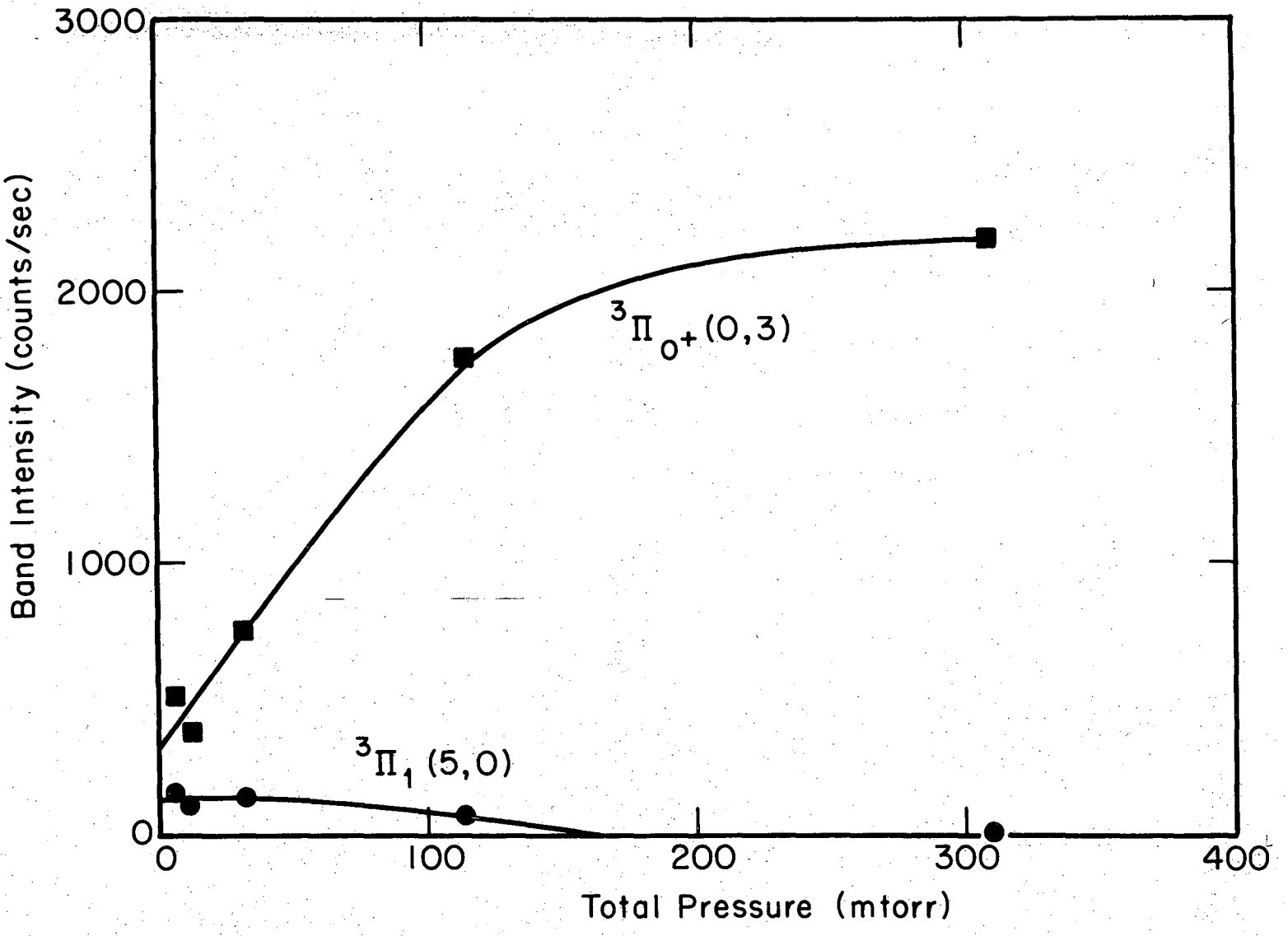

Fig. 6. Effect of increased pressure due to Ar on emission from the A and B states for the higher I_2 flow rate. Note the difference in the intensity scale between this figure and the previous figure.

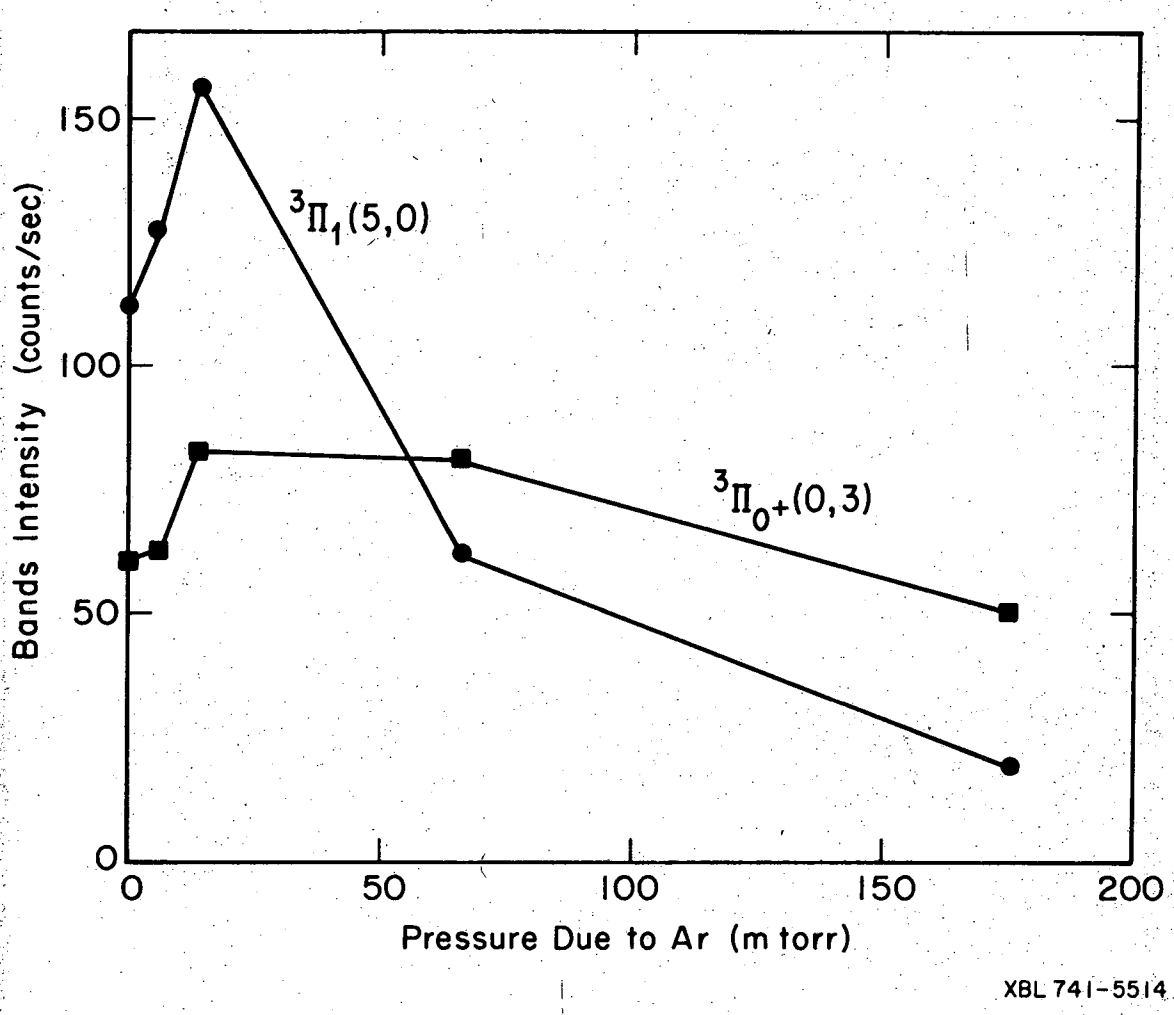

Fig. 7. Effect of pressure due to Ar on emission from the A and B states for the lower I_2 flow rate. Compare the intensity scale with that of the previous two figures.

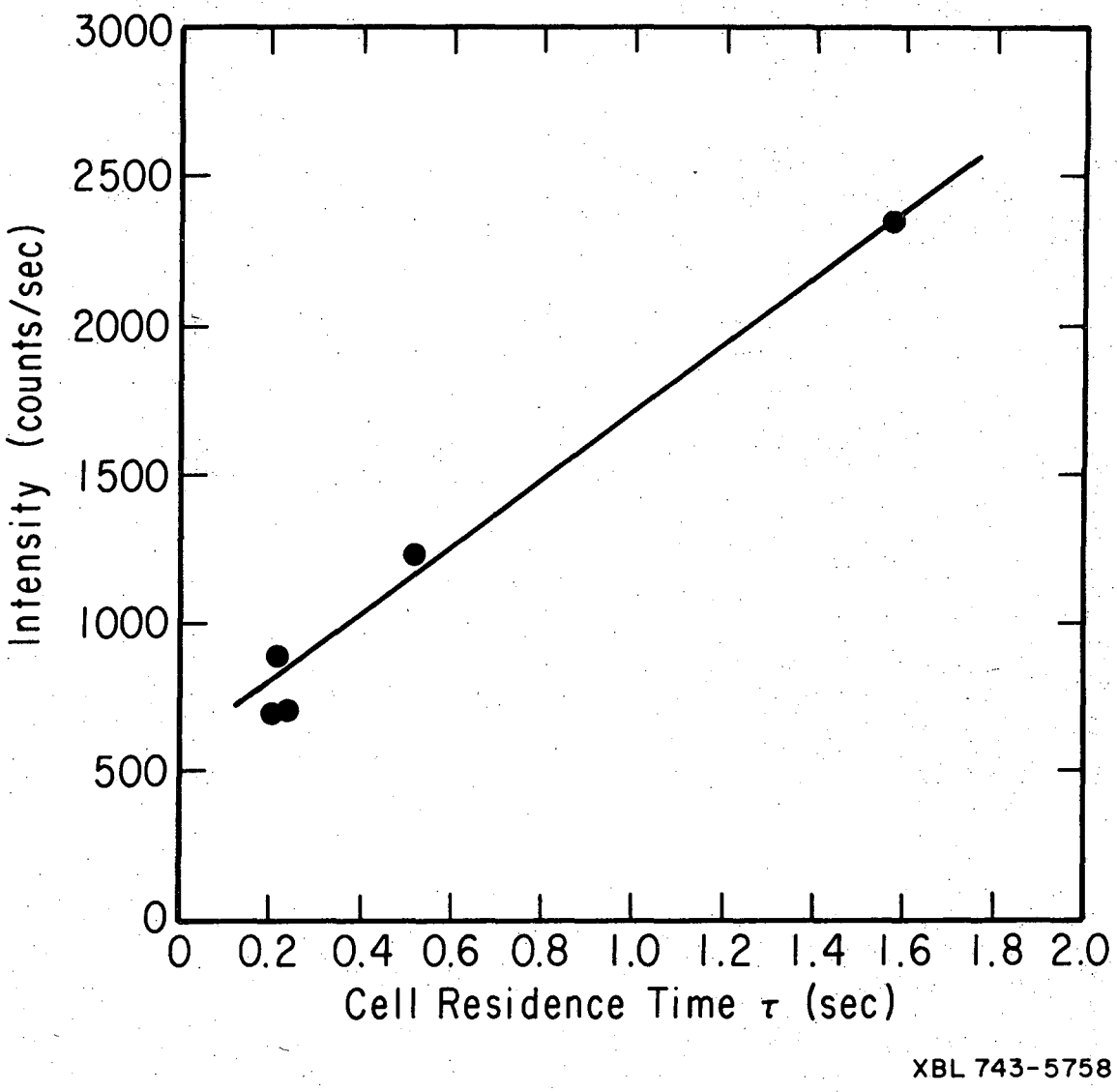

Fig. 8. Plot of the B(0,3) band intensity against the cell residence time. Compare with Fig. 6 in which a plot against pressure was strongly curved.

where $B_{v'}$ is the rotational spectroscopic constant for vibrational level v', $N_{v'}$ is the vibrational population of level v', T_r is the rotational temperature, ν is the frequency of the emission line, R_e is the transition moment and $S_{J''}^{J'}$ is the Honl-London factor. For a transition of the type of $0^+ \rightarrow 0^+$ the Honl-London factors are given by

$$\begin{aligned} R_{branch} \qquad S_{J''}^{J'} &= J' \\ P_{branch} \qquad S_{J''}^{J'} &= J' + 1 \end{aligned} \tag{2}$$

Relative vibrational populations can be determined from relative spectral intensities if the transition moment matrix elements are known. A common practice is to apply the Born-Oppenheimer[11] approximation in which the electronic wavefunction is considered to be independent of the internuclear distance. The square of the electronic transition moment may then be removed from under the integral and be considered to take on an average value $\bar{R}_e^2$.

$$\langle v' | Re | v'' \rangle^2 \approx \bar{R}_e^2 \langle v' | v'' \rangle^2 \tag{3}$$

This approximation was not found to be sufficiently accurate for the IF($B^3\Pi_{o+} \rightarrow X^1\Sigma^+$) transition. A better approximation is that due to Fraser[12] and Turner and Nicholls[13]. In this method the transition moment is considered to be a function of the average value of the internuclear distance called the $\bar{r}$- centroid. Thus,

$$\langle v' | Re(r) | v'' \rangle \approx Re^2(\bar{r}_{v'v''}) \langle v' | v'' \rangle^2 \tag{4}$$

where the $\bar{r}$-centroid is evaluated for each band in the system and is given by:

$$\bar{r}_{v'v''} = \frac{\langle v' | r | v'' \rangle}{\langle v' | v'' \rangle} \tag{5}$$

Gabelnick[8] calculated the Franck-Condon factors $\langle v'|v''\rangle$ and $\bar{r}$- centroids by the RKR method using the computer programs of Zare[14]. The results are tabulated in Table IV. The RKR potential curves for the B and X states are drawn in Fig. 9. For purposes of comparison, the A state has been drawn with arbitrary turning points.

For a given progression of bands having a common upper vibrational level the band intensities differ only by ν^3, the Franck-Condon factor, and the value of the transition moment. The square of the transition moment was evaluated as a function of the $\bar{r}$-centroid by plotting the maximum intensity of each band in a given progression of bands divided by ν^3 and the appropriate Franck-Condon factor against the $\bar{r}$-centroid for that particular band. The curve thus obtained for each progression was normalized so that the area under all such curves was the same. The normalization factors are, of course, the relative vibrational populations. Spectrum 5 was used for this determination of the transition moment as a function of the $\bar{r}$-centroid since it is free of contamination by the $A \rightarrow X$ system. Only progressions having $v' = 0,1$ and 2 could be used for this purpose since there was an insufficient number of observed bands in progressions having $v'>2$. These progressions gave values of $R_e^2(\bar{r})$ for values of $\bar{r}$ between 1.975 and 2.234 Å. Relative vibrational populations of levels $v' = 0,1$ and 2 were found to be 1.00, 0.62 and 0.46 respectively. The square of the transition moment was found to vary linearly with the $\bar{r}$-centroid as can be seen in Fig. 10. To determine the vibrational populations of levels $v' = 3$ to $v' = 8$ it was necessary to rely on a short linear extrapolation of the $R_e^2(r)$ curve to smaller values of the $\bar{r}$-centroid.

Table IV

Franck-Condon Factors and Values of the $\bar{r}$-Centroid for the B → X Band System of IF. Upper value is the Franck-Condon Factor. Lower value is the $\bar{r}$-centroid in Angstroms.

v'' \ v'	0	1	2	3	4	5	6	7	8
0	5.000-3* 2.007	2.245-2 1.991	5.302-2 1.975	8.919-2 1.960	1.195-1 1.946	1.342-1 1.932	1.316-1 1.918	1.160-1 1.905	9.456-2 1.892
1	3.039-2 2.031	9.015-2 2.014	1.307-1 1.998	1.202-1 1.983	7.176-2 1.986	2.268-2 1.953	5.947-4 1.935	7.707-3 1.928	3.008-2 1.915
2	8.784-2 2.055	1.493-1 2.038	9.737-2 2.021	1.889-2 2.003	2.891-3 1.998	3.831-2 1.978	6.704-2 1.963	6.092-2 1.949	3.343-2 1.936
3	1.602-1 2.080	1.183-1 2.061	7.914-3 2.039	2.464-2 2.032	7.322-2 2.014	5.547-2 1.998	1.153-2 1.982	1.660-3 1.980	2.405-2 1.960
4	2.065-1 2.105	3.059-2 2.084	2.965-2 2.073	8.448-2 2.053	3.050-2 2.035	1.035-3 2.038	3.567-2 2.009	5.410-2 1.994	3.098-2 1.979
5	1.998-1 2.131	3.013-3 2.125	9.732-2 2.095	2.850-2 2.074	1.032-2 2.068	5.935-2 2.046	3.822-2 2.029	1.524-3 2.003	1.303-2 2.006
6	1.507-1 2.158	6.710-2 2.142	6.683-2 2.119	7.922-3 2.112	7.015-2 2.086	2.319-2 2.066	4.745-3 2.064	4.274-2 2.041	3.920-2 2.024
7	9.057-2 2.186	1.423-1 2.168	3.554-3 2.134	7.558-2 2.130	2.783-2 2.107	1.307-2 2.101	5.573-2 2.078	1.934-2 2.059	1.904-3 2.063
8	4.400-2 2.215	1.572-1 2.195	2.915-2 2.180	6.923-2 2.154	7.234-3 2.147	6.452-2 2.119	1.037-2 2.095	1.596-2 2.092	4.550-2 2.072
9	1.742-2 2.246	1.167-1 2.224	1.103-1 2.205	6.309-3 2.171	7.149-2 2.165	1.705-2 2.139	2.450-2 2.133	4.833-2 2.111	3.729-3 2.082
10	5.667-3 2.278	6.391-2 2.254	1.478-1 2.234	2.388-2 2.218	6.012-2 2.189	1.487-2 2.180	5.769-2 2.153	8.129-4 2.101	3.269-2 2.124

*Abbreviated notation for 5.000×10^{-3}

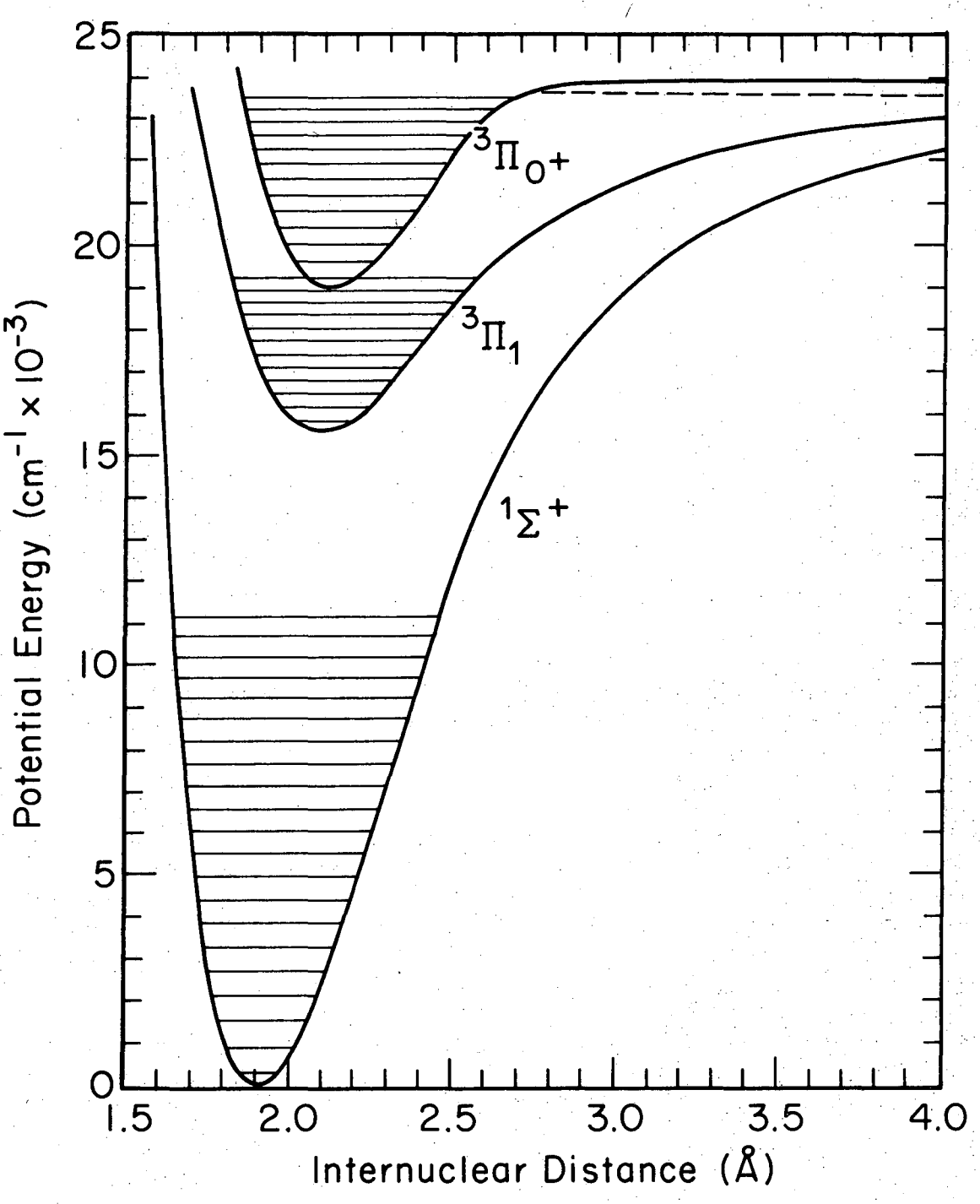

Fig. 9. Potential energy curves for the three observed electronic states of IF. The $^1\Sigma^+$ and $^3\Pi_{0^+}$ states are drawn with the calculated RKR turning points. The $^3\Pi_1$ potential curve has been drawn with arbitrary turning points. The highest positively identified vibrationally level of the $^3\Pi_1$ state is coincident with the lowest vibrational level of the $^3\Pi_{0^+}$ state. Dashed line is the assumed dissociation limit of the ground state, 23229 cm^{-1}.

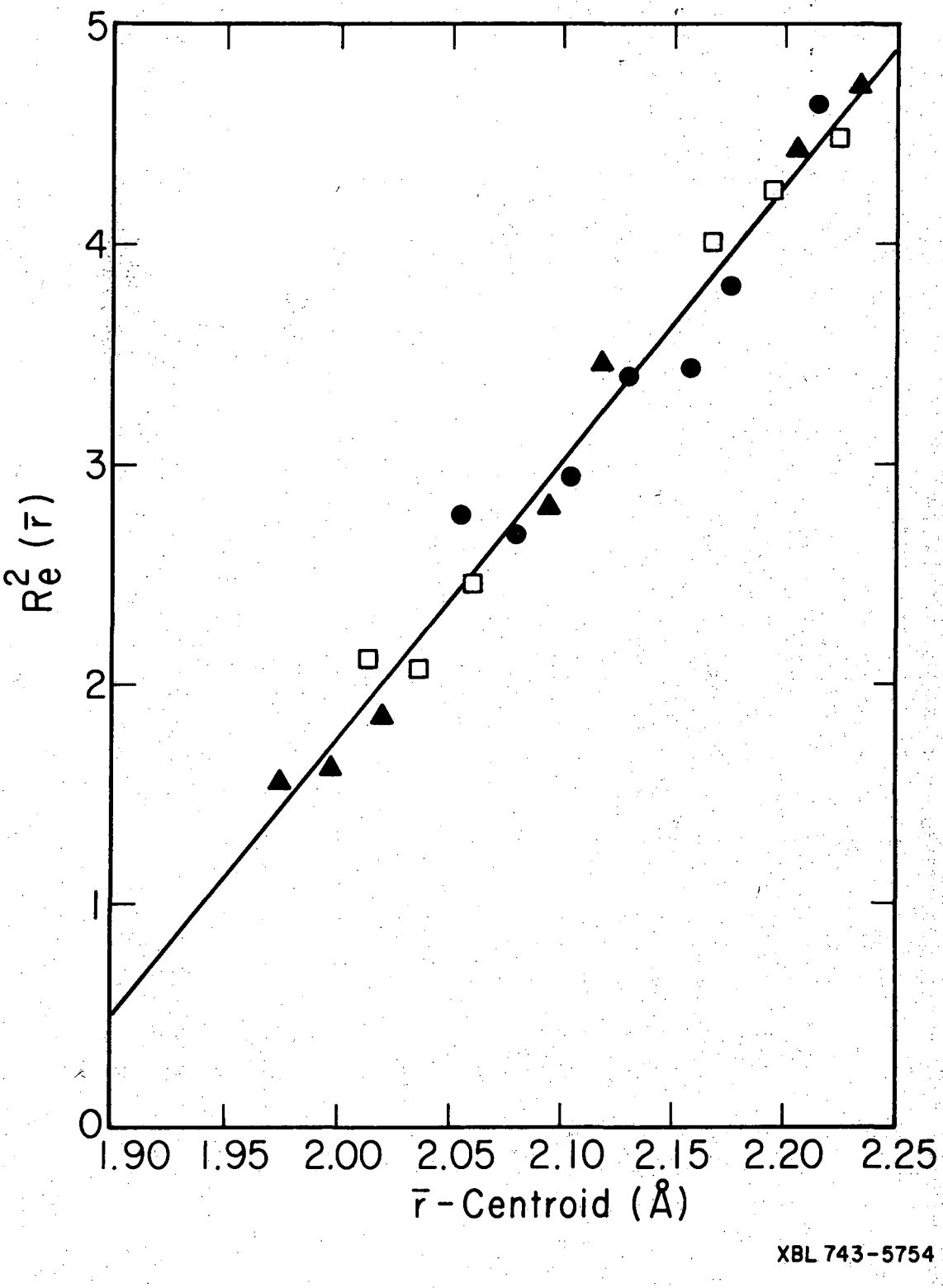

Fig. 10. Variation of the square of the transition moment with the $\bar{r}$-centroid. ● evaluated from the progression originating in v' = 0, □ evaluated from the progression originating in v' = 1, and ▲ evaluated from the progression originating in v' = 2.

For each vibrational band, theoretical band shapes were calculated for various assumed rotational temperatures by taking the convolution of the experimentally derived RC-broadened spectral slit function with the relative intensities of all rotational lines within a 20 nm envelope containing the band head. The theoretical shapes of the B(0,4) band for three rotational temperatures are given in Fig. 11. These have been normalized by the maximum band intensity. The relative rotational line intensities are given by Equation 1 without the factor $\langle v'|R_e|v''\rangle^2 N_{v'}$. By comparing the theoretical band shapes with the experimental results it was possible to determine rotational temperatures to within 100 K.

Once a rotational temperature had been decided upon, the vibrational population for levels v' = 0 to v' = 8 of the $B^3\Pi_{o+}$ state were determined by use of a least squares computer program which fit the theoretical band shapes [after multiplying the band intensities by the appropriate Franck-Condon factor and value of $R_e^2(\bar{r})$] to the ~850 spectral data points, the fitting parameters being the relative vibrational populations. In this method B_i is the total observed intensity after correction for the spectral sensitivity of the optical system, and N_j is the population of the vibrational level v' = j. We may then write

$$B_i = \sum_j A_{ij} N_j \tag{6}$$

where the term A_{ij} is the contribution to the intensity at λ_1 by all bands for which v' = j. That is,

$$A_{ij} = \Sigma\, T(j,v'') R_e^2(\bar{r}_{jv''}) \langle j|v''\rangle^2 \tag{7}$$

where $T(j,v'')$ is the intensity of the normalized band (j,v'') at wavelength λ_i.

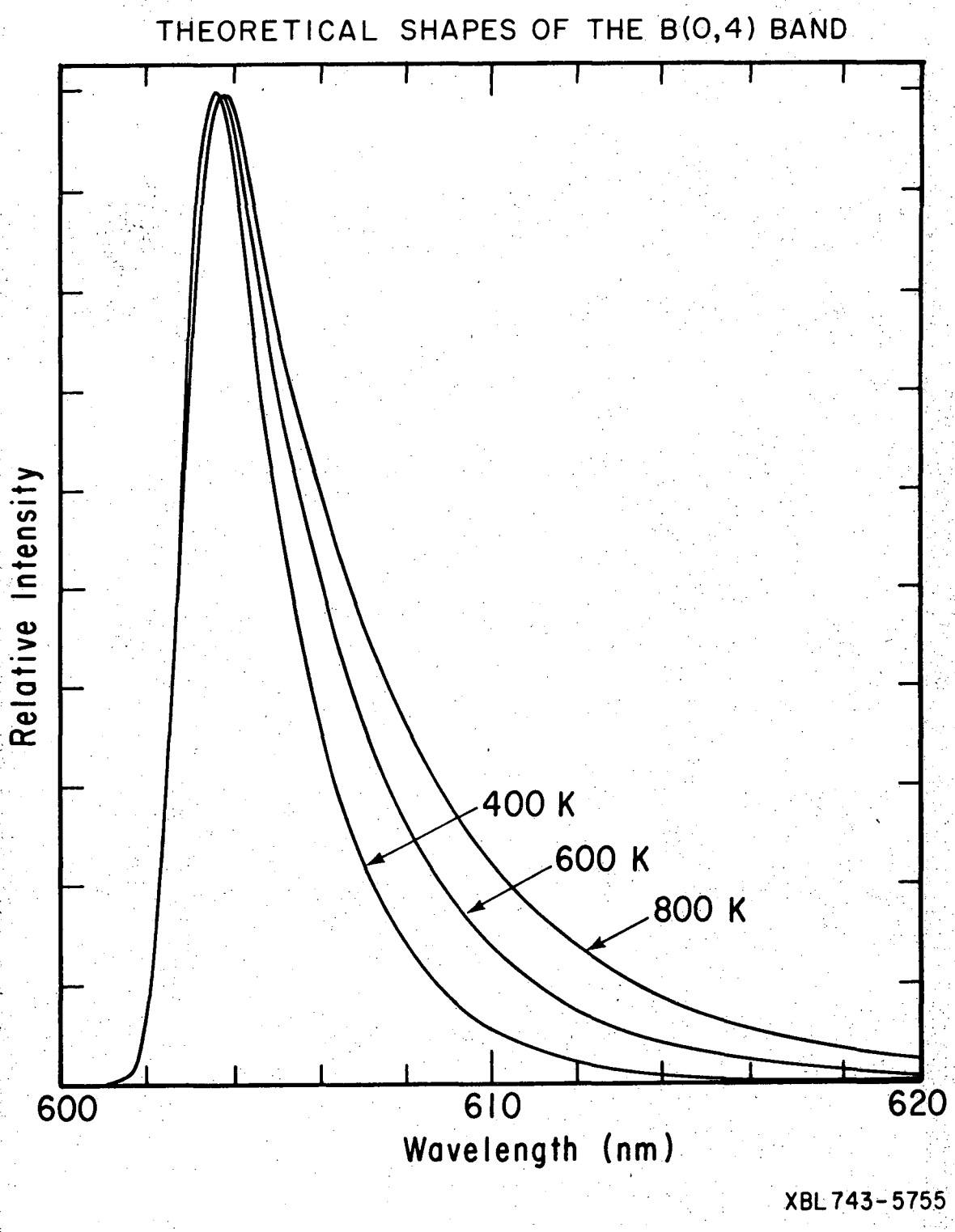

Fig. 11. Theoretical shapes of the B(0,4) band calculated for three rotational temperatures.

There are only one or two terms in the sum since there is very little overlap between bands originating in the same vibrational level. In general, the number of independent measurements of the intensity, m (∿850), is much greater than the number of fitting parameters, the vibrational populations (∿9). In order to solve the over-determined set of simultaneous equations, the method of least squares is used. A set of N_j's are found which satisfy the criteria

$$\frac{\partial}{\partial N_j} \left(\sum_{i=1}^{m} \left(B_i - \sum_{j=0}^{n-1} A_{ij} N_j \right)^2 w_i \right) = 0 \quad j = 0,1,\ldots n \tag{8}$$

where w_i is a weighting factor, chosen to be the inverse of the square of the standard deviation of the measurement. Since noise in the signal varies as the square root of the signal, the weighting factor was taken to be the reciprocal of the intensity itself. A least squares variable metric minimization program was used as a subroutine in a computer program written to determine the vibrational populations in the manner described[8].

For spectra which were overlapped by bands from the A → X transition various amounts of Spectrum 9 were subtracted from the spectrum to be fit prior to determining the vibrational populations by the least squares computer program. The fit which gave the least variance yielded the relative emission from the two excited electronic states as well as the vibrational populations of the $B^3\Pi_{o+}$ state.

Vibrational populations for Spectra 1-5 were determined in the manner just described. In this series of spectra, increasing amounts of pressure due to Ar were added with flow rates of I_2 and F_2 held constant, but the cell residence time also varied, as was previously pointed out. The vibrational populations, vibrational temperatures, rotational temperatures

and fractional amounts of $A \rightarrow X$ emission for this series of five spectra are presented in Table V. For the highest pressure spectrum (Spectrum 5) the vibrational populations can be described well by a vibrational temperature of $\sim$1250 K. At lower pressures the populations become non-Boltzmann, and the vibrational level $v' = 1$ becomes inverted over $v' = 0$.

Spectral data which have been corrected for emission from the $A^3\Pi_1$ state are compared with spectra computed from the least squares vibrational populations and theoretical band shapes in Figs. 12a-e for Spectra 1-5. There is good agreement between the computed spectra and experimentally derived spectra for Spectra 3,4, and 5. The fits to Spectra 1 and 2 are not nearly as good. This is possibly due to changes in vibrational populations of the $A^3\Pi_1$ state with pressure. That is, the low pressure Spectra 1 and 2 are contaminated by emission from the $A^3\Pi_1$ state with different vibrational populations than in Spectrum 9. As a result, correction by the use of Spectrum 9 cannot be exact. In the least squares fit some bands will be overly compensated for, while for others there is an undercompensation. This source of error does not result in a very serious effect on the calculated vibrational population of the B state, however, since the calculated vibrational populations were found to be affected only to a small extent by the amount of Spectrum 9 subtracted out.

Table V. Vibrational Populations, Vibrational Temperatures, Rotational Temperatures, and fractional amounts, f, of Spectrum 9 subtracted. Upper value is the relative vibrational population. Lower value is the calculated vibrational temperature relative to v' = 0.

v'=	Spectrum 1	Spectrum 2	Spectrum 3	Spectrum 4	Spectrum 5
0	1.00	1.00	1.00	1.00	1.00
1	1.04±.03 -1481$\bar{7}$	1.01±.02 -584$\bar{0}$	.91±.02 616$\bar{2}$	.71±.01 169$\bar{7}$	.62±.01 121$\bar{6}$
2	.81±.03 548$\bar{8}$	.78±.02 465$\bar{5}$	.73±.02 367$\bar{5}$	.49±.01 162$\bar{1}$	.46±.01 148$\bar{9}$
3	.54±.05 278$\bar{7}$	.53±.04 270$\bar{5}$	.50±.03 247$\bar{8}$	.30±.02 240$\bar{8}$	.27 ±.02 131$\bar{2}$
4	.36±.06 222$\bar{5}$	.33±.05 205$\bar{0}$	.32±.04 199$\bar{5}$	.18±.02 132$\bar{5}$	.16±.03 124$\bar{0}$
5	.21±.08 180$\bar{4}$	.17±.06 158$\bar{9}$	.19±.05 169$\bar{5}$	.11±.03 127$\bar{5}$	.10±.03 122$\bar{3}$
6	.14±.09 170$\bar{2}$	.09±.07 138$\bar{9}$	.12±.06 157$\bar{8}$	.06±.04 118$\bar{9}$	.06±.04 118$\bar{9}$
7	.06±.13 137$\bar{3}$	.03±.10 110$\bar{2}$	.04±.08 120$\bar{0}$	.03±.05 110$\bar{2}$	.04±.06 120$\bar{0}$
8	.01±.26 94$\bar{8}$	.01±.25 94$\bar{8}$	.02±.19 111$\bar{6}$	<.01	.03±.14 124$\bar{5}$
f	.47	.45	.34	.14	0.
T_r	400-500 K	400-500 K	~500 K	~500 K	500-600 K

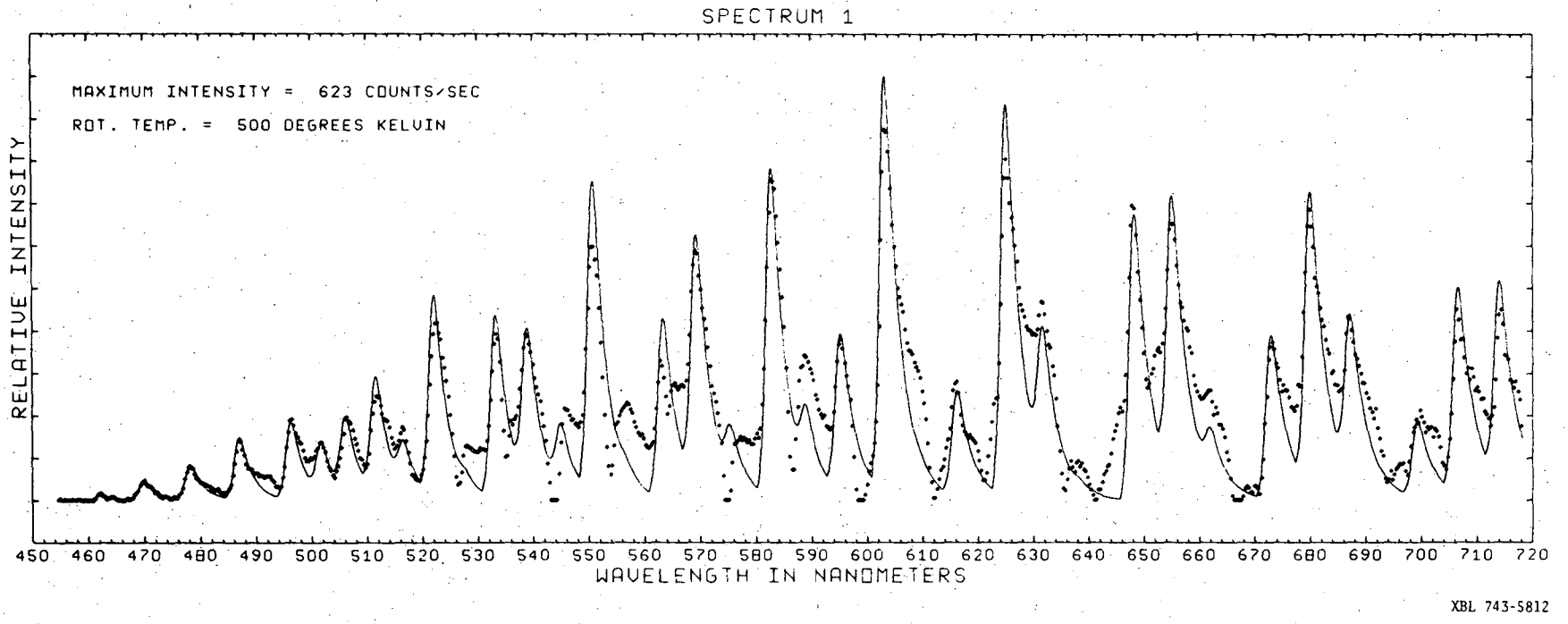

Fig. 12. a. Comparison of computed spectrum with the observed points for Spectrum 1. Fractional amount of Spectrum 9 subtracted from data points is 0.47. Total pressure for this spectrum is 4.75 mTorr.

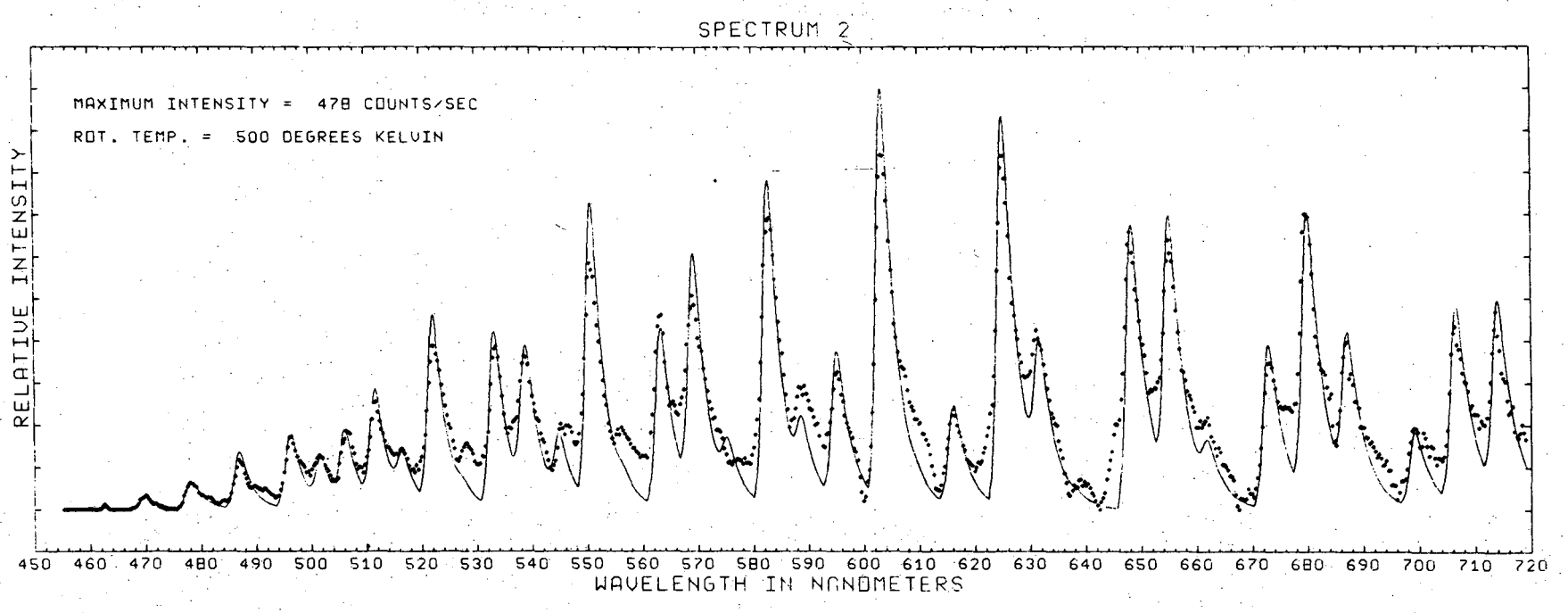

Fig. 12. b. Comparison of computed spectrum with the observed points for Spectrum 2. Fractional amount of Spectrum 9 subtracted from data points is 0.45. Total pressure for this spectrum is 12.8 mTorr.

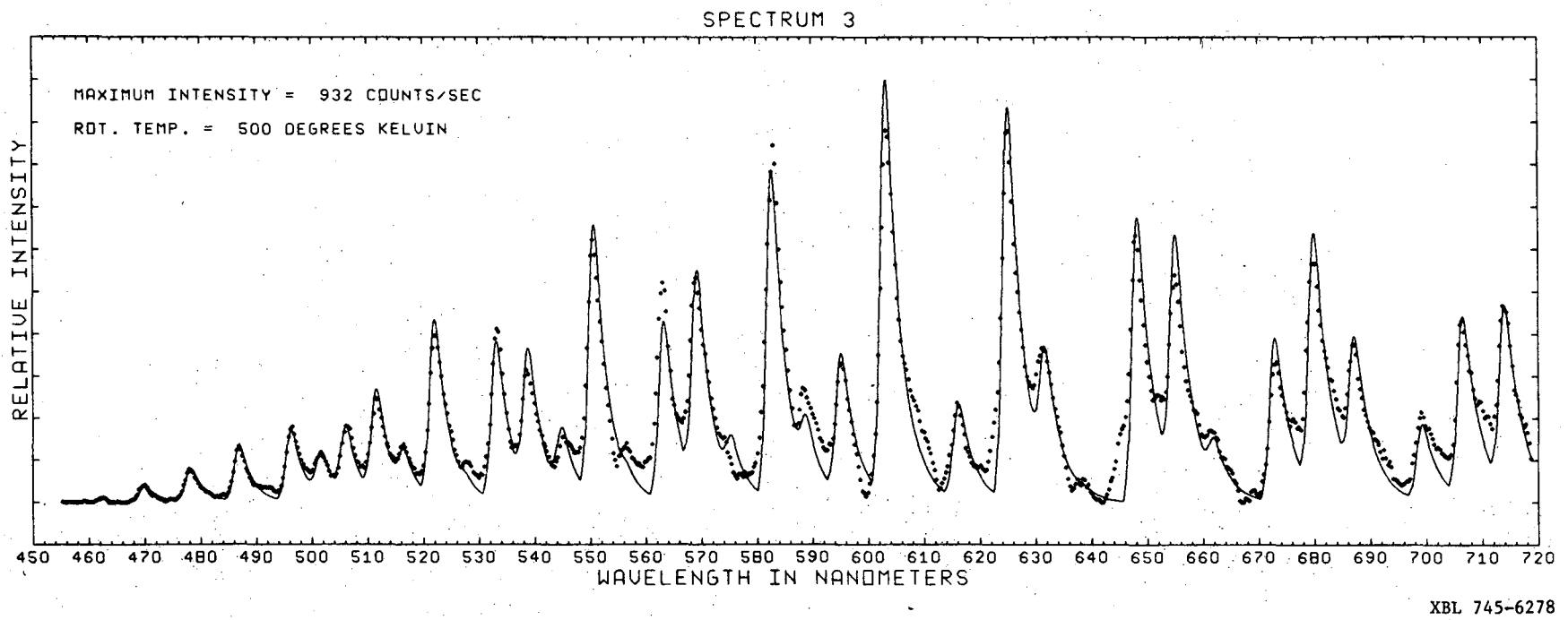

Fig. 12. c. Comparison of computed spectrum with the observed points for Spectrum 3. Fractional amount of Spectrum 9 subtracted from data points is 0.34. Total pressure for this spectrum is 32.0 mTorr.

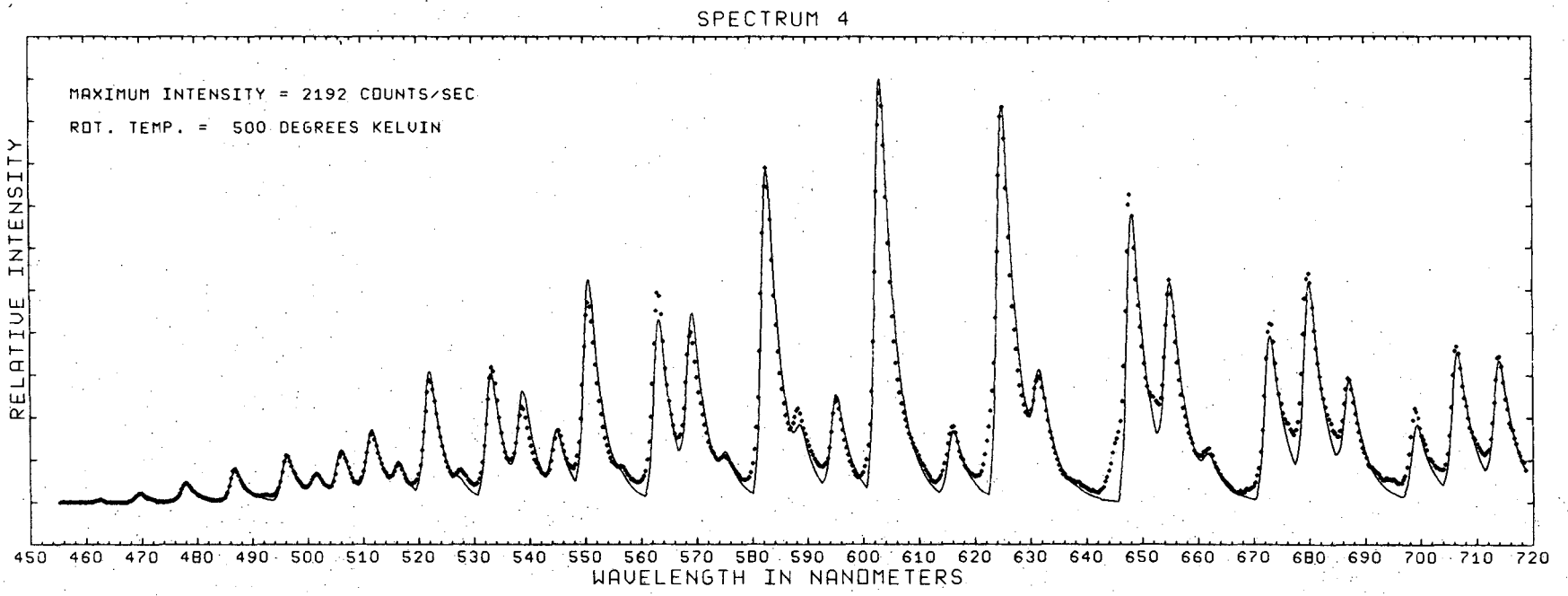

Fig. 12. d. Comparison of computed spectrum with the observed points for Spectrum 4. Fractional amount of Spectrum 9 subtracted from data points is 0.14. Total pressure for this spectrum is 115. mTorr.

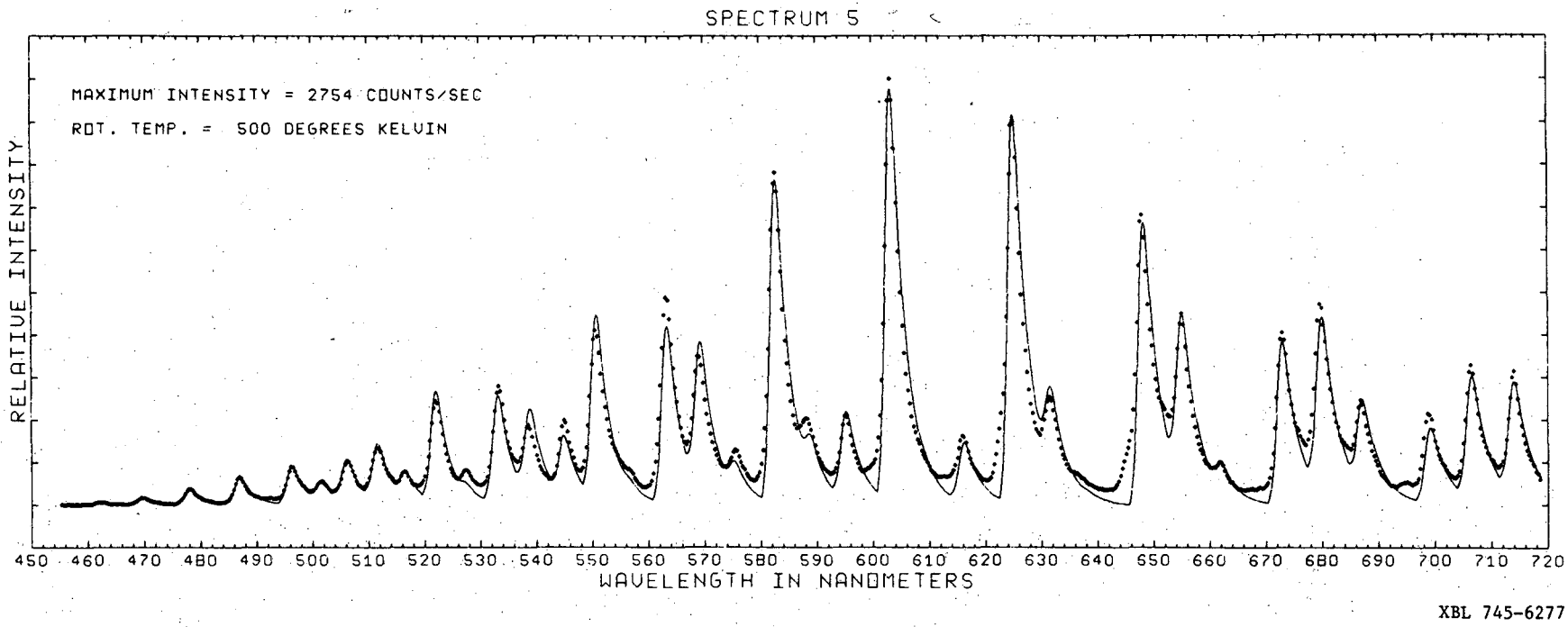

Fig. 12. e. Comparison of computed spectrum with the observed points for Spectrum 5. No correction for emission from the $A\,^3\Pi_1$ state was required. Total pressure for this spectrum is 310. mTorr.

IV. DISCUSSION

A. Introduction

All of the banded emission and absorption spectra of the halogen and interhalogen diatomic molecules have been successfully assigned thus far as transitions between the ground $X^1\Sigma^+$ state and a $B^3\Pi_{o+}$ or $A^3\Pi_1$ excited electronic state. Transitions between the ground electronic state and the $^3\Pi_{o-}$ and $^3\Pi_2$ states have not been observed apparently due to operation of the selection rules + ↮ - and $\Delta\Omega = 0, \pm 1$. The spin selection rule, $\Delta S = 0$, does not hold strictly for heavy halogen molecules in which there is strong spin-orbit coupling. The $A^3\Pi_1$ state correlates with ground state atoms, and the $B^3\Pi_{o+}$ state correlates with one ground state $^2P_{3/2}$ atom and one spin-orbit excited $^2P_{1/2}$ atom. For interhalogen molecules XY there are two $^3\Pi_{o+}$ states that correlate with $X(^2P_{1/2})$ and $Y(^2P_{1/2})$ products, respectively. There is also a repulsive state of 0^+ symmetry that correlates with ground state atoms. Interaction of the $B^3\Pi_{o+}$ state with this $Y(0^+)$ state can lead to the formation of a new $B'(0^+)$ state as in the cases of IBr[16], ICl[17], and BrF[18].

In rotationally resolved emission spectra it is possible to distinguish between the two transitions $B^3\Pi_{o+} \longrightarrow X^1\Sigma^+$ and $A^3\Pi_1 \longrightarrow X^1\Sigma^+$ since the first has no Q branch. This is due to the selection rule: $\Delta J = 0, \pm 1$ with the exception $\Delta J = 0$ (Q branch) is forbidden for $\Omega = 0 \longrightarrow \Omega = 0$ transitions. The $A^3\Pi_1 \longrightarrow X^1\Sigma^+$ emission has P, Q, and R branches corresponding to $\Delta J = -1$, 0 and + 1.

B. Previous Results for Halogen and Interhalogen Emission Spectra

Fluorine

No emission has been observed from the recombination of ground state fluorine atoms. Continuous absorption to the $^1\Pi_{1u}$ state occurs with a maximum at 34500 cm^{-1}.[10] The operation of the case (a) selection rule $\Delta S = 0$ apparently prohibits combination of the $X^1\Sigma^+$ state with either the $B^3\Pi_{o+}$ or $A^3\Pi_1$ state in this light molecule for which spin-orbit coupling is expected to be weak compared to coupling of the spin and orbital angular momenta to the internuclear axis.

Chlorine

Emission from the recombination of ground state chlorine atoms has been observed and studied by Bader and Orgryzlo[21] (1964), Hutton and Wright[22] (1965), Clyne and Coxon[6] (1967), and Browne and Orgryzlo[7] (1970). The emission has been found to originate in the $B^3\Pi_{o+}$ electronic state despite the fact that this electronic state does not correlate with ground state atoms. In these studies ground state chlorine atoms were generated by microwave discharge. No emission from the $A^3\Pi_1$ electronic state, which does correlate with ground state atoms, has been observed.

Bromine

Emission from the recombination of ground state bromine atoms has been studied by Gibbs and Orgryzlo[23] (1965), Clyne and Coxon[4] (1967), Browne and Oryzlo[7] (1970), and Clyne, Coxon, and Woon-Fat[5] (1971). The predominant emission was found to be due to the $A^3\Pi_1 \longrightarrow X^1\Sigma^+$ transition and weaker emission was assigned to $B^3\Pi_{o+} \longrightarrow X^1\Sigma^+$.

Iodine

Of the halogens and interhalogens the energy states of iodine have been studied most intensely. Emission from the direct association of an excited $^2P_{1/2}$ atom with a ground state $^2P_{3/2}$ atom, attributed to the $B^3\Pi_{o+u} \longrightarrow X^1\Sigma_g^+$ transition, has been studied by Abrahamson, Hussain, and Wiesenfeld[24] (1968). In these experiments $^2P_{1/2}$ atoms were generated by flash photolysis of CF_3I. Browne and Ogryzlo[7] (1970) assigned emission from the recombination of ground state iodine atoms to the $B^3\Pi_{1u} \longrightarrow X^1\Sigma_g^+$ transition. Predissociation for $v'>24$ of the $B^3\Pi_{o+}$ state is believed to be due to crossing of the $B^3\Pi_{o+}$ state by a repulsive $^3\Sigma_u^+$ state which correlates with two $^2P_{3/2}$ ground state atoms and belongs to the molecular orbital configuration $\sigma_g^2\pi_u^3\pi_g^3\sigma_u^2$ In case (c) terminology the $^3\Sigma_u^+$ state is a 0_u^- state.

Chlorine Monofluoride

Recombination of chlorine and fluorine atoms has not been reported. The $^3\Pi_{o+}$ state has been observed in absorption with predissociation occuring for $v' = 11$, 12, and 13.[10]

Bromine Monofluoride

Durie[1] (1951) reported the low resolution emission spectrum of BrF in a bromine-fluorine flame and found the bands to coincide with those of the previously reported high resolution absorption spectrum assigned to the $B^3\Pi_{o}^+ \longleftarrow X^1\Sigma^+$ transition. Clyne, Coxon, and Townsend[3] (1972) reported emission from the $B^3\Pi_{o}^+$ state of BrF produced from ground state atoms in the presence of singlet $\left(^1\Delta_g, {}^1\Sigma_g^+\right)$oxygen. Formation of BrF ($B^3\Pi_{o}^+$) explicitly required energy transfer from singlet oxygen.

Iodine Monofluoride

The diatomic molecule IF was discovered in 1950 by Durie[1] who recorded the emission spectrum which accompanies the reaction of fluorine with iodine, methyl iodide, and other substances containing iodine. The assignment of the emission to the $B^3\Pi_{0^+} \longrightarrow X^1\Sigma^+$ transition of IF was confirmed by Durie[2] in 1965 upon publication of the rotationally resolved spectrum. Gabelnick[8] (1969) studied the emission from the gas phase reaction of I_2 with F_2 under low resolution, and computed Franck-Condon factors and the transition moment for the $B^3\Pi_{0^+} \longrightarrow X^1\Sigma$ transition. In his lowest pressure spectra Gabelnick observed a number of unknown bands, which due to the present work can be assigned to the $A^3\Pi_1 \longrightarrow X^1\Sigma^+$ transition. Gabelnick computed vibrational populations of the $B^3\Pi_{0^+}$ emitting state for total pressures varying from 20 to 200 mtorr and found very little change in the vibrational populations over this pressure range. Clyne, Coxon, and Townsend[3] (1972) have also reported emission from the $B^3\Pi_{0^+}$ state of IF in the reaction of $I(^2P_{3/2})$ and $F(^2P_{1/2,\ 3/2})$ atoms in the presence of singlet ($^1\Delta_g$, $^1\Sigma_g^+$) oxygen. Their spectra were characterized by a higher vibrational temperature than those of Durie, possibly due to less vibrational relaxation in the absence of molecular halogens.

Bromine Monochloride

Emission from the $B^3\Pi_{0^+}$ state of BrCl has been reported by Clyne and Coxon[6,25] (1966) for the reaction between bromine atoms and ClO_2 and for the reaction of ground state bromine and chlorine atoms.

Iodine Monochloride

The association of ground state iodine and chlorine atoms was found to be chemiluminescent by Clyne and Coxon[6] (1966) with emission due to

the $A^3\Pi_1 \longrightarrow X^1\Sigma^+$ transition. In the case of ICl it has been shown by absorption spectra that there is a definate potential maximum in the $B^3\Pi_{0^+}$ potential energy curve due to a crossing of this curve by a repulsive state of 0+ symmetry correlating with ground state atoms.[17] This has also been shown to be true of BrCl[26] and IBr.[16]

Iodine Monobromide

Clyne and Coxon[4] (1967) found the emission spectrum resulting from the combination of ground state iodine and bromine atoms to belong to the $A^3\Pi_1 \longrightarrow X^1\Sigma^+$ system.

C. Assignment of Emission to Electronic States and Discussion of the Ground State Dissociation Energy of IF

The determination of the bond energy of IF by a Birge-Sponer extrapolation is not possible since the energies of too few vibrational levels of the ground state are known from the emission spectrum. The Birge-Sponer plot for the ground state is given by Fig. 13 and results in a dissociation energy of 27000 cm^{-1}. Indicated on the graph is the possibility of a much lower value for the dissociation energy of 17000 cm^{-1} for the case of extreme curvature. Such extreme curvature usually occurs when there is an avoided curve crossing, which is not possible for the ground state. There is usually some curvature in ground state Birge-Sponer extrapolations due to contribution of terms higher than squared terms to the Taylor Expansion for the energy expression. Generally, the true dissociation energy of diatomic molecules is 10-20% less than the value obtained from a long Birge-Sponer extrapolation. Based on the extrapolation for IF we would expect the ground state dissociation energy to lie between 21600 cm^{-1} and 24300 cm^{-1}.

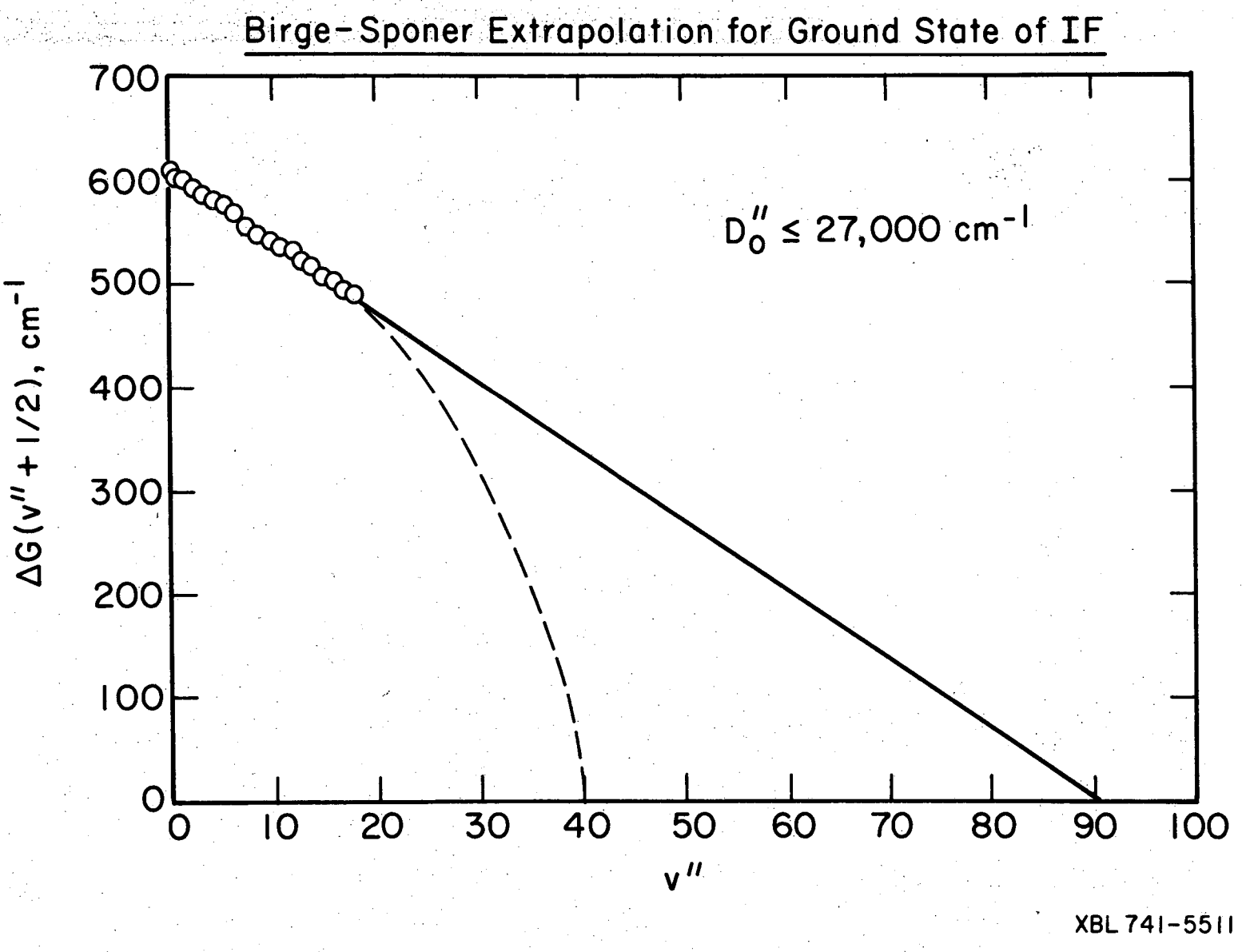

Fig. 13. Birge-Sponer extrapolation for the ground state. The long extrapolation leads to an upper limit of 27,000 cm^{-1} for the dissociation energy. The dashed line indicates the possibility of a considerably lower dissociation energy.

The accurate determination of the dissociation energy for the halogens and interhalogens has in most cases been accomplished by means of a Birge-Sponer extrapolation of one of the excited electronic states. One requires in addition knowledge of the frequency of the (0,0) band and the dissociation products of the upper state. If the upper electronic state is that of $^3\Pi_1$ there is no problem since both this state and the ground state dissociate to ground state atoms. In the case of a $^3\Pi_{0^+}$ upper state, however, there are two possibilities for the dissociation products. Durie[2] obtained the value 4680 $\pm$ 100 cm^{-1} for the dissociation energy of the $B^3\Pi_{0^+}$ state of IF by means of the strongly curved Birge-Sponer extrapolation shown in Fig. 14, and concluded that the dissociation energy for the ground state of IF must be either 16035 $\pm$ 100 cm^{-1} or 23299 $\pm$ 100 cm^{-1} depending upon the dissociation products of the upper state as illustrated in Fig. 15. A new band system belonging to an excited electronic state whose minimum lies 3348 cm^{-1} below the minimum in the $B^3\Pi_{0^+}$ potential energy curve has been described here. This new band system may originate in the $A^3\Pi_1$ state, or in the case that the $B^3\Pi_{0^+}$ state correlates with I* + F it may be the lower lying $^3\Pi_{0^+}$ state correlating with I + F*. At least eight vibrational levels of this new state lie above both the value 16035 cm^{-1} and the value 16439 cm^{-1} which are the dissociation limits for the $A^3\Pi_1$ state and the lower lying $^3\Pi_{0^+}$ state in the case that the $B^3\Pi_{0^+}$ state correlates with I* + F. Thus it would follow that the $B^3\Pi_{0^+}$ state must correlate with I + F*, and the new band system originates in the $A^3\Pi_1$ state.

The reliability of the graphical Birge-Sponer extrapolation for the

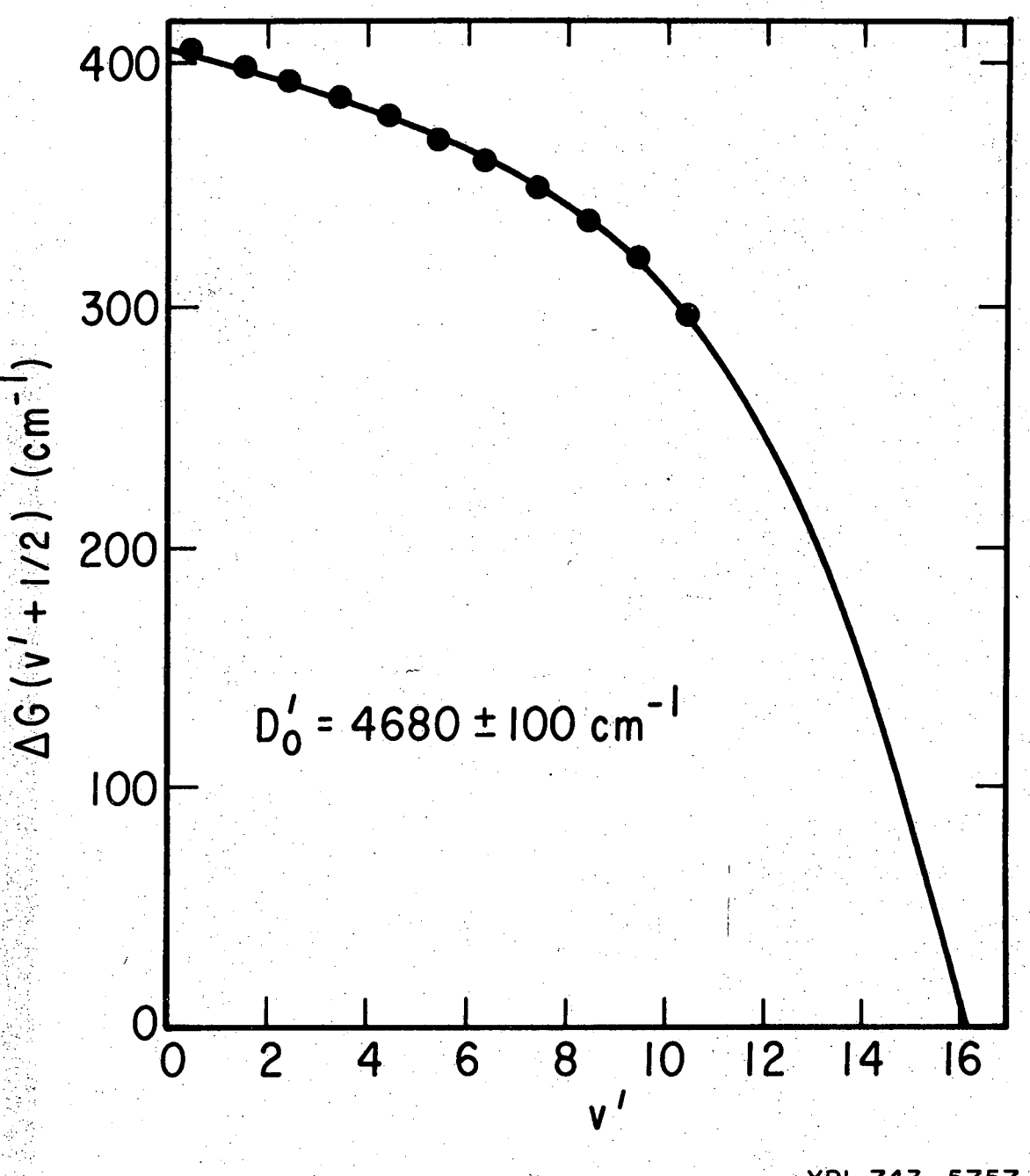

Fig. 14. Birge-Sponer extrapolation for the $B^3\Pi_{0^+}$ state of IF. The strong curvature in this plot is suggestive of an avoided curve crossing.

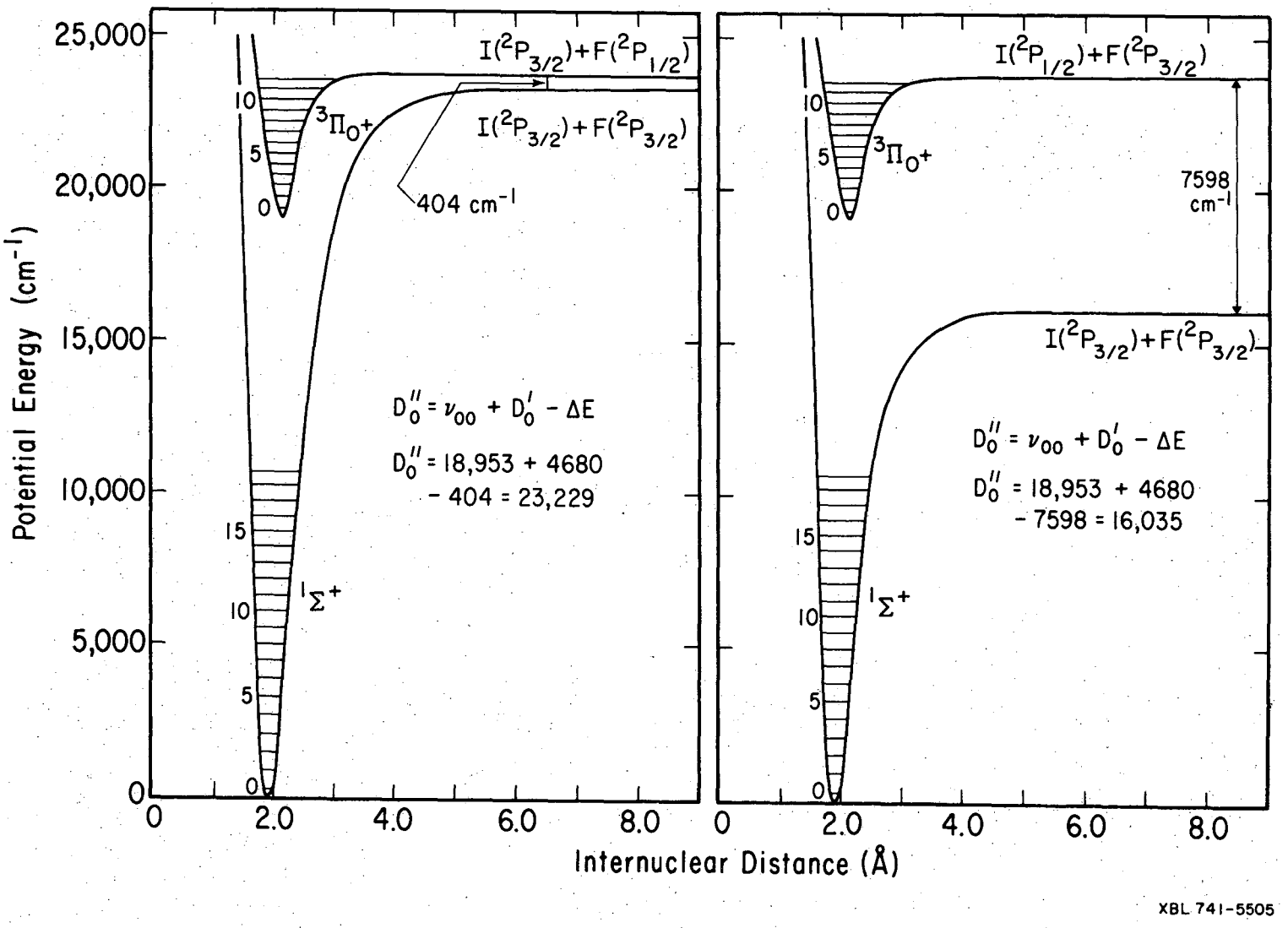

Fig. 15. Combining the dissociation energy of the $B^3\Pi_{0^+}$ state with the energy of the (0,0) band and subtracting the two possible spin-orbit excitation energies leads to the possible values of 23,229 cm^{-1} and 16,035 cm^{-1} for the ground state dissociation energy of IF.

$B^3\Pi_{o^+}$ state of IF is questionable, however, since a similar extrapolation by Durie[1] for the $B^3\Pi_{o^+}$ state of BrF was found by Brodersen and Sicre[18] to be low due to the crossing of the $B^3\Pi_{o^+}$ state by a repulsive $Y(0^+)$ curve correlating with ground state atoms. In the absorption spectrum Brodersen and Sicre[18] found the convergence limits of both the $A^3\Pi_1 \leftarrow X^1\Sigma^+$ system and the $B^3\Pi_{o^+} \leftarrow X^1\Sigma^+$ system observed in emission by Durie[1]. The difference in the convergence limits differed by a value of 3748 ± 60 cm^{-1} which is very close to the excitation energy of a $Br(^2P_{1/2})$ atom (3865 cm^{-1}). They found that all vibrational levels from $v' = 6$ to $v' = 15$ were strongly perturbed by another electronic state in the vicinity of $v' = 12$. This perturbation led to an anomalously low estimate by Durie[1] for the dissociation energy of the $B^3\Pi_{o^+}$ state of BrF since he observed levels up to only $v' = 9$ in emission.

In the case of IF, Durie[2] found that predissociation begins at $J = 45$ in the $v' = 11$ level of the $B^3\Pi_{o^+}$ state, thus establishing that the ground state dissociation energy of IF is definitely less than 23441 cm^{-1}. No emission was observed from $v' = 12$ or higher levels and there were only slight perturbations in the rotational constants for the $v' = 9$ and 10 levels. No predissociation occured in the $v' = 9$ and 10 levels even though rotational levels far above the predissociation limit were observed. The onset of predissociation at 23341 cm^{-1} is highly coincident with the higher value for the ground state dissociation energy of 23229 cm^{-1} once the rotational energy barrier of 94 cm^{-1} for $J = 45$ is taken into account. Durie[2] argued that this suggested that the $B^3\Pi_{o^+}$ state is perturbed by a state crossing nearly horizontally quite unlike the cases of

BrF[18], IBr[16] and ICl[17]. Child and Bernstein[19] have pointed out several systematic trends in the potential energy curves for the halogens and interhalogens. For example, the dissociation energies of the $B^3\Pi_{o^+}$ states of I_2, IBr and ICl are 4507 cm^{-1}, 2243 cm^{-1} and 799 cm^{-1} respectively. These states all correlate with a ground state I atom, the remaining atom being spin-orbit excited. This suggests that the $^3\Pi_{o^+}$ state of IF correlating with a ground state I atom and a spin-orbit excited F* atom is at best very weakly bound. For this reason Child and Bernstein[19] concluded that the $B^3\Pi_{o^+}$ state correlates with a ground state F atom and an excited I* atom, the low convergence limit being due to a crossing with a repulsive state of 0^+ symmetry resulting in a potential maximum as illustrated by Fig. 16. This would lead to a much stronger perturbation in the rotational structure than that observed by Durie[2], however, since such a crossing would be expected to perturb many vibrational levels. Also, for this case the ground state dissociation energy is uncertain and is only known to lie between the values 16035 cm^{-1} and 23229 cm^{-1}. A scheme is proposed here which is consistent with the type of predissociation observed by Durie[2]. This scheme is illustrated by Fig. 11b in which a weakly bound $^3\Pi_{o^+}$ state correlating with a ground state I atom and a spin-orbit excited F* atom has been added to Fig. 17 resulting in an additional avoided curve crossing. Thus, the spectroscopically observed $B^3\Pi_{o^+}$ state correlates diabatically with I* + F and adiabatically with I + F* according to this scheme. The forced correlation would result in strong curvature of the Birge-Sponer extrapolation as was observed, and predissociation would be expected to begin at an energy slightly larger than the

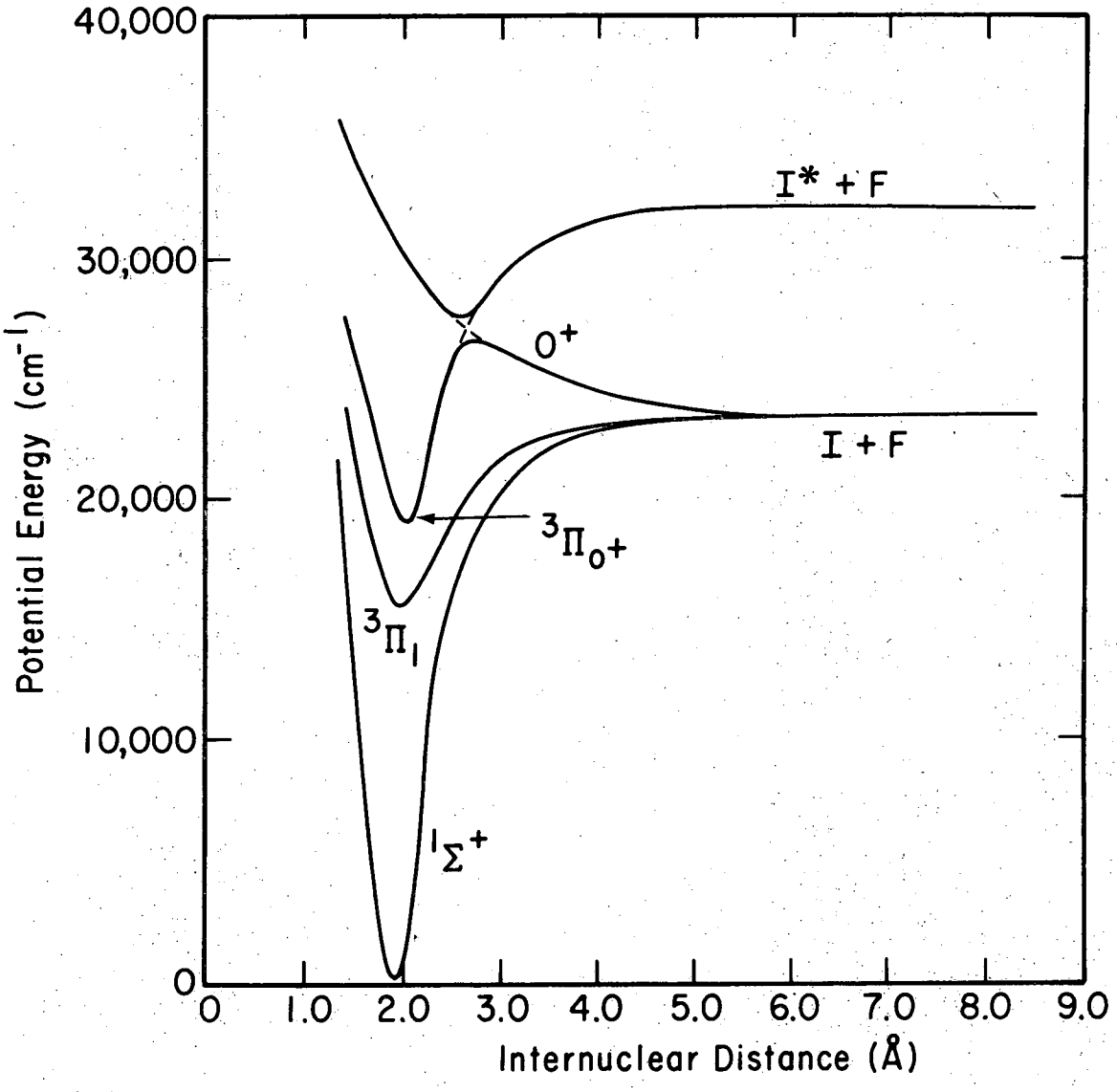

XBL 746-6539

Fig. 16. Potential energy curves drawn for IF in the case that the $B^3\Pi_{0^+}$ state correlates adiabatically with I* + F. The $B^3\Pi_{0^+}$ state is forced to correlate diabatically with ground state atoms due to an avoided crossing with a repulsive state of 0^+ symmetry. In this case the ground state dissociation energy is only known to lie between the values 16035 cm^{-1} and 23229 cm^{-1}. Predissociation in the emission spectra would be expected to begin well below the convergence limit, however, due to tunneling through the potential barrier as in the case of BrF.[18]

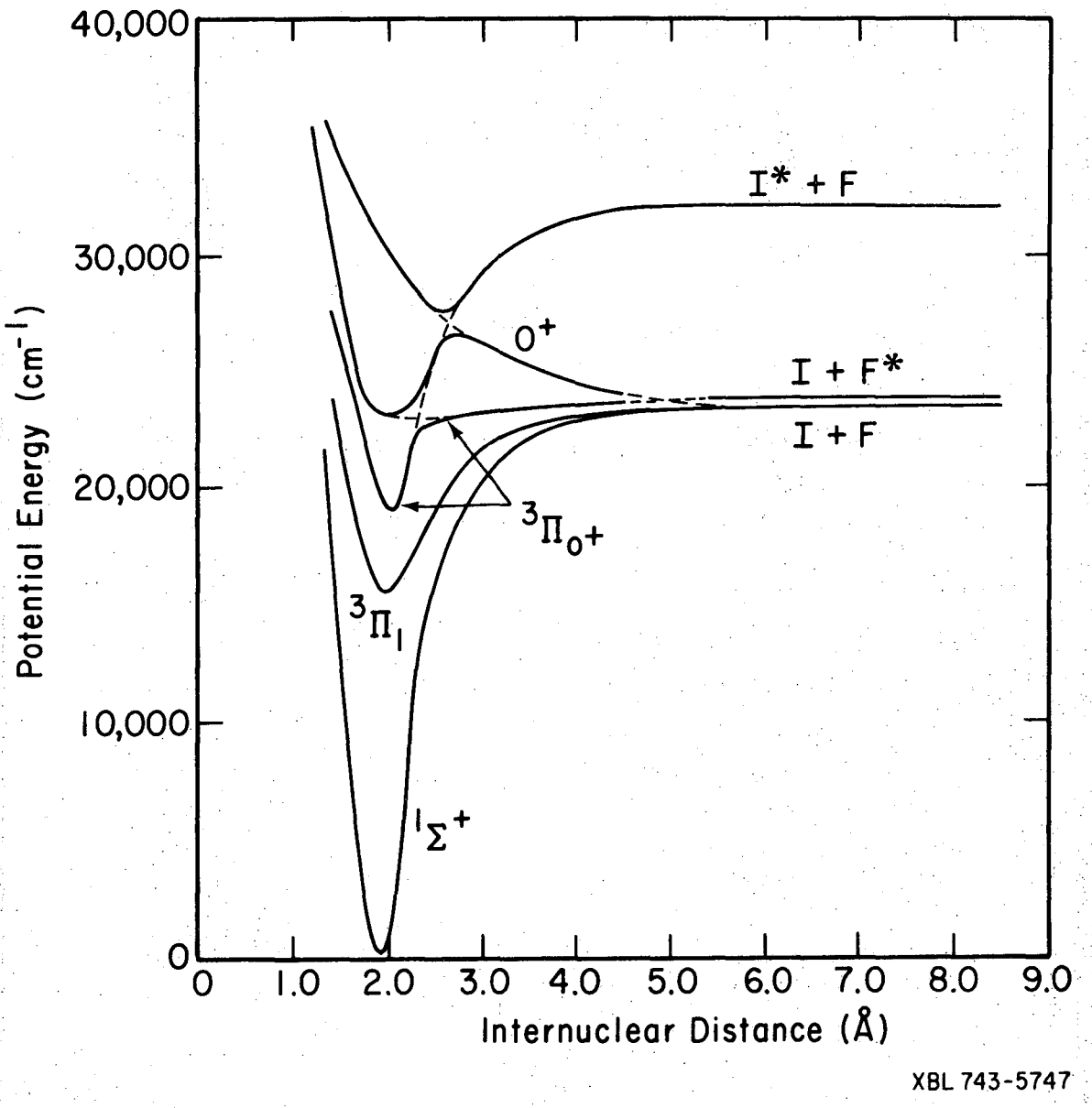

Fig. 17. Potential energy curves for IF. In this case an additional weakly bound $^3\Pi_{0^+}$ state has been drawn which leads to an avoided crossing with the $^3\Pi_{0^+}$ state of Fig. 16. The avoided crossing results in a forced correlation of the strongly bound $^3\Pi_{0^+}$ state with the products I + F*. In this case the ground state dissociation energy is known exactly to be 23229 cm^{-1} from Fig. 15, there should be a strongly curved Birge-Sponer extrapolation, and predissociation cannot occur below the dissociation limit.

dissociation energy of 23229 cm^{-1}. This value for the ground state dissociation energy agrees very well with that estimated from a long Birge-Sponer extrapolation (21600 - 24300 cm^{-1}) of the ground state.

The value of 23229 cm^{-1} for the dissociation energy of the ground state of IF leads to the values of 7638 cm^{-1} for the dissociation energy of the $A^3\Pi_1$ state and 11874 cm^{-1} for the adiabatic dissociation energy of the $B^3\Pi_{o^+}$ state. The value of 7638 cm^{-1} for the dissociation energy of the $A^3\Pi_1$ state follows the trend set by I_2, IBr, and ICl of 658 cm^{-1}, 2375 cm^{-1}, and 3684 cm^{-1}, respectively. The same series of molecules give 12546 cm^{-1}, 14660 cm^{-1}, and 17340 cm^{-1} for the dissociation energies of the ground state. The value of 23229 cm^{-1} is consistent with this trend in which the increasing bond energies are due to the increasing differences in electronegativities of the two atoms.

D. Mechanism of Population of the $A^3\Pi_1$ and $B^3\Pi_{o^+}$ States of IF

If one considers the energetics of the possible reactions between molecules consisting of iodine and fluorine atoms, one finds that there are only two possible mechanisms for the population of excited electronic states of IF in the reaction of I_2 with F_2 for a flow system such as the one described here. This is unlike the situation in an iodine-fluorine flame in which the exothermicity of the overall reaction

$$1/2\ I_2 + 5/2\ F_2 \rightarrow IF_5 \quad \Delta H = -205\ \text{kcal/mole} \tag{9}$$

is available to reaction processes by way of the high flame temperature. The first of these possible reactions is the following

$$I_2 + F_2 \rightarrow IF^* + IF \tag{10}$$

where IF* is an IF molecule in either the $A^3\Pi_1$ or $B^3\Pi_{o^+}$ electronic state.

Considering the bond energies of I_2, F_2 and the value of the bond energy for IF adopted here, emission from IF* can occur at wavelengths as short as 480 nm. This coincides well with the short wavelength cutoff in emission from the $A^3\Pi_1$ state, but emission from v' = 5,6,7 and 8 of the $B^3\Pi_{0^+}$ state occurs at higher energies with vibrational temperatures of a few thousand degrees. The lack of observation of emission from even higher levels appears to be due to the decreasing value of the transition matrix element for the (v', 0) band with increasing v' rather than the lack of population of these levels. Of course this reaction would proceed through a four-center transition complex and for this reason alone is not to be favored.

The second and more likely mechanism for the population of excited electronic states is that of three-body recombination of I and F atoms. The reactions

$$I_2 + F_2 \rightarrow IF_2 + I \tag{11}$$

$$IF_2 + F_2 \rightarrow IF_3 + F \tag{12}$$

$$IF_n + F_2 \rightarrow IF_{n+1} + F \text{ in general for } n \leq 4 \tag{13}$$

are probable sources of I and F atoms. Of the two reactions

$$F + I_2 \rightarrow IF + I \tag{14}$$

$$I + F_2 \rightarrow IF + F \tag{15}$$

the first is expected to be faster than the second since $F + Cl_2$ is much faster than $Cl + F_2$[15]. These two reactions may propagate a long chain in the explosive reaction between I_2 and F_2 if the second reaction is sufficiently fast. Neither of these reactions is exothermic enough to populate excited electronic states. Since at 300 K there are substantial

amounts ($\sim$ 13%) of $F(^2P_{1/2})$ atoms in thermal equilibrium with $F(^2P_{3/2})$ atoms both the $A^3\Pi_1$ and $B^3\Pi_{o^+}$ states may be populated up to their dissociation limits by atom recombination provided that the value of 23229 $\pm$ 100 cm^{-1} assumed here for the dissociation energy of the ground state is correct. If the dissociation energy is less than this value then atoms must pass over or tunnel through a potential barrier to populate the $B^3\Pi_{o^+}$ state. The rate of population of the $B^3\Pi_{o^+}$ state compared to that of the $A^3\Pi_1$ state would be negligible for an energy barrier of more than a few hundred wavenumbers. Thus the fact that the reaction between I_2 and F_2 populates the $B^3\Pi_{o^+}$ state of IF favors the highest possible value for the dissociation energy.

Clyne, Coxon and Woon-Fat[5] have studied the recombination of $Br(^2P_{3/2})$ atoms in the presence of singlet $O_2(^1\Delta_g, {}^1\Sigma^+g)$, and Clyne, Coxon and Townsend[3] have studied the recombination of $Br(^2P_{3/2})$ atoms with $F(^2P_{3/2}, P_{1/2})$ atoms and the recombination of $I(^2P_{3/2})$ atoms, with $F(^2P_{3/2}, {}^2P_{1/2})$ atoms both in the presence of singlet $O_2(^1\Delta_g, 1\Sigma_g^+)$. Singlet oxygen greatly enhanced the emission from the $B^3\Pi_{o^+}$ state in the case of Br_2. For both Br_2 and BrF there is an energy barrier to atom recombination which is overcome by energy transfer from singlet oxygen. Unfortunately, no determination was made as to whether singlet $O_2(^1\Delta_g, {}^1\Sigma_g^+)$ was explicitly required for emission from the $B^3\Pi_{o^+}$ state in the recombination of I and F atoms.

The recombination of I and F atoms in the presence of a third body M

$$I + F + M \xrightarrow{a} IF^* + M \qquad (16)$$

may be followed by collisional quenching of IF*

$$IF^* + M \xrightarrow{b} IF + M \tag{17}$$

or by radiative transfer to the ground state.

$$IF^* \xrightarrow{c} IF + h\nu \tag{18}$$

These three reactions lead to the following for the steady state concentration of IF*:

$$(IF^*) = \frac{a(I)(F)(M)}{b(M) + c} \tag{19}$$

If one assumes that I and F atoms are terminated primarily by the atom recombination steps I+F+M, I+I+M, and F+F+M one finds that:

$$(IF^*) \propto \frac{(I_2)\ (F_2)}{b(M) + c} \tag{20}$$

This expression is the same as that which one arrives at for the first mechanism discussed, which involves a four-center reaction between I_2 and F_2. The difference in the dependence of the $A^3\Pi_1$ and $B^3\Pi_{o^+}$ emission on the concentration of I_2 (Fig. 5) can be explained on the basis of the radiative lifetimes of the two states, according to Equation 20, if I_2 is primarily responsible for electronic quenching so that $I_2 \equiv M$. In the case that emission from the $A^3\Pi_1$ state is in the high pressure limit of Equation 20 then the dependence on (I_2) is removed, as was observed. The $B^3\Pi_{o^+}$ state must be in the low pressure limit to fit the experimental results, thus predicting that the $A^3\Pi_1$ state, has a much longer radiative lifetime than the $B^3\Pi_{o^+}$ state for similar quenching constants. As will be discussed below, the radiative lifetime of the $B^3\Pi_{o^+}$ state is short enough to be competitive with the vibrational relaxation time at the pressures studied. Addition of an inert gas such as Ar would be expected to decrease emission from the $A^3\Pi_1$ state at sufficiently high pressures, as was observed (Figs. 6 and 7). Small flow rates of Ar would be expected

to increase emission from the $A^3\Pi_1$ state by increasing the cell residence time and thus the F_2 concentration. Increasing flow rates of Ar would be expected to increase the emission from the $B^3\Pi_{o+}$ state by increasing both the concentrations of F_2 and I_2. Thus the effect of flow rates of F_2, and I_2 and Ar on the relative emission from these two excited electronic states can be explained in a qualitative way by either of the two mechanisms discussed. The atom recombination mechanism is to be preferred on the basis of energetics in the case of the $B^3\Pi_{o+}$ state, however, so that the $A^3\Pi_1$ state is probably also populated by atom recombination.

E. Effect of Pressure on Vibrational Populations of the $B^3\Pi_{o+}$ State

The vibrational populations for Spectra 1-5 are given in Table V and the vibrational populations for the two extremes in pressure are compared graphically in Fig. 18. For this series of spectra the flow rates of I_2 and F_2 into the cell were held constant and the total pressure increased from the value of 4.8 mtorr to as high as 310 mtorr by an increased flow of Ar. Increasing the flow rate of Ar increased the cell residence time by decreasing the pumping speed of the system and thus increased concentrations of I_2, F_2, and reaction products in the cell, as discussed previously. For this reason changes in vibrational populations cannot be attributed solely to increased pressures of Ar, and in fact are probably due to the increased pressures of halogens and interhalogens as these molecules are excellent energy transfer agents. For this reason the effect of increased pressure on the vibrational populations will only be discussed in a qualitative manner.

Increasing the pressure to 310 mtorr with Ar increased the cell residence time from 0.2 to 1.6 sec (Fig. 8) so that the pressure of

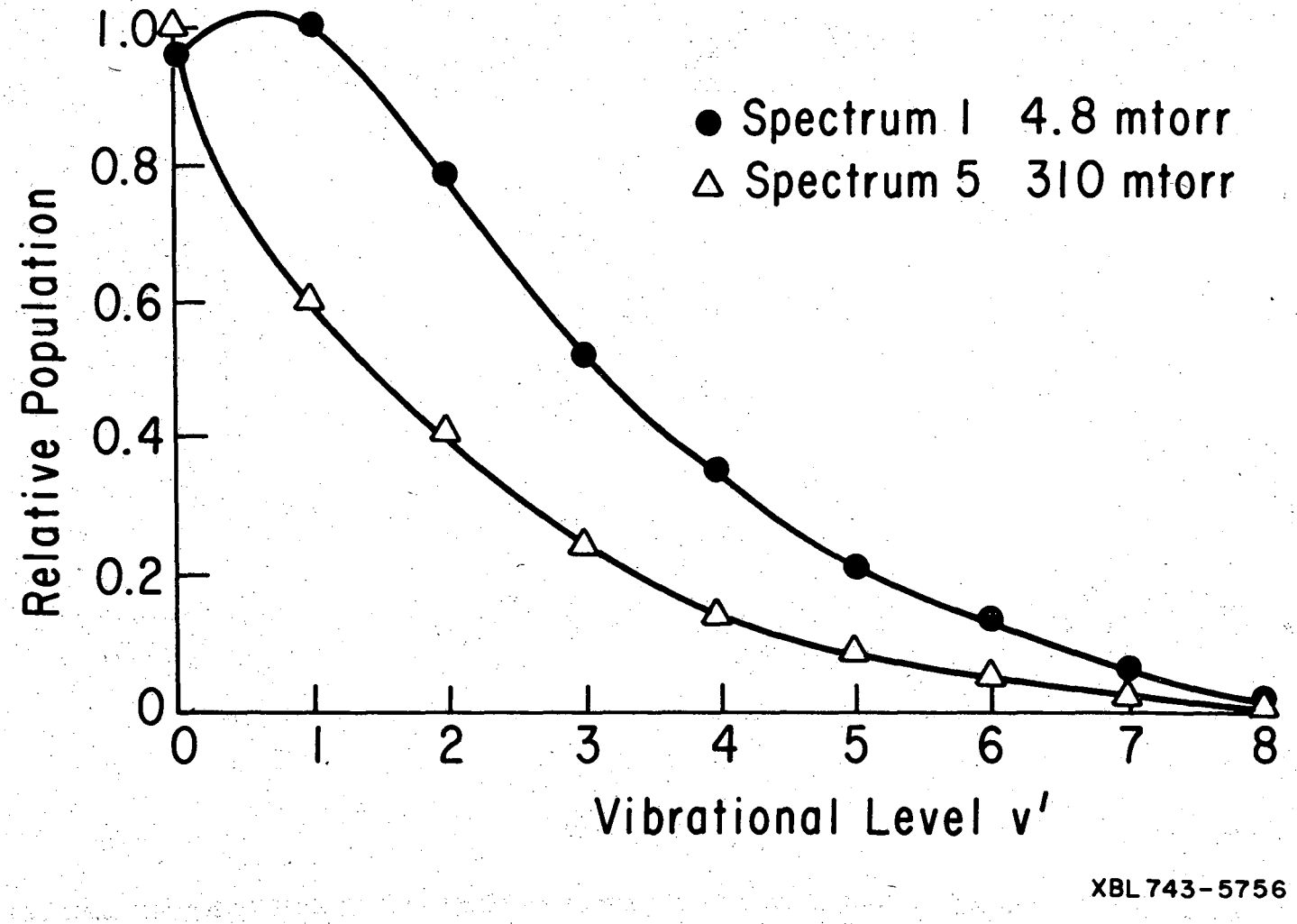

Fig. 18. Comparison of vibrational populations calculated from Spectra 1 and 5.

halogens increased from about 5 to 40 mtorr. Moderate pressures (up to 32 mtorr) of Ar (Spectra 2 and 3) had little effect on the cell residence time and little effect on the vibrational populations (Table 5). The substantial changes in vibrational populations brought on by larger flow rates of Ar (Spectra 4 and 5) appear to be due to the increased deactivation by halogens and interhalogens as a result of the increased cell residence times.

Measurement of vibrational relaxation times of homonuclear halogens by Millikan and White[27] resulted in a typical value of 10^{-7} for $p\tau_v$ where p is the pressure in atmospheres and τ_v is the vibrational relaxation time. The vibrational populations change substantially over the halogen pressure range of 5 to 40 mtorr so that over this pressure range the radiative lifetime must be competitive with the vibrational relaxation time. This yields a radiative lifetime of about one millisecond for the $B^3\Pi_{0^+}$ state of IF. The cell residence time is long compared to this value for the radiative lifetime so that essentially all molecules formed in excited states emit before passing out of the cell.

A radiative lifetime of about one millisecond for the $B^3\Pi_{0^+}$ state of IF is intermediate between that of $I_2(7 \times 10^{-7})$[28] and that of F_2 which has not been measured, but is expected to be very long due to the forbiddenness of the transition which only becomes allowed for heavy molecules for which there is strong spin-orbit coupling.

The lowest pressure spectrum, Spectrum 1, is non-Boltzmann and exhibits a slight population inversion for $v' = 1$. One goal of this study was to obtain the "initial distribution" of molecules among vibrational energy levels. In the low pressure limit a newly formed molecule will radiate before colliding with another molecule so that the vibrational

populations represent the rates of reaction into each of the vibrational levels. In atom recombination the higher vibrational levels are populated at a more rapid rate than lower vibrational levels, and one would expect the initial distribution to be highly inverted. In these experiments the trend with reduced pressure is clearly in this direction, but the vibrational distribution is far from that expected for the initial distribution. This is despite a reduction in total pressure by an order of magnitude over that used by Gabelnick[8] and an increased call volume from 1 to 350 liters to reduce deactivation at the walls. The inability to obtain an initial distribution for this reaction is due to two factors. The first is that emission intensity nessarily decreases with decreasing concentration of reactants and thus pressure. The second is that at lower pressures the emission from the $B^3\Pi_{o+}$ state was masked by emission from the $A^3\Pi_1$ state.

REFFRENCES

1. R. A. Durie, Proc. R. Soc. A 207, 388 (1951).
2. R. A. Durie, Can. J. Phys. 44, 337 (1966).
3. M. A. A. Clyne, J. A. Coxon and L. W. Townsend, J. Chem. Soc. Faraday Trans. II 68, 2134 (1972).
4. M. A. A. Clyne and J. A. Coxon, J. Mol. Spec. 23, 258 (1967).
5. M. A. A. Clyne, J. A. Coxon and A. R. Woon-Fat, Trans. Far. Soc. 67, 3155 (1971).
6. M. A. A. Clyne and J. A. Coxon, Proc. R. Soc. A 298, 424 (1967).
7. R. J. Browne and E. A. Ogryzlo, J. Chem. Phys. 52, 5774 (1970).
8. S. D. Gabelnick, Ph.D. Thesis, University of California, Berkeley, Lawrence Berkeley Laboratory Report UCRL-18623 (1969).
9. J. C. DeVos, Physica 20, 690 (1954).
10. G. Herzberg, Molecular Spectra and Molecular Structure I. Spectra of Diatomic Molecules, 2nd ed. (Van Nostrand, Princeton, 1950).
11. M. Born and R. Oppenheimer, Ann. Physik 84, 457 (1927).
12. P. A. Fraser, Can. J. Phys. 32, 515 (1954)
13. R. G. Turner and R. W. Nicholls, Can. J. Phys. 32, 475 (1954).
14. R. N. Zare, Lawrence Berkeley Laboratory Report UCRL-10925 (1963).
15. R. T. Watson, Private Communication.
16. W. G. Brown, Phys. Rev. 42, 355 (1932).
17. W. G. Brown and G. E. Gibson, Phys. Rev. 40, 529 (1932).
18. P. H. Brodersen and J. E. Sicre, Z. Phys. 141, 515 (1955).
19. M. S. Child and R. B. Bernstein, J. Chem. Phys. 59, 5916 (1973).
20. L. Mathieson and A. L. G. Rees, J. Chem. Phys. 25, 753 (1956).

21. L. W. Bader and E. A. Ogryzlo, J. Chem. Phys. 41, 2926 (1964).

22. E. Hutton and M. Wright, Trans. Far. Soc. 61, 78 (1965).

23. D. B. Gibbs and E. A. Ogryzlo, Can. J. Phys. 43, 1905 (1965).

24. E. W. Abrahamson, D. Husain and J. R. Wiesenfeld, Trans. Far. Soc. 64, 833 (1968).

25. M. A. A. Clyne and J. A. Coxon, Chem. Comm. 10, 285 (1966).

26. W. G. Brown, Work never published but referred to in several references including Ref. 6.

27. R. C. Millikan and D. R. White, J. Chem. Phys. 39, 3209 (1963).

28. L. Brewer, R. A. Berg and G. M. Rosenblatt, J. Chem. Phys. 38, 1381 (1963).

29. O. K. Rice, J. Phys. Chem 65, 1972 (1961).

ACKNOWLEDGMENTS

I am thankful for the assistance and guidance afforded me by many people during my studies at Berkeley. My research director and mentor was Professor Harold Johnston, who provided me with many stimulating problems. His approach to graduate education, which allows the student to develop as independently as possible has in the long run proved very beneficial to myself. In his courageous stand against the pollution of the stratosphere by SST airplanes, he has provided me and my fellow graduate students with a faith in scientific honesty and a desire to see truth prevail.

My sincere thanks go to Professors Henry Schaefer and William Miller who assisted me with the theoretical work. Thanks are also extended to Dr. Dean Liskow for assistance with the computer calculations.

I am grateful to Dr. Steven Gabelnick of Argonne National Laboratory for many discussions of the IF work and to Dr. Don Secrest of the University of Illinois for a helpful discussion of the potential energy surface.

I am appreciative of the friendship extended to me by my fellow graduate students and for the many good times we have had together.

I am most thankful to Karen and Krishna for their many sacrifices during the course of my education, and for the encouragement they have always provided. I am also thankful to my parents for their constant friendship and support.

Financial support from both the Department of Chemistry and the Inorganic Materials Research Division of the Lawrence Berkeley Laboratory is gratefully acknowledged.

TECHNICAL INFORMATION DIVISION
LAWRENCE BERKELEY LABORATORY
UNIVERSITY OF CALIFORNIA
BERKELEY, CALIFORNIA 94720